ALMA MATER STUDIORUM - UNIVERSITÀ DI BOLOGNA

SCUOLA DI INGEGNERIA E ARCHITETTURA

DIPARTIMENTO di
INGEGNERIA DELL'ENERGIA ELETTRICA E DELL'INFORMAZIONE
"Guglielmo Marconi"
DEI

CORSO DI LAUREA IN INGEGNERIA DELL'ENERGIA ELETTRICA

Tesi di Laurea Magistrale
in

AZIONAMENTI ELETTRICI per APPLICAZIONI INDUSTRIALI

INVESTIGATION ON ENERGY EFFICIENCY FOR SERVO CONTROL APPLICATIONS

CANDIDATO: RELATORE:

Simone Morini   *Prof. Angelo Tani*

                                               CORRELATORI:

                                               Ing. Loredana Matea

                                               Prof. Luca Zarri

Anno Accademico 2015/2016

Sessione III

To my parents and their inspiring curiosity

<<The Buddha, the Godhead, resides quite as comfortably in the circuits of a digital computer or the gears of a cycle transmission as he does at the top of a mountain or in the petals of a flower. To think otherwise is to demean the Buddha, which is to demean oneself.>>

Robert M.Pirsig,

"Zen and the art of motorcycle maintenance"

CONTENTS

ABSTRACT in LINGUA ITALIANA

Lo scopo del lavoro è stato migliorare la previsione del consumo energetico di applicazioni per servo controllo. La tesi è stata proposta e supportata dalla divisione Meccatronica di un'azienda locale. Un'analisi più accurata dell'efficienza in specifici cicli di lavoro, che portano i componenti a lavorare lontano dai punti nominali di funzionamento, può aiutare nella selezione ottima degli stessi e nel calcolo del loro costo operativo di vita.

L'analisi prende in considerazione particolari componenti quali inverter con controllo vettoriale, motori brushless a magneti superficiali e riduttori planetari a gioco ridotto. Questo tipo di componenti massimizzano la dinamica e la precisione del controllo. Le perdite più importanti vengono descritte teoricamente. Successivamente si presenta un'indagine sullo stato dell'arte dei più diffusi modi per ridurre le suddette perdite.

Per il motore elettrico viene elaborato un algoritmo in grado di ricavare delle mappe di efficienza, ovvero il valore delle perdite e dell'efficienza in ogni punto del diagramma coppia velocità. L'algoritmo considera diverse temperature di funzionamento cercando di predirle dal tipo di funzionamento operativo. Laddove venga misurata la resistenza e la temperatura della cassa del motore si possono ottenere informazioni più dettagliate sulla temperatura degli avvolgimenti e si possono quindi calcolare le perdite Joule con maggiore precisione.

L'obiettivo è fornire uno strumento di facile implementazione, come un'equazione polinomiale, con cui si possano calcolare le perdite del componente per ogni particolare fase del ciclo di lavoro. Inevitabili approssimazioni che non considerano le reali condizioni operative devono essere verificate per validare la correttezza del metodo. E' stato condotto un esperimento in cui si calcolano le perdite di un motore flangiato ad un riduttore. Nel calcolo delle mappe infatti i componenti sono considerati da soli in una differente situazione di scambio termico. Le misure reali condotte confermano un errore nella stima dell'efficienza da parte delle mappe del motore e del riduttore soprattutto ad alta velocità quando le temperature delle casse sono alte. Si nota inoltre come le perdite sull'inverter sono comparabili con quelle degli altri componenti e si consigliano ulteriori analisi che esulavano dagli scopi di questo lavoro.

Per concludere si presenta l'integrazione del metodo nella selezione ottima dei componenti che usa una più accurata previsione delle perdite e quindi dei consumi energetici annui.

ACRONYMS

THD	Total Harmonic Distortion
TCO	Total Cost of Ownership
PWM	Pulse Width Modulation
FEM/FEA	Finite Element Method/Analysis
CFD	Computational Fluid Dynamics
PM	Permanent Magnet
PMSM	Permanent Magnet Surface Mounted
IPM	Interior Permanent Magnet
SVPWM	Space Vector Pulse Width Modulation
DPWM	Discontinuous Pulse Width Modulation
WBG	Wide Band Gap
FOC	Field Oriented Control
BMR	Bonfiglioli Mechatronic Research
MDS	Mechatronic and Drives Solutions
VSI	Voltage Source Inverter
MTPA	Maximum Torque per Ampere ratio

SYMBOLS

P_i	*Active Power*	*[W]*
W_i	*Energy*	*[J]*
V_i	*Phase Voltage*	*[V]*
$V_{ce\,sat}$	*Collector-Emitter Voltage*	*[V]*
I_o	*Output current*	*[A]*
R_s	*Stator Resistance*	*[Ω]*
J	*Current density*	*[A/m^2]*
I_s	*Stator phase current*	*[A]*
Θ	*Temperature*	*[K]*
T	*Torque*	*[Nm]*
θ_m	*Angular position (mechanical)*	*[rad]*
f	*Frequency*	*[Hz]*
B_m	*Flux density*	*[T]*
σ	*Conductivity*	*[Si/m]*
ρ	*Resistivity*	*[Ω m]*
μ	*Mobility or friction*	

μ_t	Magnetic permeability	[H/m]
F	Force (radial)	[N]
v	Velocity	[m/s]
δ	Air gap length	[m]
n	Rotational mechanical speed	[rpm]
p	Number of pair poles	
D	Diameter of the stator	[m]
H	Magnetic field	[A/m]
e_i	Electromotive force	[V]
ω_m	Rotational speed	[rad/s]
ω	Pulsation	[rad/s]
J_m	Inertia of the motor	[Kg/m^2]
J_g	Inertia of the gearbox	[Kg/m^2]
L_s	Inductance of the Stator	[H]
M_{se}	Mutual Inductance	[H]
φ_{em}	Magnetic Flux	[Wb]
τ	Pole pitch	[m]
P_m	Permeance	[H]
N	Number of conductors	
X_s	Stator Reactance	[Ω]
V_{pk}	Peak Voltage	[V]
I_{pk}	Peak Current	[A]
R_{pp}	Phase to phase resistance	[Ω]
i	Ratio of reduction	
r	Inertia mismatch	
J_L	Inertia of the load	[Kg/m^2]
η	Efficiency	

LIST OF FIGURES and TABLES

Chapter 1

INTRODUCTION TO SERVO DRIVES

This chapter introduces the reason and the purpose of the project. Servo drives include many different types of application characterized by the need of high dynamic and position accuracy. The choice of the size of the components nowadays does not include accurate efficiency analysis but it focuses mainly on the mechanical strength, robustness and thermal loadability. Due to the increasing importance of efficiency, this work aims at a more accurate analysis of the efficiencies of the components in the varying working cycle. This kind of approach allows the optimization in the selection of the sizes also from energy consumption prospect.

1.1   Problem Background

After Kyoto Protocol, new law about Minimum Efficiency Standard for electric motors and a grown sensitivity of industries and people to environmental issues, the efficiency of the mechatronic solutions became a crucial point of the field. The product that succeeds, combines high performance, high dynamic response, high density to reduce the size and eventually high efficiency.

Besides the need to save energy for the grown green consciousness and to contribute to fight the climate change, being efficient might mean great savings in the electricity bill of the companies.

This work was proposed, encouraged and assisted by the Industrial Mechatronic Drives Solutions division of Bonfiglioli Riduttori s.p.a..

It is determining for this field of application being able to provide to the customer efficient products and therefore an efficient drivetrain.

Nowadays the initial cost of a product is not considered anymore so important but customers look at the Total Cost of Ownership (TCO). This parameter is the sum of the cost of the product in its entire operating cycle. Fig. 1.1 shows an example of TCO for a pump.

The Fig. 1.2 depicts, instead, that a little improvement in the efficiency can provide a relevant reduction of the total cost permitting to save money on the long period with a slightly bigger initial cost.
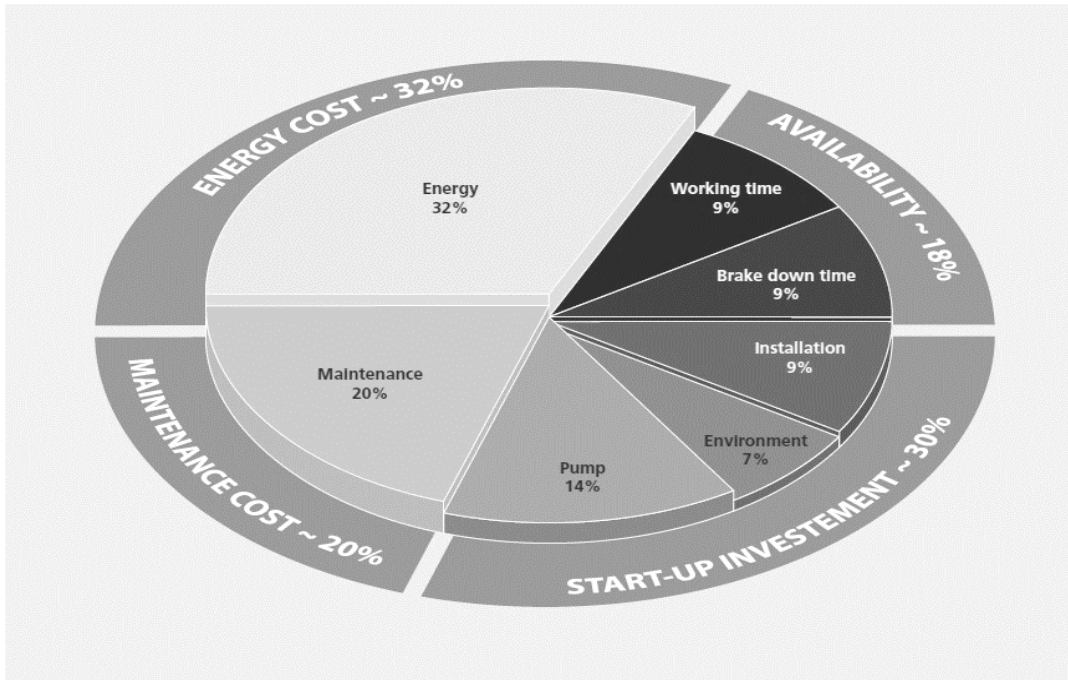
FIGURE 1.1: TOTAL COST OF OWNERSHIP OF A PUMP [1].
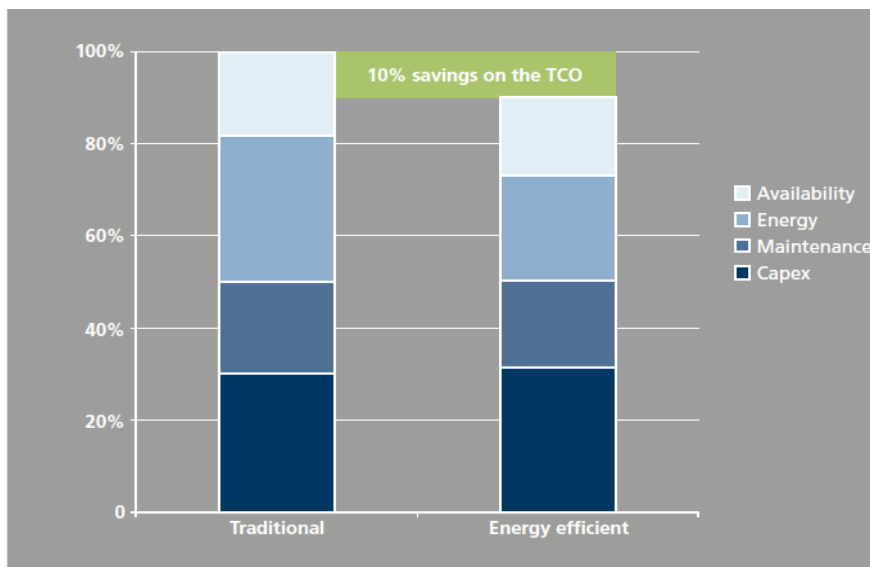
FIGURE 1.2: EFFECT of AN IMPROVEMENT IN EFFICIENCY on TCO [1].

Inside the Industry application the company has separated the business units dedicated to Power Transmission solutions and the Mechatronic ones. The project was proposed by this latter that presents the solutions with the highest efficiency. The author received support from the business unit MDS (Mechatronic and Drive Solution). For this reason, the products considered are the ones designed, built and sold by this division of the company.

The solutions considered are SERVO drives and combine a Servo inverter with an optional Sensorless control, a Permanent Magnet Surface Mounted motor with high torque density and a high precision planetary gearbox. Each component dissipates part of the energy in heat that does not contribute to the power transmission as in Fig. 1.3.
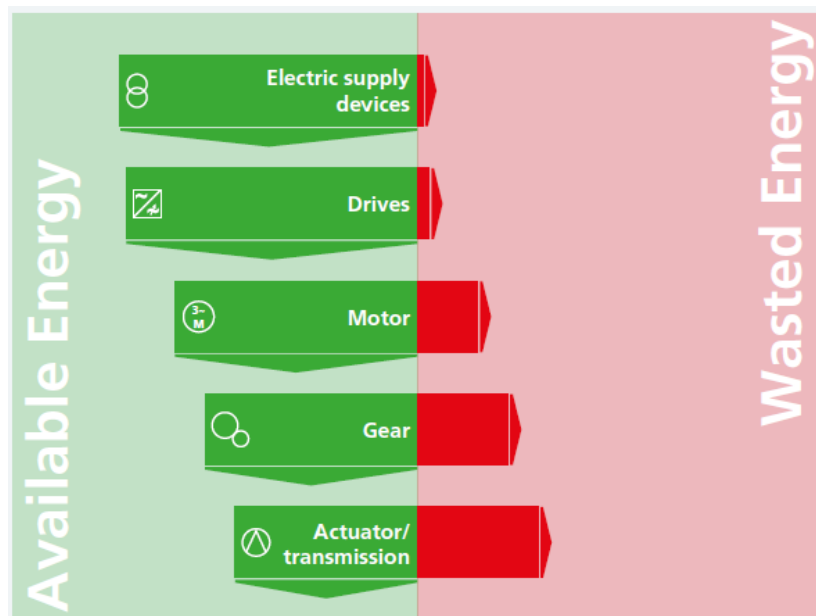
FIGURE 1.3: WASTED ENERGY IN THE MECHATRONIC CHAIN [1].

Some examples of application of Servo Drives are:

- Machine tools
- Packaging
- Conveyors
- Cranes and Hoist
- Textiles
- Robotics
- Paper and Paperboard
- Electronics Assembly
- Semiconductor
- Elevators and Escalators

To properly evaluate how and where the energy is being wasted in the entire chain (Variable frequency converter- Electrical Motor- Gearbox) it is important to watch the components altogether. The gearbox often may be the weak point. Since the global efficiency is the product of the efficiency of the 3 products if one of them has a very low efficiency, improvements in the others would be less effective.

High precision planetary gearbox, due to their technology and their construction process, allows higher input speed and higher efficiency. Thus, for a Servo axis the size of the motor is usually reduced in respect of industrial application. This reasoning is valid with types of gearboxes with low efficiency as the worm gears or generally with older or less expensive industrial gearboxes that have nominal efficiency between 50% and 90%. The planetary gearboxes have instead a nominal efficiency over 95% therefore in Servo drives (or whenever a high efficiency gearbox is chosen) all the 3 components matter as suggested in Fig. 1.4 where typical products for Industrial applications are depicted along with their nominal efficiency.

Therefore, the sizing procedure plays the crucial role in the optimization of cost and energy consumption.

Usually the efficiency point of view is still seen as marginal in the selection of the components. Often, to avoid complicated issues further discussed, the nominal efficiency of the component is assumed constantly or slightly dependent on the speed or torque. However, when each component is furtherly investigated it is undeniable that the losses of the electrical motors and of the gearboxes depend on both torque and speed. Therefore, considering the nominal efficiency as a valid value in many working points, which are different from the one in which that value is calculated, may be incorrect. The efficiency with low percentage of the nominal torque and at very low speed may vary significantly in comparison with the nominal one. A selection that aims to decrease only the weight or the cost (as it is common) may end up in selecting a very low efficient drivetrain for the specific cycle asked by the load. Selecting the components that run in working points with low efficiency might increase the TCO.

A method to derive a detailed characterization of the efficiency of these two components is proposed. A similar strategy was not developed for the inverter but the results from experiment demonstrate that the efficiency of inverter also drops at low speed. This suggests the need of characterization also for the converter and it should be verified in future works. The focus of the thesis is mainly on the electrical motor since the field of the

study of the author is electrical engineering. Moreover, the ratio of the gearbox is the main degree of freedom of the selection so when the ratio changes the size of the motor, the speed and the torque asked change with it.

FIGURE 1.4: POSSIBLE CHOICE OF TYPE OF COMPONENTS AND THEIR NOMINAL EFFICIENCY [1].

Then, it can be said that with the same number of stages of reduction the same type of gearboxes shows similar efficiency results. Thus, it seemed reasonable that the optimization of the ratio was made considering mainly the efficiency of the motor.

1.2 Content of the thesis

Chapter 2 describes the main types of losses and their physical reasons. The converter frequency has mainly conduction and switching losses. Conduction losses are proportional

to current and so to the torque asked by the load. Switching ones are basically proportional to the switching frequency chosen and so they may be linked to the desired quality of the current (high switching frequency guarantees a lower THD).

Electrical motors dissipate Joule losses (or Copper losses) due to the finite conductivity of the metals and Iron losses on the stator and rotor core. These last ones are a particular complicated subject. Moreover, losses on the magnets may be significant and windage losses should be considered.

Gearbox losses are even more difficult to be calculated precisely since in the planetary gearboxes independent load losses are more significant. These losses are the results of fluid dynamical events of the oil and the air. The operating condition of the gearboxes change the temperature and so the viscosity, CFD analysis are needed. Furthermore, meshing losses are due to friction and they are load dependent. Also, bearing and seals losses are included.

Chapter 3 includes a review of the state of art of inverter and PMSM motor. Different strategies to optimize the efficiency and the performance are presented trying to focus on the most popular techniques in the industry and the most attractive improvements.

For the inverters, emerging wide band gap (WBG) materials seem very promising and offer several benefits. More complex topology as multilevel inverter (as Neutral Clamp Pointed 3 level converter for instance) may improve the quality of power conversion. Eventually peculiar choice in the modulation technique of the Pulse Width Modulation may decrease the switching losses without compromising the THD.

Electrical motors present nowadays several different technologies but for the Servo drives application the Permanent Magnet motors are used to maximize the torque density and Maximum Torque/Ampere ratio. Briefly the equations of the equivalent model in the synchronous reference frame are presented to investigate the operational limits. Then considerations about the materials, the structure and the control are developed. The materials are quite consolidated in the windings while iron powder or iron alloy may improve the torque density. The magnets as Neodymium Iron Boron are definitely the most powerful on the market. Insulators also play a key role.

Furthermore, the structure of the PMSM motor can be optimized to increase the power density with a high number of poles and with the adoption of the concentrated windings. Nevertheless, the issue about the pulsations of the torque are introduced and the most common method to have a sinusoidal waveform of EMF and to reduce the cogging torque are mentioned. Field Oriented Control optimizes the relative position of the magnetic fields

producing the torque and nowadays Sensorless control is becoming more and more popular because it avoids the use of speed measurement tools.

Chapter 4 deals with the method employed to derive the efficiency map for the electrical motor. The efficiency is plotted on the torque-speed diagram and it can be therefore simplified in a polynomial function of the variables. The main principle is to consider that copper losses are proportional to the square of the torque while iron losses are somehow proportional to the speed of the motor. The accuracy of the map depends on the level of detail of the information used. The author received from Bonfiglioli Mechatronic Research several data of FEM simulations of some motors of the company. Thanks to this detailed information a script generates the map and a prediction of the efficiency in each working point is available. A case is presented showing the division of the total losses between copper, iron and mechanical ones.

Chapter 5 includes the description of the test conducted in Bonfiglioli Mechatronic Research. Since the map of the motor and of the gearbox (that was received from the author from BMR) are validated with the component alone, the values of efficiency are expected to decrease when the components are flanged together. The heat exchange in fact is very different and the temperature would increase. The test analyses the real efficiency in the real operating condition. The error committed by the prediction of the maps is quantified and justified. Moreover, a verification of the maximum overtemperature of the windings is presented. Finally results of the inverter efficiency are shown.

Eventually chapter 6 focuses on an improvement in the optimization of the ratio of the gearbox with the more accurate information obtained about the efficiency. The sizing procedure has to take into account different selection criteria and so far the mechanical strength and thermal loadabillity are the most investigated. Since the increasing accuracy of the efficiency, a more reliable prediction of the energy consumption may be achieved. Therefore, after presenting the main matters in the selection of the components and in the choice of gearbox ratio, the efficiency maps are integrated in the method.

An example is presented to show that the minimization of the energy consumption might not coincide with the minimization of the initial cost.

1.3 Purpose of the project

The purpose of this project was mainly practical: it aimed to give a simple and effective tool to Customer Application engineers to analyse the efficiency of different scenarios

during the sizing procedure. Especially in Europe, where the cost of energy is higher the Total Cost of Ownership of a mechatronic solution deeply depends on its own energy consumption and a bigger investment in initial cost may be repaid back in a certain time. The demanding improvement was enhancing the accuracy of the efficiency calculation paying attention to consider the exact working cycle in which the components will work.

To correctly calculate losses on the mechatronic solution in a general approach valid for a wide range of applications the losses on each component are investigated. Due to the complexity of the subject it is not convenient to try to obtain a detailed model of equations that would calculate the losses for each torque and speed. The real efficiency in fact is strictly linked to the operating and environmental conditions in which the solutions will work. A precise calculation is not completely possible and all the results are an approximated prediction of the real efficiency. Therefore, developing a very complex algorithm able to model all the losses would present a great computational effort and anyhow the accuracy of the prediction is quite poor.

Beside the operating and environmental conditions the first approximation made in the development of the efficiency map is considering the component alone. When the component is working in the real condition, instead, the gearbox and the motor are flanged together and the quality of the heat exchange is decreased and so the efficiency may vary. The temperature inside the gearboxes or the temperature of the windings are fundamental information to properly estimate the efficiency but they are also very difficult to be predicted precisely and dynamically. Moreover, the quality of heat exchange depends on the temperature itself and makes the calculation iterative. The test described in Chapter 5 aims to quantify the difference in the efficiency calculation between these two conditions. The tool developed should be able to offer a rapid analysis of how the efficiency varies between different scenarios. The intent of the author was to find a proper trade-off between an academic approach with the typical more practical approach of a company. While the first needs mathematics and physics phenomenon interpretation, the second may be based often on experience and rules of thumb. The main issues of the mechatronic are investigated more deeply where the practical approach may lack of accuracy.

Reference Chapter 1:
[1] Bonfiglioli MDS Catalogue-2015.

Chapter 2

THEORETICAL EVALUATION OF THE LOSSES ON EACH COMPONENT

To discuss about the efficiency of the entire drive solution the first step is to deeply understand where and how part of the energy is lost. Several non-ideal behaviours of the nature cause different losses, instead of transmitting the entire power to the next component a percentage of that is dissipated in heat without contributing to the transmission. In this chapter the most relevant losses are described.

In order to design and control our devices focusing on their efficiency it is crucial to know the physical phenomena that cause the losses. The scheme in Fig. 2.1 summarizes the losses described in this chapter. The choice of the motor will be explained later.
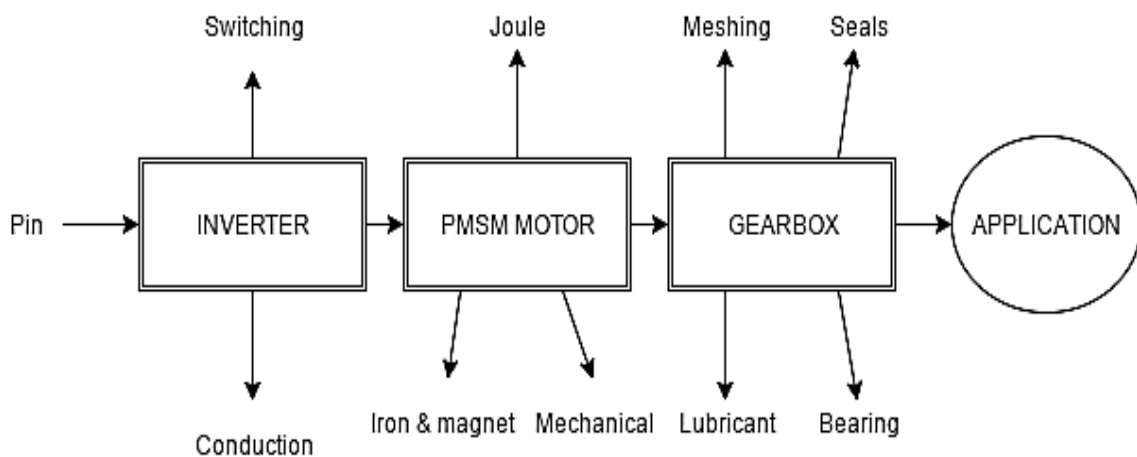
FIGURE 2.1: LOSSES DISTRIBUTION SCHEME.

The calculation of the losses of each component has a very broad literature. This topic, in fact, is widely investigated for many reasons. Firstly, the thermal analysis needs some information about the heat produced by the components. Moreover, the optimal design of the dissipation system of the components needs to know the amount of losses produced in the nominal point.

In the chapter a brief description of the physical reason is followed by an analysis of the most common method calculation of each type of loss. Losses in the iron and in the lubricant, require FEM and CFD calculation respectively. As previously mentioned, for the purpose of the project these complicated method calculations were not investigated deeply. Moreover, indirect methods to derive the iron losses are often used to avoid the computational effort. For these reasons, in the chapter only the analytical formulas are presented.

2.1 Inverter Losses

The structure of a VSI inverter is the one shown in Fig. 2.2:
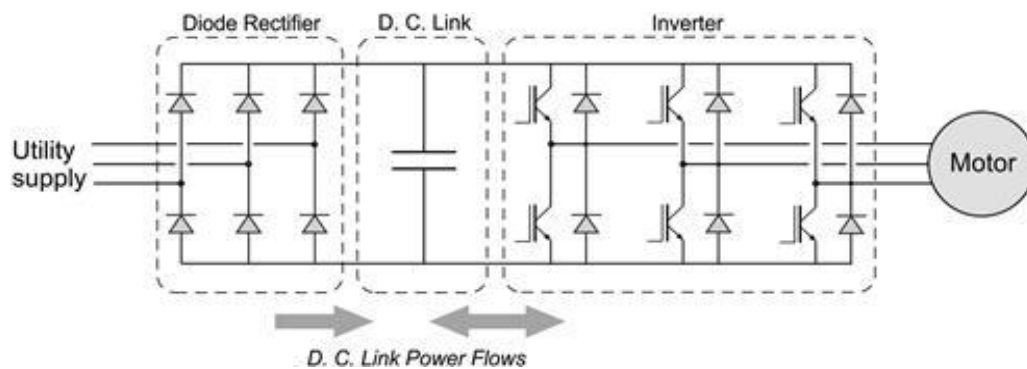
FIGURE 2.2: TYPICAL STRUCTURE OF VSI INVERTER.

Since the maximum junction temperature should not be reached at any time, the losses produced by a converter frequency are studied to select the proper components checking the thermal loadability. There are different types of losses that need to be considered:

- conduction losses occurring in the ON state
- switching losses in any turn-on/off of the components
- off-state (stand-by) losses (not discussed)

2.1.1 Conduction Losses

The conduction losses are mainly due to the finite resistivity of Silicon and to the presence of the internal resistances both on the diodes and the IGBTs. The conductivity is the product of the number of free carriers times the electrical mobility (μ) that describe the tendency of

electrons to be moved. The number of free electrons in the semiconductors varies with the temperature, while instead it is constant for metals and insulators. At the environmental temperature, a proper doped silicon (pn junction) can be considered already a good conductor over the threshold voltage. The mobility instead can be manipulated in the design of the semiconductors. It depends mainly on the impurity level, temperature and electrons or holes concentrations. The internal resistance of the power devices is linked to the width of the Drift region (n- region in Fig. 2.4), that presents a lower density of free carriers to provide a higher breakdown voltage. Fig. 2.3 shows an equivalent circuit of IGBT.

 IGBTs are widely used in many kinds of power frequency converter. They combine the advantages of Mosfets in the switching behaviour with the better ON state behaviour of bipolar transistors. IGBTs present in fact, very low on state voltage drop along with a superior current density at high breakdown voltage. Moreover, they require low power drive circuit thanks to the MOS input. All in all, they have a wider Safe Operating Area in comparison with both the other 2 traditional devices (Mosfet and BJT). The value of that internal resistance is about order of mΩ and it doesn't change drastically at high voltage breakdown like in the Mosfet [1].

The value of the internal resistance (called Ron) increases with the width of the drift region. To achieve higher breakdown voltages the width should be larger so a trade-off is in any case needed in the design.
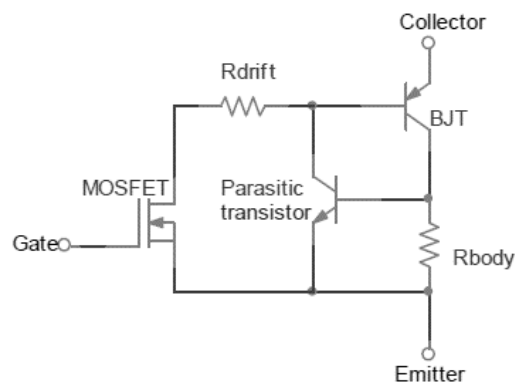
FIGURE 2.3: MID-LEVEL DETAILED IGBT MODEL.
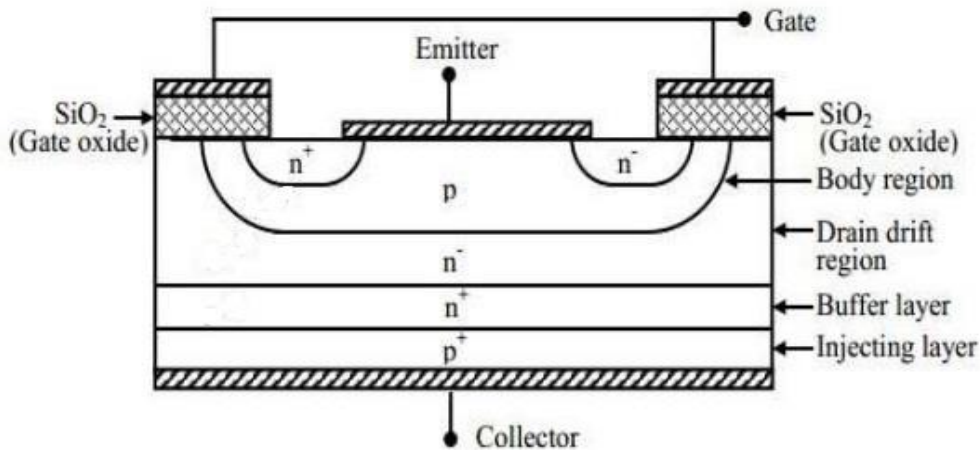
FIGURE 2.4: STRUCTURE OF IGBT.

The conduction losses on the rectifier are the power dissipated by the diodes. To calculate them the same approach that will be discussed for the inverter can be used. Both diodes and IGBTs in fact present a similar ON state behaviour with the drop voltage due to the threshold of the junction plus the internal resistance.

Different methods are proposed to calculate conduction losses on the inverter [2][3]. Different level of detail of the model of the devices are also proposed but basically, they all require specific data that are not provided in the Datasheets as the one depicted in Fig. 2.3.

However, from the I-V characteristic curve of the device it is easy to obtain the value of the internal resistance (*Ron*) that can be used in the simple but quite accurate ON-state model [2] shown in Fig. 2.5.
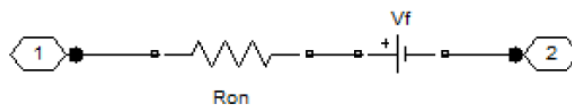
FIGURE 2.5: SIMPLIFIED MODEL OF ON-STATE.

Due to the dependence of the resistance on the junction temperature the right curve has to be chosen in the data sheet output characteristic shown in Fig. 2.6. The conduction losses can be calculated as in [1] as:

$$P_{T/Dcond} = \frac{1}{\tau}\int_0^\tau V_{ce}\,I_a\,d\tau = \frac{1}{\tau}\int_0^\tau (V_{T/D} + R_{onT/D}I_a)I_a\,d\tau \|_{\text{T/D conducts}} \quad (2.1)$$

12

Where V $_{D/T}$ is the threshold voltage of the diodes or the transistors. τ is the period of time in which the component considered is conducting. The IGBTs conduct both when the signal of the switch is 1 (upper one ON) and the phase current *Ia* is positive and when the switch is 0 (lower one ON) and the current is negative. Vice versa for the diodes.

An example of Data Sheets (from Infineon) with the static characteristics of IGBTs is shown in Fig. 2.6. From this chart, it is possible to derive a value for the internal resistance of the device. The junction temperature and the voltage of the drive gate change the internal resistance therefore they should be considered during the choice of the chart. As a result, the conduction losses are linearized by an internal resistance and by the threshold voltage. The value is multiplied by 3 to obtain the losses of the three legs since the same switching pattern, ac currents and voltages are applied to all the phases.

Figure 6. Typical output characteristics
(T_j = 150°C)
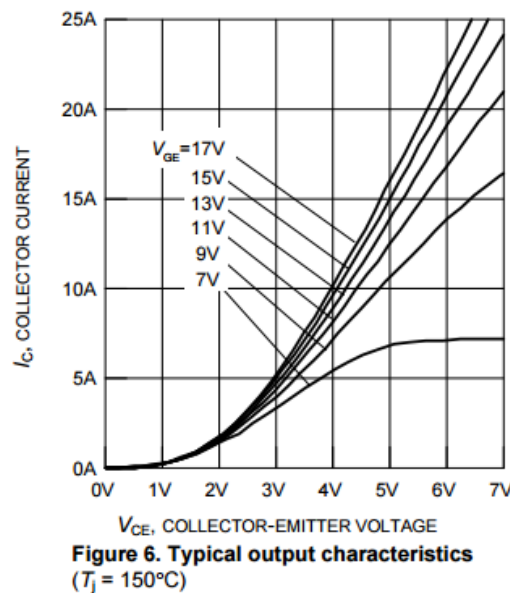
FIGURE 2.6: I-V CHART FOR IGBTs.

2.1.2 Switching Losses

The switching losses, instead, take place only in the time period in which the IGBTs or the diodes are switched. It is not possible to achieve a switching time equal to zero due to physical reason. The amount of losses becomes such important nowadays when the

converters use switching frequency up to Megahertz. Caused by different inherent delay of the components as the rise and fall time but also delay time (as reverse recovery and tail current time), switching losses correspond to the dissipation that occurs when both current and voltage are changing. Switching losses exist because in that interval the components have contemporary voltage and current very different from zero and it produces a power dissipation of V times I.

Generally, they can be calculated as:

$$W_{on/off} = \int_0^{t_{on/off}} v(t)i(t)dt = \int_0^{t_{on/off}} V_{ce}(t)I_a(t)dt$$

(2.2)

Fig. 2.7 shows an approximation of the evolution of the voltage and current.
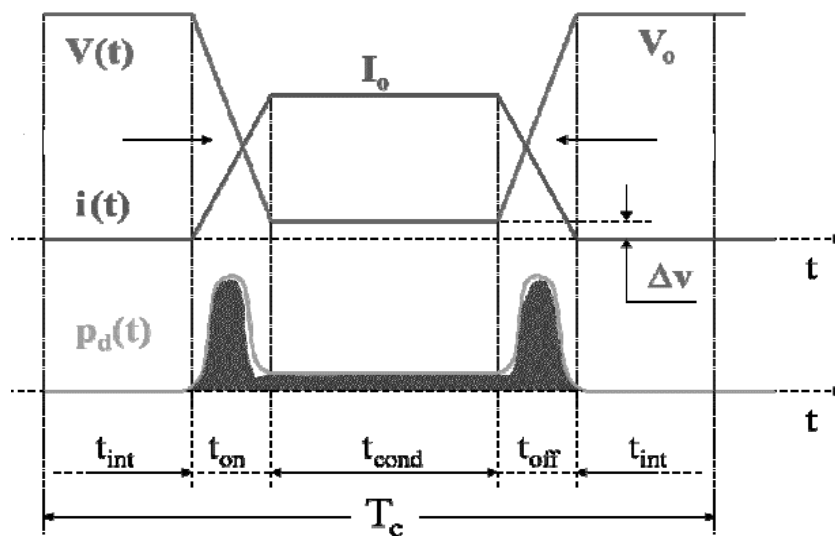
FIGURE 2.7: SWITCHING AND ON-STATE BEHAVIOUR APPROXIMATION.

The physical reason that avoids an instant switch is the presence of a stored charge. The diode exhibits the phenomena of reverse recovery current that delays its turn off. In Data sheets the parameter *Err* describes this event. The IGBTs have a more complex structure but the major contribution to the delay times is due to its bipolar behaviour. In Fig. 2.8 and 2.9 the evolution of the turn on and off is depicted in a more detailed way. The delay time is clearly visible. The first, in Fig. 2.8c, is the drain source voltage in the turn on that slowly enters in its hard saturation area before the drop voltage reaches its final (saturation) value.

14

Instead, in the turn off behaviour the drain current (Fig 2.9b) exhibits the typical tail current of the bipolar behaviour: chargers are stored in the drift region and before stopping the conduction these carriers must be removed.

Generally, also for IGBTs an approximation is made between the two different slopes of the curve due to the MOS/bipolar behaviour.

As in [3] they can be calculated with approximation of the waveform of the Voltage and the current but the value of the parasitic capacitors are needed to calculate the constant time of the RC circuit and therefore the delay times.

A faster approach is however suggested in [2] exploiting data sheets that provide different value of the energy consummated by the process. From this value the switching losses can be easily determined with a good accuracy. The sign of the current and the duty cycle chosen determine different configurations and different paths of the current therefore all the possibilities must be considered.
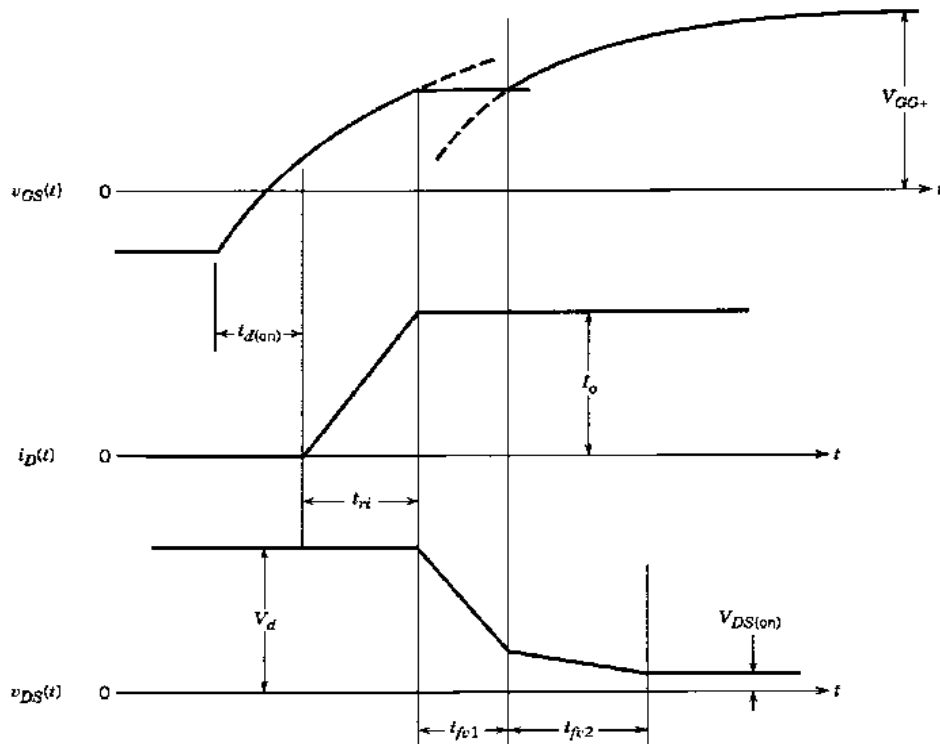
FIGURE 2.8: DETAILED EVOLUTION OF TURN-ON OF IGBT.
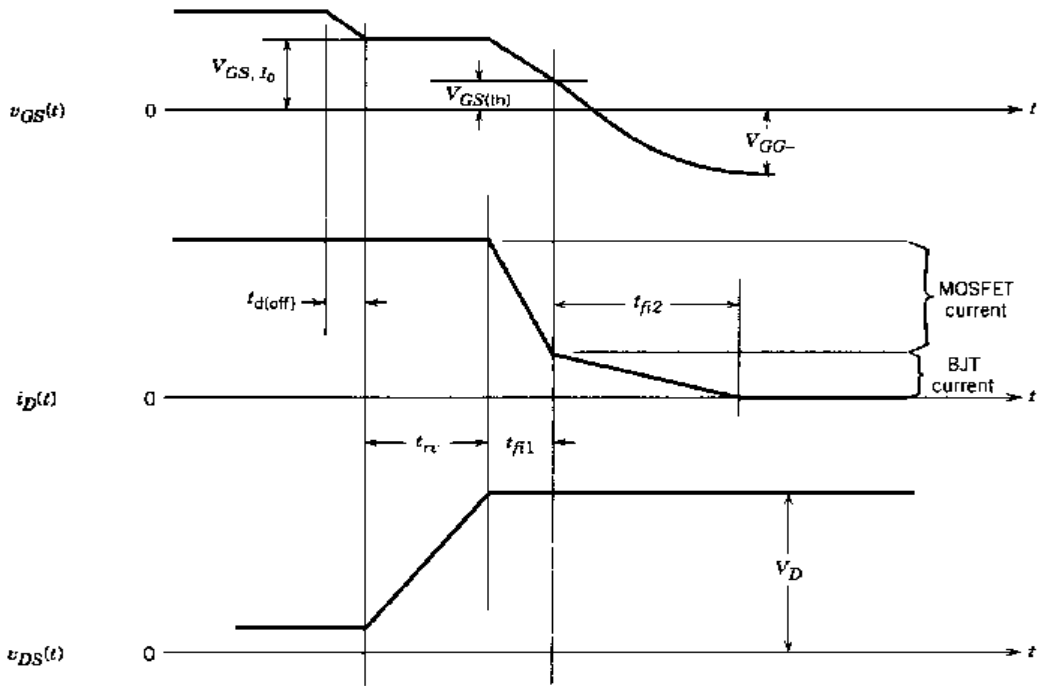
FIGURE 2.9: DETAILED TURN-OFF OF IGBT.

The chart of Energy/collector current, shown in Fig. 2.10, is taken from a datasheet of Infineon and it presents respectively the total, turn on and turn off losses including the reverse recovery of the anti-parallel diode.
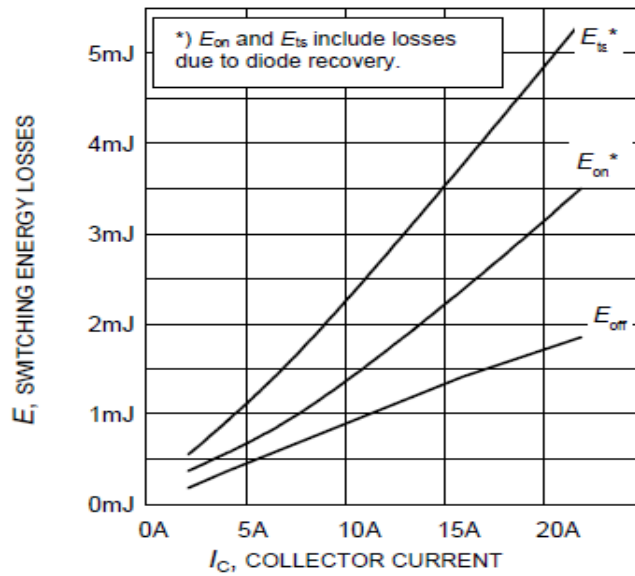
FIGURE 2.10: ENERGY LOSSES IN THE SWITCHING (ON, OFF, TOTAL) VS CURRENT.

16

Some points can be selected and fitted using a second order polynomial through the function Polyfit in Matlab as suggested in [2]. This permits to achieve an analytical expression of the dissipated energy function of the off-state voltage and of the collector current. A Simulink model and a code to simulate the duty cycle are also needed. After obtaining the proper function the total switching losses can be calculated knowing the level of the gate signal and the sign of the collector current. The calculation is iterated for every switching cycle using the turn on or the turn off losses for both the transistor and the diode. In [3] different suggestions are proposed. From the datasheet, also information about the condition test may be used, therefore the total energy losses are scaled with the change of Current, Voltage (*Vce*) and the value of the gate resistance as well as temperature.

$$E_{tot} = (E_{on} + E_{off}) \frac{V}{V_{test}} \frac{I_{ce}}{I_{test}}$$

(2.3)

2.2 Motor Losses

The type of motor analysed as previously mentioned is the PMSM motor. Obviously with different motors the type of losses and their relevance can remarkably change [4]. In chapter 3 the main advantages of this kind of motors will be presented. This chapter only deals with the description of the losses. In comparison with the other most common choices, as Induction Motors, the rotor copper losses are removed. However, magnet losses may be more significant in the high-speed region in comparison with Reluctance (SynRel) motors or Interior Permanent Magnet motors. The typical structure of a permanent magnet surface mounted motor is shown in Fig. 2.11.
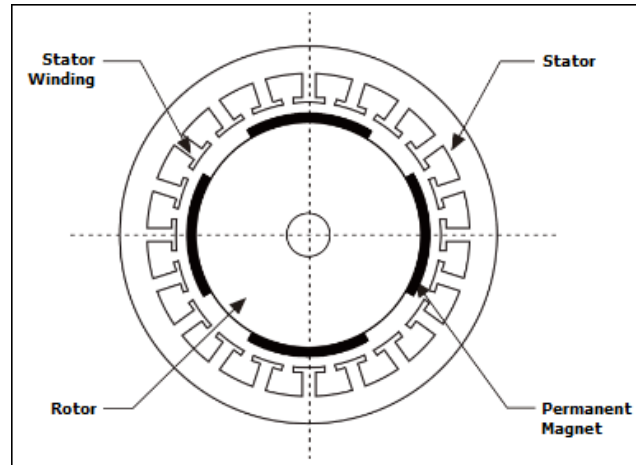
FIGURE 2.11: TYPICAL STRUCTURE OF PMSM MOTOR.

2.2.1 Copper Losses

The physical reason for the conduction losses is that none of the materials presents an infinite electrical conductivity at environmental temperature. The best conductors are typically metals and Copper or Aluminium are the most common ones thanks to their good mechanical properties, light weight, easy supply and almost stable price.

The metallic bond leaves some atoms free to circulate when an electrical voltage difference is applied. But, at the environmental temperature, the atoms already have their own vibration due to thermal (or kinetic) energy. While an electron is moving, it wastes part of its energy crushing with the other electrons around it. The resistance of metals increases with the temperature because the electrical mobility of electrons decreases due the increasing reticular vibration.

Moreover, as known, the skin effect can reduce the section involved in the conduction process therefore in the calculation of copper losses it is important to take into account the frequency of the current. In particular, for motors with a high number of poles it can be common to use high nominal frequency. This may reduce the skin depth to a value smaller than the radius of the conductor. The calculation for copper losses uses the Joule's formula for the power dissipation:

$$P_{cu} = \rho_{cu} Vol_{Cu} J^2 \qquad (2.4)$$
$$P_{cu} = 3 R_{ac}(\Theta) I_s^2$$

18

Different dimensions or different number of conductors can modify the joule losses. Some considerations about the influence of the design on the copper losses are presented in chapter 3.

As known, the stator resistance increases proportionally with the temperature. Equation (2.5) is widely used to take into account the increase of resistance but also to verify the maximum temperature reached by the windings in the nominal working point. α is 3.93e-3 [K^{-1}] for copper and 4.26e-3 [K^{-1}] for aluminum. The second one is easier to be applied for different ambient temperature and it is considered for copper.

$$R_{\theta avg} = R_{20°C}(1 + \alpha \Delta \theta) \qquad (2.5)$$

$$R_{\theta avg} = R_{20°C} \frac{(234.5 + \Delta \theta + T_{amb})}{(234.5 + 20)}$$

2.2.2 Iron and Magnet Losses

The issue about the iron losses is one of the historical problems of electrical engineering and research is still proposing improvements in efficient FEM calculation [5]. A high level of accuracy requires many resources and in Chapter 4 that deals with the calculation of the efficiency maps assumptions will be unavoidable. In [6] different methods are compared in accuracy and resources demand. To enhance the accuracy, the losses are divided between yoke and teeth because both contribute to hysteresis and eddy currents losses but the value of the flux density may be very different.

The phenomenon of ferromagnetism is linked to the magnetic permeability that describes the tendency of a material to be able to orient the magnetic momentum of its atoms in the same direction. Very few elements in the periodic table exhibit this quality. Inside a PMSM motor the phenomenon is exploited in different ways. The iron provides the proper path for the magnetic flux. It is necessary to have soft magnetic elements with a little cycle of hysteresis and little coercivity to avoid huge losses as seen in Fig. 2.12. While the permanent magnets, that is Neodymium Iron Boron, exhibit a very large cycle that provides a strong magnet with high saturation level, residual magnetism and coercivity (Hard ferromagnetic).
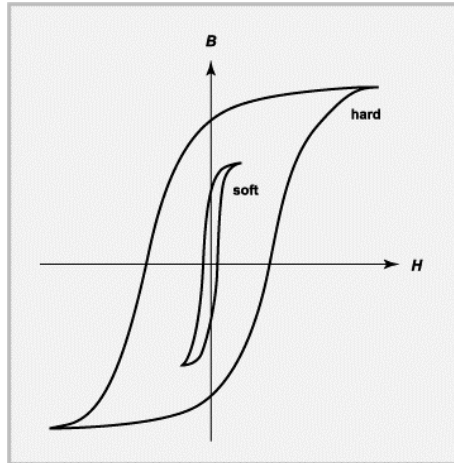
FIGURE 2.12: DIFFERENT HYSTERESI CYCLES FOR FERROMAGNETIC MATERIALS.

All the Iron losses are mainly due to the variability of the magnetic flux and they all depend on the frequency of the current that generates the magnetic field and therefore on the speed requested by the motor.

Commonly, the stator core losses are divided in hysteresis and eddy-currents losses. Someone adds extra current-losses, and investigations considering the increase with the harmonic content are presented in [8] [9]. The well-known Bertotti's equation gathers these 3 terms. Moreover, rotor eddy-current losses should be considered, too. They can be placed specifically on the magnets or on the rotor steel and depend on the shape of the magnets and on the harmonic content of the air gap field. All in all, the iron losses can be divided as:

- hysteresis Losses
- eddy-Currents losses
- additional eddy-currents losses
- magnet and rotor losses

Concerning the stator core losses that are the sum of the first 3 terms of the list, it is worth to point out [7] that the division of the losses represents a difference in the scale of the magnetization. Hysteresis losses describe the localized jump of small domain walls due to the Barkhausen effect. Classical eddy currents are linked to a uniform change of magnetization throughout the sample and their path strongly depends on the dimensions and the shape. Finally, the scale of the additional eddy current losses is the domain walls and they don't depend so much on the shape of the sample. From this consideration, the initial approach to have a reliable model is to divide the kind of losses on their dependence on the frequency of the varying magnetic field and therefore:

$$\frac{P}{f} = C_{hy} + C_{ed}f + C_{add}\sqrt{f} \qquad (2.6)$$

Hysteresis (literally "delay" in the ancient Greek) means that during the magnetization cycle of a magnet the path followed changes during the process and it maintains a memory inside. This brings to the fact that the energy given as input (current that produces the magnetic field H) is not followed by the air gap field B that is the output we desired to be achieved as depicted in Fig. 2.13. Part of the energy is dissipated in heat inside the material, in an entire cycle these losses are exactly the area of the hysteresis cycle. Hysteresis losses depend on the magnetic characteristic of the ferromagnetic material.
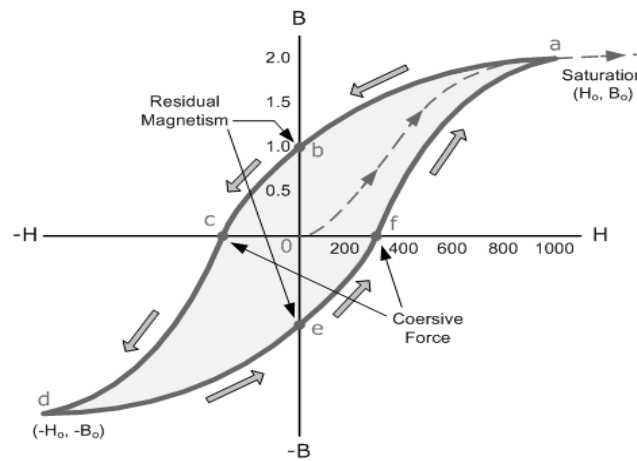
FIGURE 2.13: TYPICAL HYSTERESIS CYCLE FOR A MAGNET.

Hysteresis losses don't depend on the thickness of the material. To calculate hysteresis losses Steinmetz equation is still widely used:

$$P_{hy} = K_i f B_M^{\alpha} \qquad (2.7)$$

In (2.7) α is a coefficient found by Steinmetz and it can vary from 1.6 to 2.2. It depends on the level of the induction field that is mainly calculated in 1 or 1.5 T. While the coefficient *Ki* depends on the material, on the impurity and the geometrical structure of the stator. However, from the Fig. 2.14 it is clearly visible that each different point of the domain exhibits different value of the flux density due to the geometrical shape of the stator. Moreover, the produced magnetic field is far from a perfect sinusoidal waveform.

A)
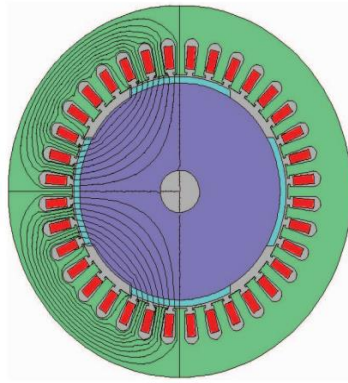
B)
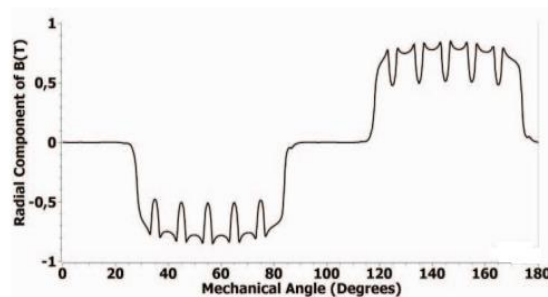
FIGURE 2.14: IN A) FLUX LINE MAP IN B) FLUX DENSITY DISTRIBUTION ALONG THE AIR GAP.

Therefore, the use of analytical formulas brings many assumptions that are often not true. Assuming the maximum value of the induced magnetic field for all the points of the stator is not correct and it may bring to errors [8]. Mainly for this reason, for the calculation of all the different iron losses a FEM analysis at least 2D is required.

Regarding the second term of (2.6), to avoid classical eddy-currents it is well known that the iron is laminated and any kind of electrical machine is assembled with many thick layers of iron, insulated between each other (Fig. 2.15). Moreover, the market offers mainly alloy of Silicon-Iron or Silicon-Steel to decrease the conductivity of Iron. The percentage of Silicon cannot be over 5/6% to avoid losing mechanical strength.

Eddy currents are the natural consequence of Faraday's Law (2.8).

When a variable magnetic field is applied, in the perpendicular direction an EMF is created. Eddy currents circulate in closed loop on parallel planes.
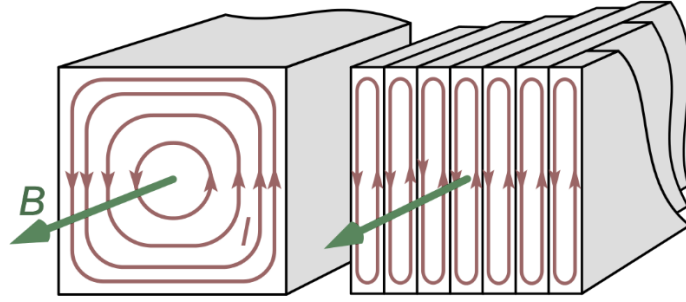
FIGURE 2.15: BENEFIT OF A LAMINATED CORE AGAINST EDDY CURRENTS.

$$\nabla \times \bar{E} = -\frac{\partial \bar{B}}{\partial t}$$

(2.8)

A common expression for stator eddy currents is

$$P_{ed} = K_{ed} f^2 B_m^2$$

(2.9)

This analytical expression requires coefficients that strongly depend on the material and on the geometry of the magnetic sheet. Even though these values can be derived from the data sheets the accuracy achievable with this approach is quite poor. Furthermore, in the data sheets losses density is present for each different shape and dimensions. To have an approximate but reasonable value of the losses they offer a faster approach.

To increase the accuracy FEM analysis are needed to consider the different value of the varying maximum magnetic field in the different part of the stator. Moreover, other information about the material, the geometry and the air gap field are required. With this approach the Bertotti's equation is often used in the calculation.

$$P_{fe} = K_h f B_m^\alpha + \frac{\sigma d^2}{12} \frac{dB}{dt}^2 + K_e \frac{dB}{dt}^{1.5}$$

(2.10)

The first term is for the hysteresis losses while the second is for the eddy currents losses. The last one is the excess eddy currents losses [7]. Another important consideration is that for permanent magnet motor the waveform of the air gap field is far from sinusoidal and so to enhance the accuracy a precise description of that is needed.

While the iron losses of the stator are a secular topic of electrical machine, the theme about magnet losses is quite new in comparison but it grew in importance with the diffusion of pm motors. For the thermal constraints of the magnets this topic was investigated by many authors in order to predict the amount of losses produced and to avoid reaching the demagnetization temperature of the latter [9], [10]. The main contribution to magnet and rotor losses are eddy currents, hysteresis losses are generally smaller.

The physic principle is similar to the stator eddy-currents. But concerning the magnets the particular reasons can be individuated in: the lack of uniformity of the stator and the presence of harmonic content in the air gap field. Since the stator has often an open slot design, the magnets encounter alternatively part of iron and part of air that have very different permeance. This geometry causes additional harmonic as explained in [11]. Moreover, nowadays the problem is more and more important due to the use of power converters that can provide a high harmonic content in the currents that produce the magnetic field. As mentioned this kind of losses becomes significant in the PMSM machine and so it cannot be neglected [9]. The eddy currents path on the magnet is shown in Fig. 2.16.

The magnet and rotor losses are due to the presence of different harmonic contents in the magnetomotive force. In [11] it is explained that there are 3 different sources of harmonic content for the air gap field. This consideration is important also for chapter 3 in which the design, and the quality of the torque, will be discussed:

- space harmonics: armature windings and permanent magnet
- time harmonics: ripple of the current generated by the inverter
- slot permeance harmonics: iron and air alternate in open slot design

When the rotor runs, the magnet faces alternatively short air gap length areas under the iron and long air gap length under the slot. This causes an air gap field with a strong harmonic content that induces eddy currents in the magnet. The common adoption of not over-lapping concentrated windings increases the space harmonics [13], open slot design is very popular also and so slot permeance harmonics are significant. Moreover, the broad use of power converters frequency arises the problem of time harmonics.
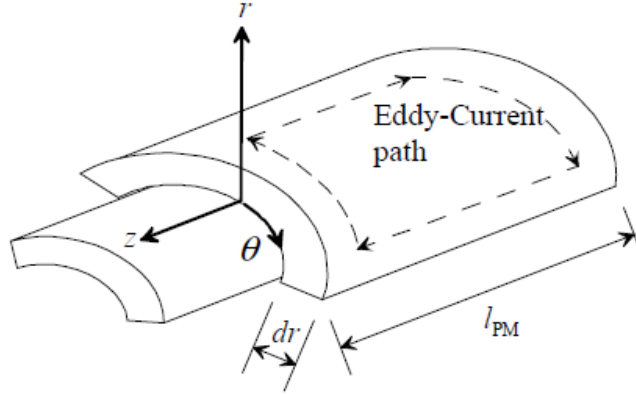
FIGURE 2.16: EDDY CURRENTS ON THE PM.

The analytical expression is very complicated and it can be found in [10] and [12]. The stator windings are considered as an equivalent current sheet and the linear current density. The issue is that the current density of the rotor needs the solution of the magnetic vector potential that is often too complicated.

In [12] the losses are summarized with:

$$P \sim l_s \sum_j \int \frac{J_e^2}{\sigma} dS$$

(2.13)

Where J_e is the current density of the eddy currents on the magnets. Others [11] derive the expression of the current density from Maxwell equation after the FEM analysis for the varying air gap field source of the voltage that produces this current.

Often the indirect method is used to calculate total iron losses. With different expedients, it is possible to measure losses in peculiar working points in which they should be only joule losses and mechanical. Because they can be estimated with a good accuracy without many efforts iron losses can be derived as the difference between total losses measured and the sum of joule and mechanical losses. The limit is that the test on the benchmark takes time and the evolution is very slow for the high thermal constant of the motor.

25

2.2.3 Mechanical Losses

The mechanical losses can be divided in bearing losses and windage losses. Bearing losses depend on the type of bearing, its lubricant but also rotor speed and load. An analytical expression can be found in [14]:

$$P_B = 0.5\omega_m K_B F D_B$$

(2.14)

Where ω_m is the speed of the rotor, k_B is a constant loss for the type of bearing, D_B is the diameter and F is the force acting on it. This latter can be derived from the configuration. Losses on the bearing are mainly due to the friction losses and a part of independent load losses in the lubricant.

Windage losses instead occur when friction is created between a rotating part and air. Unlike frictional losses they increase non-linearly with the force applied. The following expression can be used to calculate them:

$$P_w = 0.0315\omega_m^3 \pi K_{ct} K_r \rho_{air} D_r^4 l_r$$

(2.15)

Where D_r and l_r are the diameter and length of the rotor. Kr is a coefficient for the roughness. Kct is the torque coefficient and it can be derived separately: the Reynolds number has to be calculated to tell which kind of motion is occurring. Equations are found in [14]:

$$N_{Re} = \frac{\rho_{air}\omega_m D_r l_{ag}}{2\mu_{vis(air)}}$$

(2.16)

$$K_{ct} = 2\frac{(2l_{ag}/D_r)^{0.3}}{N_{Re}^{0.6}}$$

(2.17)

Where μ_{vis} is the dynamical viscosity of the air at the temperature considered.

2.3 Gearbox Losses

The losses of the gearbox are a complicated issue, moreover it was not deeply investigated during the academic period because the field of study of the author is mainly electrical. Nevertheless, it is a component almost always present in the mechatronic chain and in many different applications. More recent technologies as direct drive try to avoid the use of gearboxes but this kind of application has a limited diffusion. There are many different types of industrial gearbox but the advantages of the choice of the planetary ones are remarkable. They may achieve better torsional stiffness and lower backlash than any other. However, the model of the losses becomes even more difficult for the increased significance of the independent load losses [17].

For this reason, this issue was not investigated in its singular details as CFD analysis. In chapter 4 a way to derive the efficiency maps is reported. Despite the complexity and the other difficulties just mentioned, efficiency evaluation are needed also on the gearboxes. Thus, the first step is to understand which losses are present.

Without the support of Doctor Franco Concli I would not have been able to obtain the efficiency map and to understand how they are calculated. Luckily, he already deeply analyzed the problem by a theoretical point of view [16].

In Fig. 2.17 the structure of a planetary gearbox is shown; a two-phase fluid of lubricant and air is present inside the case. The lubricant is continuously moved by the motion of the planets, its temperature and viscosity change and the two phases may mix up creating foam. The losses of a planetary gearbox can be divided in load dependent and load independent as in Fig. 2.17. No load (or independent load) losses occur even without power transmission while load dependent losses happen in the contact between the transmitting components. Moreover, they can be linked also to the different part of the gearboxes: meshing (or gears), bearing, seals and auxiliaries. The no load losses of gears and bearing are the losses due to the lubricant. It is worth to notice that even though they are usually classified load independent, because they strongly depend on the temperature, and a change of the load may change them. Fig. 2.18 shows a classification of the main gearbox losses dividing them on their dependence on the load.
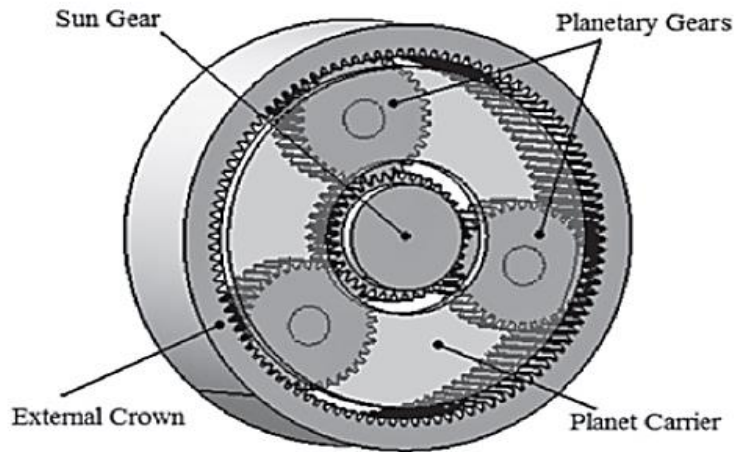
FIGURE 2.17: STRUCTURE OF A PLANETARY GEARBOX.
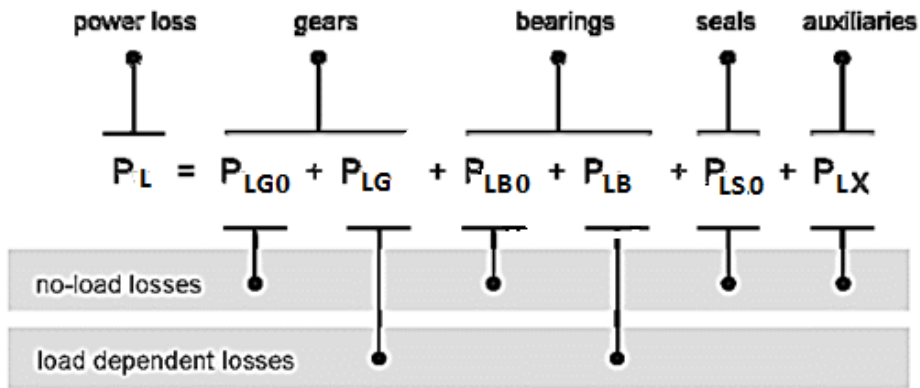
FIGURE 2.18: CLASSIFICATION OF GEARBOX LOSSES [15].

For each of these losses a model is needed. All the losses are the results of complicated phenomena but analytical formulas that can calculate the losses only with the data from geometry and boundary conditions exist. In the planetary gearbox [16] the no load gears losses include also the fluid dynamics ones. Due to the structure and to the presence of the planet carrier [17] these losses arise in importance. The independent load losses are treated in a different way and rely on CFD analysis. They are the sum of churning, squeezing and windage losses. Basically, they are linked to the losses due to fluid dynamics reason of the two-phases fluid oil and air that lubricate the contact between the gears.

2.3.1 Meshing Losses

Load dependent

These kinds of losses are mainly due to the friction between the gears, in fact during the power transmission the motion is affected by sliding and rolling of the gears. Thus, they are proportional to the amount of torque transmitted. The most common formula to calculate them is [15]

$$P_{LG=}F_R v_{rel} = F_N \mu_m v_g$$

(2.18)

Where F_R is the friction force, F_N is the normal force, μ_m is the friction coefficient achievable from a formula in [16] (need to notice that is function of the dynamical viscosity of the lubricant) and finally V_g is the sliding velocity.

Independent load losses

Specifically, for this kind of gearbox the churning and windage losses acquire particular significance because of the translational motion of the planets and the presence of the planet carrier [17]. The CFD analysis use the geometry of each different combination of teeth and ratio and calculate the field of pressure and speed of the two-phases fluid. The motion of the oil is complicated by viscosity and density changing with the temperature, moreover the motion of the planetary forces the oil to move and to mix with air. The oil tends to occupy particular areas, and to mix with air in others, to be squeezed near the contact of the gears while it is changing its properties due the changing of the temperature.
Churning losses are linked with the motion of the two-phases fluid and the unavoidable churning between itself and the planet-carrier of the planets. Furthermore, the contribution is divided between the resistant torque (viscous) due to the field of speed (2.19) and the inertial one due to pressure (2.20). Once the CFD analysis has obtained the velocity and pressure field they can be postprocessed.

The used formulas are generally (2.19) and (2.20) for each finite volume of the mesh grid [16]:

29

$$T_{LG0\tau=} \sum v_\iota \rho_{mix\iota} \frac{\partial U_i}{\partial x_i} A_i r_i \qquad (2.19)$$

$$T_{LG0p=} \sum p_\iota A_i r_i \qquad (2.20)$$

Where ν is the viscosity, ρ the density, U is the velocity, A is the area of the i-th cell, r is the radial distance of the i-th cell from the axis and p is the pressure field. The procedure is extended in case of a major number of stages for high transmission ratio repeating the simulation with the intermediate input (torque and speed) occurring at the second stage.

2.3.2 Bearing losses

As for the gear losses, they can be divided in load dependent and no load. The load dependent losses are due to the sliding between elements of the bearings, e.g. rings and rolling elements.

Independent load losses instead depend on the lubricant and on the geometry. They can be calculated knowing the properties of the oil and its interaction during the sliding of the rings. Bearing manufacturers investigated deeply the issue and propose analytical coefficient to derive bearing losses. An example of estimation of bearing load dependent losses [18]:

$$P_{LB} = 1,05 \times 10^{-4} \, M \, n \qquad (2.21)$$

Where M is the total frictional moment, n is the speed.

2.3.3 Seal Losses

Seal losses are not dependent on the load. They are basically due to the sliding between the shaft and the seals themselves. Several reliable estimation methods are present in literature. Here (2.22) expresses a common way to calculate seal losses.

$$P_{vD=} \lambda d^2 \frac{n}{1000} \qquad (2.22)$$

λ is a coefficient that depends on the geometry and it describes the operating condition and temperature. d is the diameter and n is the rotational speed [16]

Eventually, it is worthy to notice that all these kinds of losses depend strongly on the temperature. Therefore, the model works only if the temperature in which the gearbox is working is known.

The amount of losses changes the heat dissipated and therefore the temperature. It is clear then that an iterative procedure is needed in the model.

As known, the viscosity of the lubricant decreases with higher temperature so, the friction coefficients and the load independent losses as well tend to decrease with an increase of the temperature along with the decrease of the viscosity and density of the lubricant. In fact, total gearbox losses exhibit a decrease with the increase of the temperature. The iterative procedure can reach an equilibrium point between the heat power dissipated (proportional to the temperature) and the losses that decrease with the temperature [16].

References Chapter 2

[1] Mohan N., Undeland T., Robbins W. - Power Electronics (II edition), John Wiley&Sons Inc.

[2] J. Pou, D. Osorno, J. Zaragoza, S. Ceballos, and C. Jaen, "Power Losses Calculation Methodology to Evaluate Inverter Efficiency in Electrical Vehicles," *IEEE Trans. Power Electron.*, pp. 404–409, 2011.

[3] P. Sanjeev, "Analysis of Conduction and Switching losses in two level inverter for low power applications," *2013 Annu. IEEE INDICON*, 2013.

[4] L. Song, "Efficiency Map Calculation for Surface-mounted Permanent-magnet In-wheel Motor Based on Design Parameters and Control Strategy," *ITEC Asia-Pacific*, no. 2, pp. 1–6, 2014.

[5] G. Almandoz, G. Ugalde, J. Poza, and A. J. Escalada, "to Finite Element Software for Design and Analysis of Electrical Machines," *INTECH*, 2012.

[6] Zijian Li (2012). Politecnico di Torino, Doctoral Thesis. Fractional slot concentrated winding surface-mounted permanent magnet motor design and analysis for in-wheel application.

[7] W. Roshen, "Iron Loss Model for Permanent-Magnet Synchronous Motors," *IEEE Trans. Magn.*, vol. 43, no. 8, pp. 3428–3434, 2007.

[8] Wu, X., Zhang, C., Wang, Y., Gang, D., Zhu, W., & Pan, L. (n.d.). The Electromagnetic Losses Analysis of Surface-mounted Brushless AC PM machine Driven by PWM.

[9] N. Zhao and W. Liu, "Loss Calculation and Thermal Analysis of Surface-Mounted PM Motor and Interior PM Motor," *IEEE Trans. Magn.*, vol. 51, no. 11, pp. 2–5, 2015.

[10] K. Atallah, D. Howe, P. H. Mellor, and D. A. Stone, "Rotor Loss in Permanent-Magnet Brushless AC Machines," *IEEE Trans. Ind. Appl.*, vol. 36, no. 6, pp. 1612–1618, 2000.

[11] J. Alexandrova, H. Jussila, and J. Nerg, "Comparison Between Models for Eddy-Current Loss Calculations in Rotor Surface-Mounted Permanent Magnets," *XIX Int. Conf. Electr. Mach. 2010, Rome*, 2010.

[12] S. Steentjes, S. Boehmer, and K. Hameyer, "Permanent Magnet Eddy-Current Losses in 2-D FEM Simulations of Electrical Machines," *IEEE Trans. Magn.*, vol. 51, no. 3, pp. 3–6, 2015.

[13] Dutta R., Chong L., Rahamn F, "Analysis and experimental verification of losses in a concentrated wound interior permanent magnet machine." Progress In Electromagnetics Research B, Vol. 48, 221–248, 2013. (2013), *48*(November 2012), 221–248.

[14] D. K. Athanasopoulos, V. I. Kastros, and J. C. Kappatou, "Electromagnetic Analysis of a PMSM with Different Rotor Topologies," *IEEE*, vol. 1, 2016.

[15] Hohn, B. Michaelis, K., Hinterstoißer, M. "Optimization of gearbox efficiency."

Gomabn (2009) Volume: 48, Issue: 4, Pages: 462-480

[16] F. Concli, "Thermal and efficiency characterization of a low-backlash planetary gearbox: An integrated numerical-analytical prediction model and its experimental validation".

[17] Conli F. Gorla C. "Le perdite per sbattimento in un riduttore epicicloidale." Organi di trasmissione, (January 2012).

[18] SKF, Catalogo generale, 6000 IT, SKF, 2006.

Chapter 3

STATE OF ART of EFFICIENCY in SERVO DRIVES

This chapter presents the state of art to reduce the losses described in chapter 2 during the design process and in the control. To design an interesting product for customers it is obvious that increasing the efficiency cannot be the only goal. Thus, the discussion does not deal only with the efficiency problem but it mentions also the most common strategies used to obtain the best performance of the components.

As explained in the introduction, the field of application chosen is the Servo control. Due to high dynamic demand of Servo application, very compact and stiff components are needed to fulfil the requirements of the load. The highest power density and a very low inertia are therefore needed in order to develop an attractive solution and to satisfy the requirements. An investigation on the state of art of components is hereby presented focusing on the improvements more popular in the industry. The investigation is interested in benefit provided to these aspects:

- efficiency
- power density
- maximum performance (static and dynamic)
- quality of the transmission: both electrical and mechanical power.
- reliability

Typically, engineers look at possible improvements from three different approaches:

- materials
- structure, dimensions or topology
- control

Materials are always the key point but often the attractive property does not meet with all the other properties needed as cost, a trustful and stable supply, workability and transportability. Science will never stop to present new materials that will improve efficiency of all the 3 components. In power electronics, more discussion will be presented. The power electronics are a quite new field of research in comparison with electrical machine or speed reducer therefore many innovations are continuously presented. For

instance, the emerging wide band gap materials (WBG), as Silicon Carbide (SiC) or Gallium Nitride (GaN) are slowly spreading in the market. In other fields the materials are quite consolidated and the discussion is mainly focused on the last two approaches. The process of production is not investigated even though it plays a critical role as for example in the sintering of the magnets and of iron powder.

Specifically, about the electric motor, Servo applications require firstly high torque density and high acceleration capability but also the quality of the torque produced is fundamental and many strategies are developed to increase it in the design procedure. Different kinds of structure of the motor may be compared but AC Synchronous PM motor guarantees the best performance. An important mention is then, the so-called Direct Drives, a peculiar structure of the motor permits to meet the request of some load eliminating the speed reducer but it still has a marginal diffusion.

Regarding the control, the method known as FOC (field oriented control) provides the complete exploitation of the machine with high dynamic performance (Maximum Torque per Ampere control). An actual topic is instead the Sensorless control that does not need an encoder and it is attractive wherever maintenance and reliability play an important role.

For the needs of this field of application the planetary gearboxes are the speed reducer chosen thanks to their high-density power transmission. Moreover, the efficiency of these types is particularly high and higher transmission ratios are achievable in a single stage (up to 10-12). In this field of application often a high torsional stiffness is required along with a very low back-lash angle (positioning control, motion control). As mentioned this argument exceeds from the field of the study of the author therefore it is not further developed.

3.1 Inverter

The increase of the demanding performance of the converter is pushing the state of art forward. Desired specific requirements can be summed up in:

- high power density transmission (linked to devices)
- minimization of current ripple and of the losses

The most desirable characteristics of the devices that can influence the performance are:

- low internal resistance
- large breakdown voltage
- heat dissipation capability

- fast turn-on and turn-off

Final evaluations of the performance are current ripple, power factor and efficiency. As known it is generally necessary a tradeoff. In fact the ripple can be decreased with high switching frequency but losses increase.

The analysis is limited to low voltage application because it is the most common source for Servo drives: 600V on the DC link is generally the value considered.

Nowadays in the industrial world IGBTs are the most common devices thanks to their peculiar characteristics. This component in fact combines the conduction benefit of a low on state resistance with a fast switching capability.

3.1.1 Materials for Power Electronics

Emerging WBG devices as Gallium Nitride (GaN) and Silicon Carbide (SiC) will increase the breakdown voltages of a single device and increase the density of current capability. Moreover as depicted in Fig. 3.1, SiC has a better thermal conductivity and it achieves a better power dissipation that permits higher performance. The commercial market of this
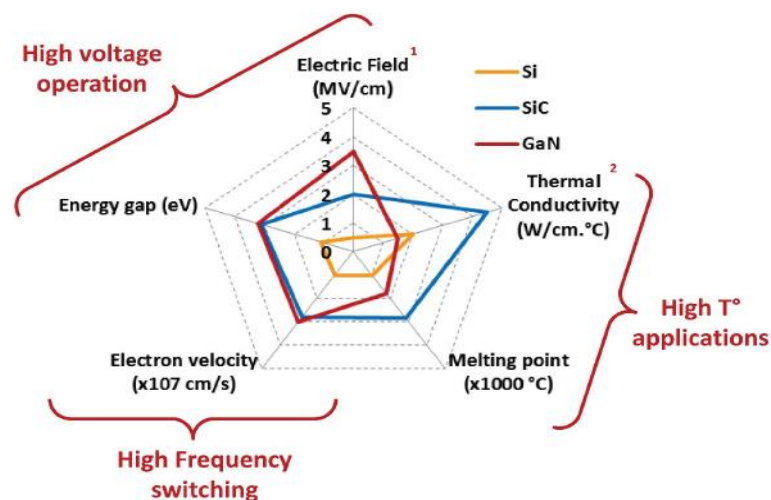
FIGURE 3.1: SEVERAL BENEFITS OF THE WIDE BAND GAP MATERIALS IN COMPARISON WITH SILICON.

devices is growing but, like any new technology, it needs time to ensure its own reliability to the customers and to increase the number of devices produced in order to decrease the

initial cost. Nevertheless, a broad diffusion of these emerging devices will increase the efficiency and the performance of the inverter.

Silicon Carbide has about 10 times the critical breakdown voltage of the Silicon, therefore the width of the drift region is 10 times thicker. This allows a large reduction in the internal resistance of the component and so the conductivity losses are decreased as shown in Fig. 3.2.
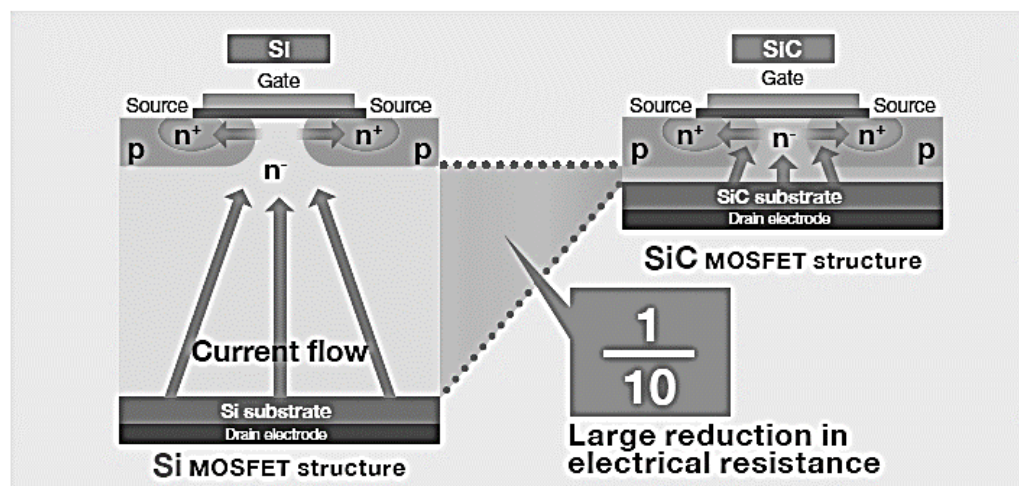
FIGURE 3.2: REDUCTION OF THE WIDTH OF DRIFT REGION IN SiC DEVICES.

The heat dissipation is increased of about 3 times thanks to the higher thermal conductivity of Silicon Carbide. Furthermore, the higher wide band gap allows higher temperature operations because it prevents any leakage currents (they may create abnormal operation in traditional silicon devices). Finally, along with the reduction of the losses they allow also shorter delay times for the absence of stored charge. Thus, higher switching frequency can be used and an improvement in the current ripple might be achieved.

The possibility of increasing the breakdown voltage of a single device seems a very attractive characteristic for medium voltage application. By the way in low voltage applications as well the SiC devices provide all the described benefits. Nowadays diodes, Mosfet and IGBTs for low voltage applications [1], [3] in Silicon Carbide are the most efficient choice.

3.1.2 Topology for Power electronics

The second degree of improvement is the topology of the converter that means how the devices are connected between each other. To improve the performance, multilevel converters are chosen in several applications for their peculiar benefits. This technology is well established in medium voltage application but also in low voltage it provides better performance. The Fig. 3.3 shows the topology of a 3-level converter where it can be seen the division of the DC link voltage in a higher number of devices than for the conventional 2 level converters. To increase the breakdown voltage, multilevel converters use a series of "level". This structure arises a complicated problem as the voltage sharing and it needs complicated PWM strategies [6] but it permits many advantages in the current ripple and in the efficiency because a lower switching frequency is required. The number of level may be increased furthermore but for low voltage applications is not so convenient and hereby only the 3 level Neutral Point Clamped Converter is mentioned. Other popular possibilities use different topology as Cascaded multilevel inverter or Flying capacitor that don't have the issue about the voltage sharing.

The main advantages provided in comparison with the 2 level inverters are:

- a higher output voltage
- lower switching frequency
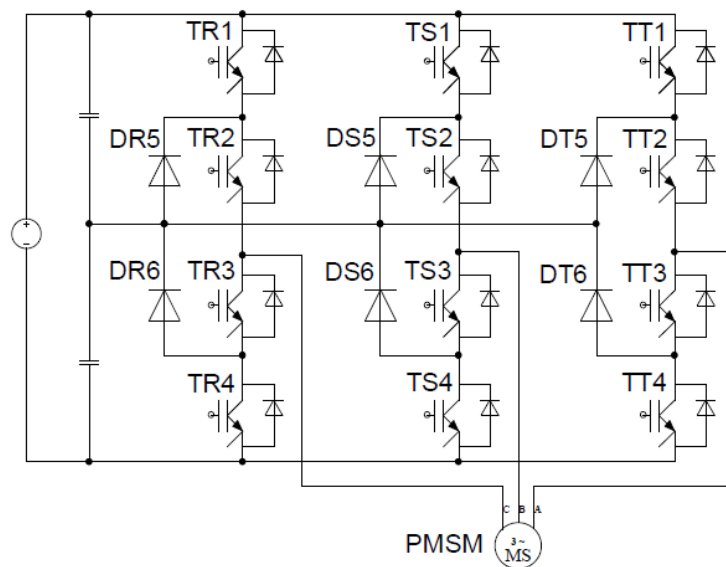
FIGURE 3.3: GENERAL TOPOLOGY OF A 3 LEVEL INVERTER [4].

Mecke in [4] specifically analyzes the case of a NPC with a PMSM motor. The quality of the current and voltage with this type of motor is particularly important. Firstly, the low value of the stator inductance makes the motor sensitive to high level of THD that would increase significantly harmonic active power losses. Secondly, as explained later in the chapter, the quality of the torque produced may depend on the current ripple of the converter. The adoption of multilevel converters reduces the harmonic content in comparison with 2 level inverters [4]. Furthermore, the efficiency is increased: the use of devices with a lower blocking voltage allows the adoption of devices with smaller size (600V IGBTs instead of a 1200V IGBTs) and thus a better optimization. Total losses are decreased in comparison with 2 level inverters [4].

3.1.3 Control and modulation techniques

Regarding the switching losses several strategies are found in literature in order to better exploit the converter. The most common modulation technique in industry is the Space Vector Modulation (or SVPWM) as in Fig. 3.4. It provides the maximum output voltage with low THD and it is suitable for microprocessor implementation.

In order to decrease the switching losses different PWM strategies are developed [7], [8], [9]. In all the modulation techniques for an inverter a tradeoff between the quality of the output and the amount of switching losses occurs. With a high value of the switching frequency the ripple of the current can be almost removed but with an exaggerate amount of losses. It is worth to mention that Zero Switching inverter was developed to avoid drastically switching losses and therefore they make possible the use of very high switching frequency. This advantage is quite desirable because it decreases the size of the transformer whereas a galvanic insulation is essential. However, it seemed unlikely that this technology could phase out the traditional Hard switching therefore only those latter are discussed.

Because these losses depend on the number of switching that we ask to the converter, peculiar PWM strategies as Discontinuous PWM permit to drastically decrease the number of switching.

The DPWM proposes a different pattern of the switches in comparison with the SVPWM to reduce the number of commutations. The SVPWM produces the required voltage using two active vectors and one or two zero vectors. Fig. 3.4 shows how to generate a general

voltage reference. Once the sector is individuated, using the two adjacent active vectors and the zero vectors, any voltage reference can be built in magnitude and phase angle.
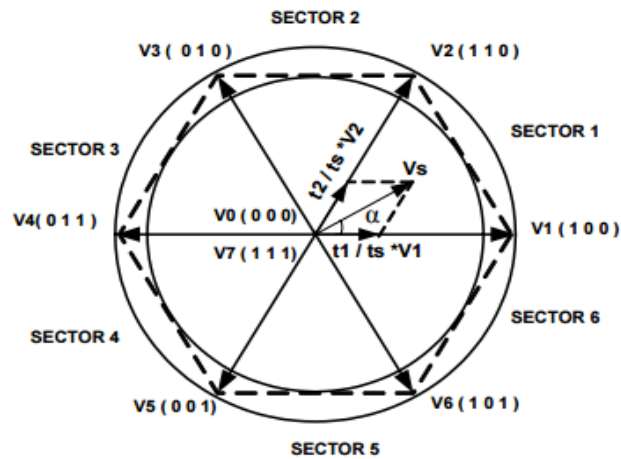
FIGURE 3.4: SPACE VECTOR OPERATION.

The zero vectors are needed during the dwell time whenever the magnitude of the output required is smaller than the maximum value. The pattern of the switching should be symmetrical to increase the quality of the output as it can be seen in Fig. 3.5; thus, the zero vectors are commonly applied at the beginning, in the middle and at the end of the cycle.
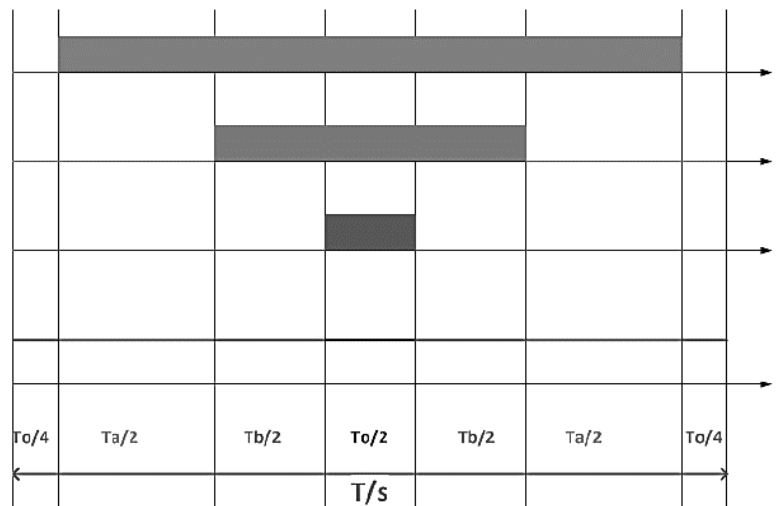
FIGURE 3.5: TRADITIONAL SVPWM SYMMETRICAL PATTERN WITH BOTH ZERO VECTORS.

To better understand a parameter called modulator ratio is defined as [7]:

$$\mu = \frac{T_7}{T_0 + T_7} \qquad (3.1)$$

T_7 is the time in which the vector V_7 (1,1,1) is applied while T_0 when V_0 (0,0,0) is applied. This ratio describes how the dwell time is divided between the upper and lower devices. SVPWM uses μ=0.5, in fact in each switching cycle the two zero vectors are used for the same amount of time. This choice minimizes the current ripple [7]. Traditional SVPWM has moreover the purpose of equalizing the thermal stress between the upper and lower devices. Discontinuous PWM chooses instead to use only one zero vector for a certain time: μ=0 or μ=1. In DPWM the number of switching would decrease from 6 to 4 in each cycle. In fact, instead of using a zero vector in the middle of the cycle as in Fig 3.5 it uses only at the beginning and at the end of the cycle. If μ=0 one of the leg has the lower device more stressed, vice versa if μ=1 one of the leg conducts only on the upper device.

In Fig. 3.6 and 3.7 DPWM1 and DPWM3 are shown respectively. They change the zero vectors every 60° degrees of the period of the reference but with different phase angle. V_a^* is the sinusoidal reference, V_{a0}^* is the generated signal and V_h is the zero-voltage signal.
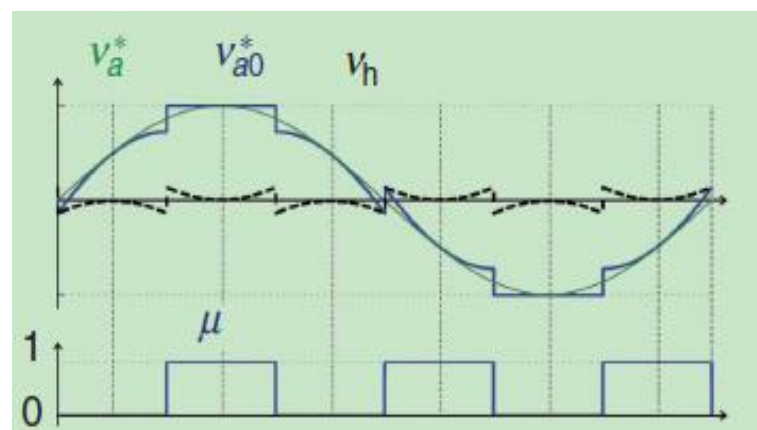
FIGURE 3.6: DPWM1 OPERATION AND MODULATION RATIO [7].
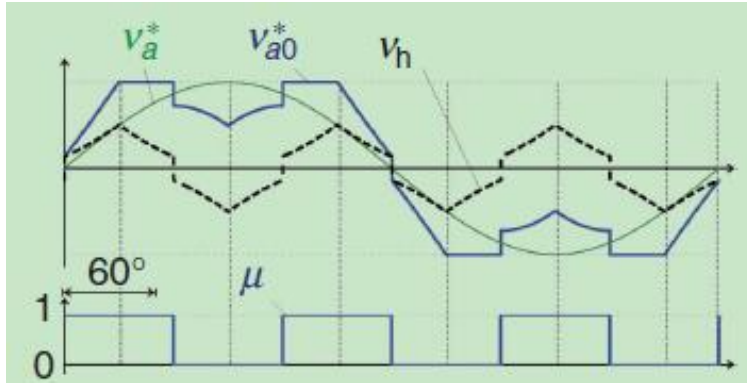
FIGURE 3.7: DPWM3 OPERATION AND MODULATION RATIO.

While in Fig. 3.6 the modulation ratio changes in the middle of the period, DPWM3 exhibits a lag factor of 60° degrees. There are many different possibilities in the choice of the phase shift.

The switching losses are decreased with the lower number of switching but the higher harmonic content of the current generates more conduction losses. Continuous modulations are superior in term of harmonic distortion as it is clear from the non-sinusoidal profile of the Fig. 3.6 and Fig. 3.7. However, with the same switching time, in high modulation range discontinues modulations provide less harmonic losses [10]. This may bring to a switch between the two modulations according to the specific load situation. Different choices of the phase shift of the discontinuous operation can be optimized with the phase angle of the load.

3.2 Electrical Motor

In servo drives applications, the main requirements for the motor are: high acceleration capability, high torque density and a constant, stable and smooth torque. For several reasons the permanent magnet motor are the type of motor that meet all these needs. Thanks to the presence of the magnets that provide the excitation field, the rotor copper losses are eliminated. Nevertheless, the size of the rotor is reduced and so the inertia. Then, the main losses are produced on the stator and they are easier to be dissipated, therefore higher torque density and torque/ampere ratio can be achieved in comparison to other machines. The drawback of the use of the magnets are the high price, the risk of a demagnetization with high temperature or high current and significant rotor losses at high speed. The most common characteristics in industry are considered so the machine has a radial-flux and inner rotor geometry. Fig. 3.8 shows a common structure of PMSM motor.

FIGURE 3.8: PMSM MOTOR.

The last choice regards the geometry of the magnetic circuit and therefore the position of the magnets. They can be inserted like in Fig. 3.9(a) on the surface or buried inside the rotor as in Fig. 3.9(b).
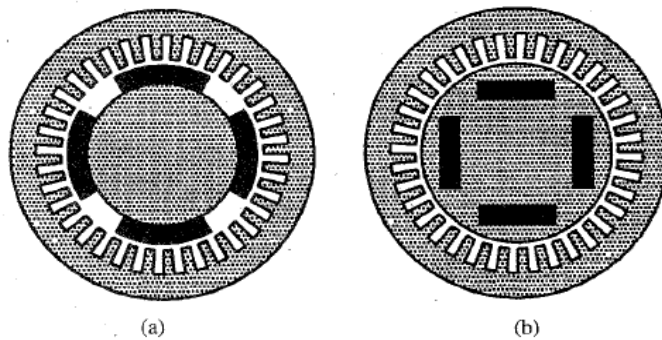
FIGURE 3.9: PERMANENT MAGNET SURFACE MOUNTED (a) INTERIOR PERMANENT MAGNET (b).

The Permanent Magnet Surface Mounted (PMSM) motors are isotropic (not salient-pole) and they are the most common type in automation. Interior Permanent Magnet (IPM) have a salient-pole geometry and they are an interesting choice for high speed application. Thanks to the aid of the reluctance torque, they need less power from the magnets therefore the back electromotive force may be smaller.

When working in the field weakening region is needed, salient pole motors are more attractive. The switched reluctance motor (SynRel) and Interior Permanent Magnet motor are widely investigated for the growing electric traction market.

The motor hereby discussed is therefore the PMSM machine. A discussion about the operational limits of this motor is developed starting from the machine equations.

Very detailed model of isotropic synchronous machine can be found in [11]. The equations will be presented in the dq reference frame after the use of three-two phase transformation (Clarke) and the change of the reference frame (Park transformation). The purpose is to show the operational limit of the machine.

$$V_{sd} = R_s I_{sd} + L_s \frac{dI_{sd}}{dt} - \omega L_s I_{sq} \tag{3.2}$$

$$V_{sq} = R_s I_{sq} + L_s \frac{dI_{sq}}{dt} + \omega(L_s I_{sd} + M_{se} I_e) \tag{3.3}$$

$$T = \frac{3}{2} p \varphi_{em} I_{sq} \tag{3.4}$$

As better explained in the paragraph of the control, in these kinds of motor the Maximum Torque per Ampere strategy is researched. The first limit is given by the maximum current of the motor or of the converter. The limit operation can be depicted on the d/q graphs as in Fig. 3.10 and Fig. 3.11. The other limitation is given by the maximum output voltage achievable from the converter, this depends on the DC link voltage and on the modulation used. To figure out how the limits are linked to each other the (3.2) and (3.3) are considered in steady state and the resistance is neglected.

$$V_{max} = \sqrt{V_{sd}^2 + V_{sq}^2} = V_0 \tag{3.5}$$

$$(\omega L_s I_{sq})^2 + (\omega L_s I_{sd} + \omega \varphi_{em})^2 < V_0^2 \tag{3.6}$$

By dividing the (3.6) by ω times the stator inductance.

$$(I_{sd} + \frac{\varphi_{em}}{L_s})^2 + I_{sq}^2 < \frac{V_0^2}{\omega L_s} \tag{3.7}$$

Fig.3.10 shows the current and voltage limit. When the speed increases the last term of (3.7) decreases the radius of the voltage circle (green). When the green circle intersects the

blue one, the nominal (or base) speed is reached and the field weakening region begins as shown in Fig. 3.11.
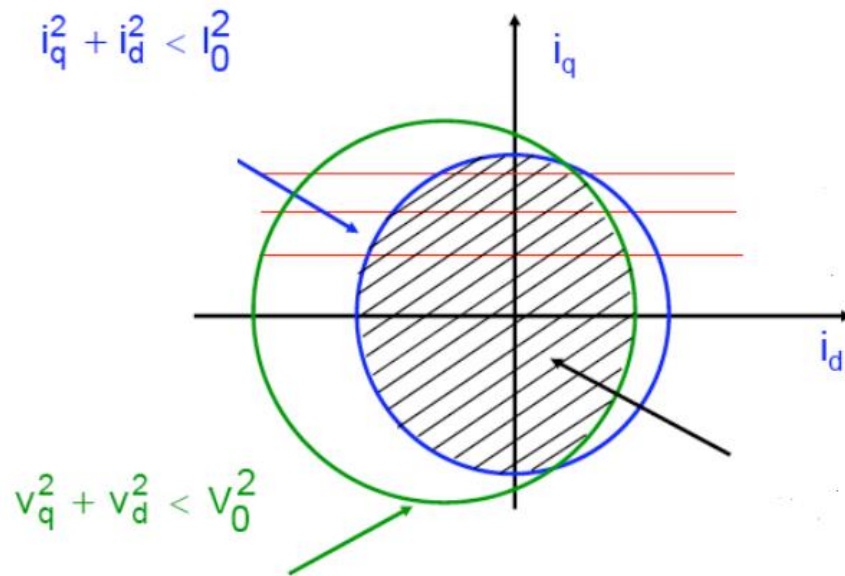
FIGURE 3.10: OPERATIONAL LIMITS OF CURRENT AND VOLTAGE ON D-Q PLANE.

These kinds of machine have a wide air gap for the presence of the surface magnets and therefore they have a low value of the stator inductance. This brings that the center of the voltage circle is out of the circle of the maximum current: as it can be seen from (3.7) and in Fig. 3.11.
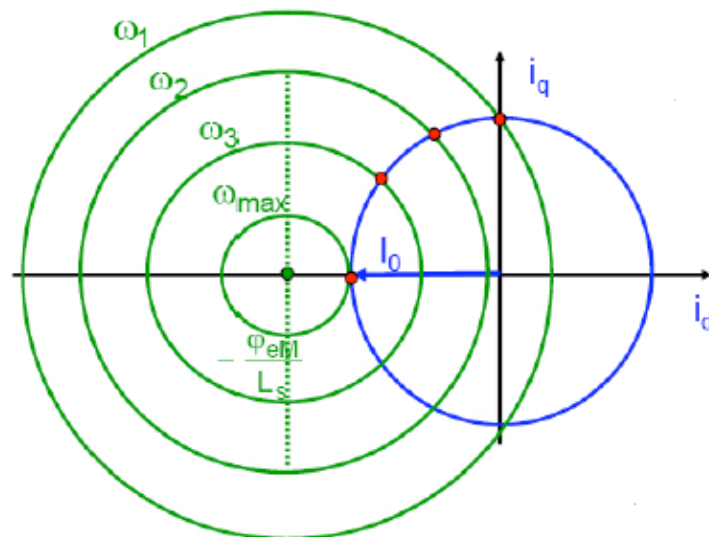
FIGURE 3.11: MTPA UNTIL THE BASE SPEED.

The field weakening region needs a negative value of the d axis current in order to counteract the magnetization of the magnet. The principle is very similar to the DC machine in which the excitation voltage is decreased. In this case, the magnet can be counteracted by a specific current on the machine. However, the field weakening region is not deeply discussed because for Servo drives the most important operating region is the constant torque area. So with the d axis current kept to zero the Fig. 3.12 shows the typical profile of the operation limit of PMSM motor.
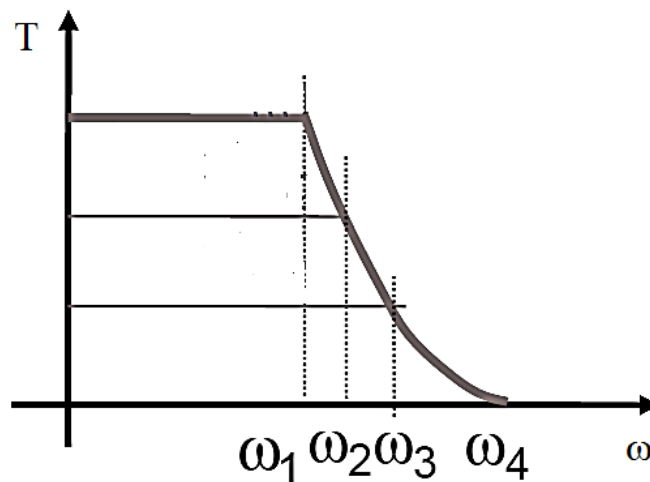
FIGURE 3.12: OPERATIONAL LIMIT ON TORQUE SPEED PLANE.

Thanks to the thermal inertia of the motor there is a limit for continuous operation and one for the peak torque achievable only for short period of time. These aspects will be discussed in Chapter 6.

Once the operational limits are defined the discussion follows with consideration about efficiency and performance in the design process of a PMSM motor.

The main requirements for Servo motor are:

- high torque density (MTPA)
- high acceleration capability (lower inertia rotor)
- high quality of the torque (reduction of pulsations of the torque)

The table 3.1 shows the main strategies developed to achieve these requirements from three approaches of the design process. The amount of losses produced is linked to the maximum performance with the same heat dissipation structure. The operational limit is given by the

maximum temperature that the insulator of the windings can reach. With the same thermal exchange a reduction of the power losses increases the maximum nominal current and so the maximum performance.

	Materials	Structure	Control
High Torque Density	Iron Powder, Iron alloy Powerful and light magnet (NdFeB)	High number of poles Concentrated winding Low rotor inertia	Field Oriented Control Sensorless
Losses Reduction/High performance	Soft Iron, %Silicon, Insulator	Lamination stator core Concentrated winding	MTPA
Quality of Torque	___	Fractional # slot/pole Double layer-fractional pitch winding (if not concentrated) Skew of the rotor Shape of the magnet	Possible current ripple reduction, control against torque ripple

Table 3.1: Sum of strategies for servo motor.

3.2.1 Materials for electrical machine

The stator core is a pack of laminated layer of an alloy called electrical steel. The stator core is generally laminated up to 0.2 [mm] and made of alloy of Iron. Silicon is present in the alloy (up to 5% for workability) in order to reduce the electrical conductivity. This expedient reduces the eddy currents of the iron core. Moreover, usually Manganese, Aluminum, Carbon and impurities are present. The benefit of Silicon is also to reduce the size of the grain in the structure of the Iron, and this helps to reduce hysteresis losses. This type of material is called soft magnetic iron and it presents a very narrow cycle of hysteresis and therefore it minimizes also this part of the losses. Grain oriented steel may provide improvement and a higher permeability even at high flux density but for electrical motor application is generally not used.

Newest possibilities in this field of material are the iron sintered powder that can increase the power density.

Soft Magnetic Composite is an alloy of iron powder, binder and other materials that provide good permeability characteristics and a very low weight. The production is quite complicated and the quality of the composite depends very much upon the quality of the process.

The Datasheet of the electrical steel sheet provides the value of the specific total loss power. This value should be calculated for different flux density and frequency. From two data of the specific loss power the coefficient for hysteresis and eddy currents can be derived. The amount of density of losses describes also the quality of the sheet. The choice of a low value for the specific losses may increase the price but it may also decrease the size of the motor itself and of the converter.

For the windings, there are no more choices than copper or aluminum and no more discussion are developed. The fascinating scenario of the use of the superconductors in motors seems difficult to be developed for lack of workability and flexibility. Moreover, it seems that this technology will never spread for its own management complexity. The insulator plays a crucial role in the limit operation allowed to the machine. The thermal class, in fact, defines the maximum temperature to avoid decreasing the life of the insulator. The field of study about electrical machine insulators is too wide to be discussed inside this work. Development in chemistry and in the technology of the winding procedure may bring improvement and cost reduction as well.

In the rotor, there are permanent magnets of NdFeB and other electrical steels. This magnet entered in the market after the SmCo and it exhibits the highest energy density ever seen in a commercial magnet (shown in Fig. 3.13). Its diffusion was coupled with the diffusion of this type of high efficient brushless motor. The main worry about this magnet is the presence of the Neodymium, a rare-earth element. The production and the market of this material is almost completely managed by China. An exclusive access, almost as a monopoly, of a single country to such a strategic material may be synonymous of high oscillations of the price and of the availability. Historically Japanese researchers focused on finding comparable permanent magnets without the use of rare earth metals [13]. A monopoly of such a spreading material may generate a geopolitical power that should be considered also by engineers. Nevertheless, the high-power density of this kind of magnet is the main reason of the high-power density of PMSM motor. Different strategies may be investigated to reduce the amount or the quality of the magnet needed but until the price of NdFeB remains affordable it will continue in its worldwide diffusion.
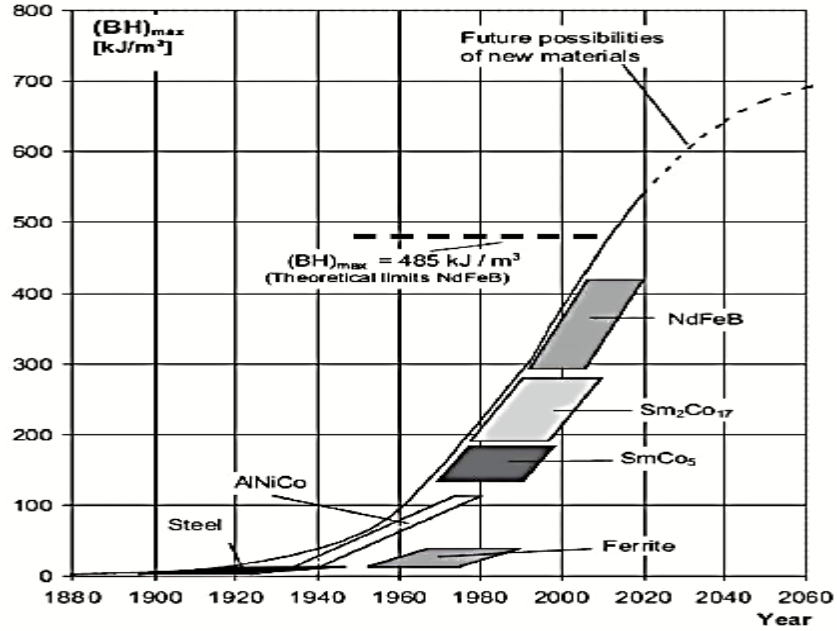
FIGURE 3.13: ENERGY DENSITY OF MOST COMMON MAGNETS.

3.2.2 Structure of PMSM machine

In order to enter more detailed in the structure it is worth to repeat the objectives of the servo motors. First, the higher acceleration capability is basically linked with the rotor inertia, therefore there is no other way than reduce as much as possible the size and the weight of the rotor.

High torque density is linked with the techniques to reduce the size and the weight of the stator. The general expression of the electromagnetic torque produced by two rotating magnetic fields is [14]:

$$T = \mu_0 \delta L p^2 \tau H_1 H_2 \sin(\alpha) \tag{3.8}$$

While the maximum value is

$$T = \frac{1}{2} \mu_0 \delta L \pi D p H_1 H_2 \tag{3.9}$$

49

From (3.8) once the dimensions of the motor are chosen (LD), the torque is proportional to the amplitude of the magnetic field, their relative orientation and the number of poles. The orientation is optimized with the control. While for the structure, (3.9) suggests that torque density is proportional to the number of poles. Generally, a higher number of poles reduces the height of the stator yoke therefore the amount of iron necessary to create the same torque is decreased. The end of the winding occupies less space in comparison and so the power density increases [15]. This brings to higher value of the ratio Nm/kg for these kinds of machines. However, a higher number of poles means also a higher frequency to reach a reference speed. This can bring to an increase in Iron losses that are more than proportional to the frequency. Moreover, higher fundamental frequency may also be difficultly controlled by the inverter or introduce higher current ripple that affects copper losses. Other important development that became popular nowadays is the adoption of concentrated windings instead of the traditional distributed ones shown in Fig. 3.14.
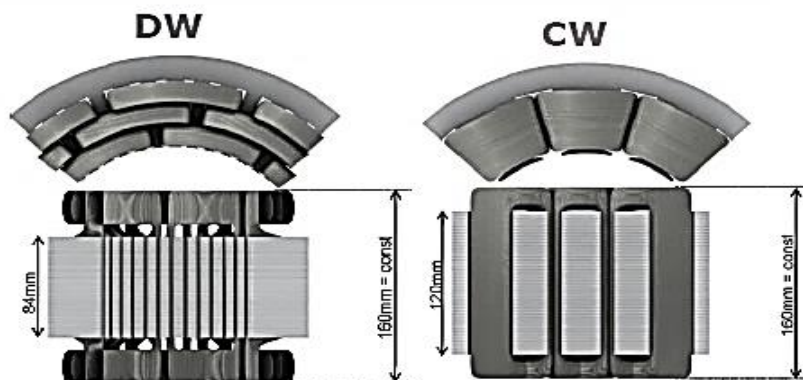
FIGURE 3.14: DISTRIBUITED AND CONCENTRATED WINDINGS.

Many advantages are linked with this choice [15]:

- reduction of the end coil ends therefore increase of power density
- reduction of copper losses
- increased fill factor

However, the main drawback is that concentrated windings are not overlapping and so their choices excludes the presence of fractional pitch windings. Therefore, they provide more harmonic space content. As described later the torque ripple depends also on the geometry of the stator and the choice of this type of windings may increase it [16]. As already

mentioned the choice of the concentrated windings can be considered a way to decrease copper losses because it decreases the length of the conductors.

Furthermore, the discussion now deals with a very important topic for PMSM motor: the torque pulsations (shown in Fig. 3.15). The torque ripple is a parasitic effect inherent with the structure of the motor. Different techniques are used to reduce it [16], [17], [18]. These kinds of motors are needed in application like packaging, machine tools, positioning control and others. It is clear therefore that the possible smoothest torque is required. But especially for motors with permanent magnets on the rotor the issue of the cogging torque arises. The torque produced by the interaction of the stator and the rotor field can be expressed as following [14]:

$$T = -\sum_{i=1}^{m} \frac{e_i I_i}{\omega_m} + \frac{1}{2} F_m^2 \frac{dP_m}{d\theta_m} \tag{3.10}$$

The first member in the right side represents the main contribution to the torque produced while the second one describes the cogging torque oscillation. The torque ripple is produced by both members. The first one in fact contains the harmonic content due to the current ripple produced by the inverter with the EMF given by the geometry of the windings. The back-EMF voltage for each order of harmonic may be expressed as:

$$e_\rho(t) = \frac{\omega}{2\sqrt{2}} N K_{\alpha\rho} K_{skew} \frac{2}{\pi} B_m(t) L\tau \tag{3.11}$$

The first coefficient $K_{\alpha\rho}$ is the winding factor results of the distribution and pitch factor. The second one is the skew factor that is the results of peculiar position of the magnets. From (3.10) therefore, the interaction between the air gap flux density and the geometry of the rotor produces harmonic content (multiple and submultiple of the fundamental harmonic). The design process of the motor offer possibilities to improve the EMF and reduce the space harmonics. Many strategies are found in order to improve the quality of EMF waveform. Acting on the winding factor, both distribution and pitch factor, provide many solutions. Moreover, the skew of the stator and of the magnets may help to reduce the order of harmonics more annoying [18].

In order to provide an electromotive force as sinusoidal as possible, a common technique is the use of a double-layer fractional pitch winding that can selective eliminated some low order harmonics but this excludes the use of concentrated windings.

Then, a high number of slot per pole per phase would be needed to increase the distribution factor for the fundamental harmonic [14].
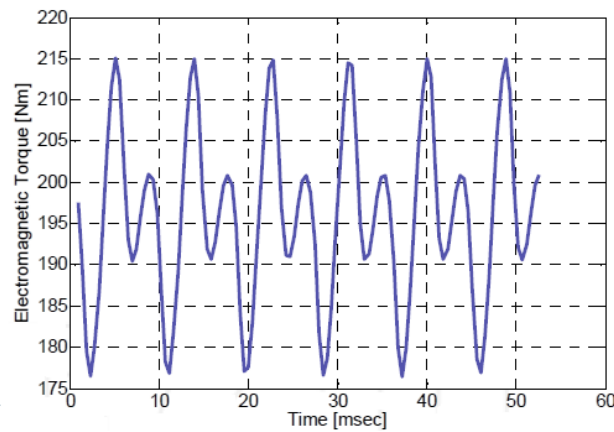
FIGURE 3.15: PULSATING TORQUE FOR PMSM MACHINE.

Moreover the second member of the (3.10) is considered. This contribution is called cogging torque and it grows significance in the permanent magnet motor due to the geometrical structure of the machine. In particular, to the interaction between the magnets and the slots of the stator.

As depicted in Fig. 3.16, the cogging torque is caused by the variation of the energy of the magnetic field of the magnet with the angular position of the rotor.
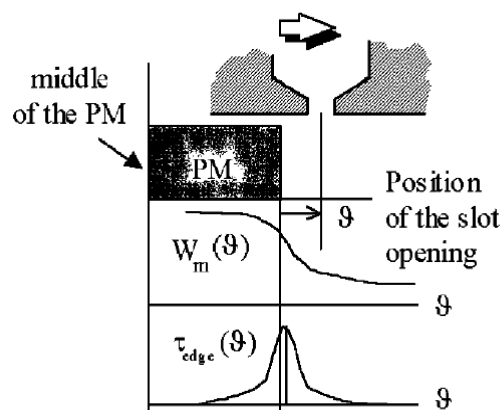
FIGURE 3.16: REASON OF THE COGGING TORQUE [17].

52

For the stator with open slot there are inherently some positions of equilibrium due the varying permeance of the geometry.

The rotor tends to stop in the position of minimum potential. This phenomenon generates a pulsation of the rotor. It shows a null average value as shown in Fig. 3.17. If the stator is not slotless, this pulsation is always present but the geometry of the stator can be designed to decrease the relevance of the cogging torque.

The number of period of the cogging torque waveform depends on the number of slots and on the number of pair poles. The purpose is to decrease the magnitude of the cogging torque so a small period would be needed. Vice versa if the number of periods is high the amplitude of the cogging torque is decreased.

The number of periods is calculated as [17]:

$$N_p = \frac{2p}{HCF\{Q, 2p\}} \qquad (3.12)$$

Where Q and p are the number of stator slots and motor pair poles respectively and HCF is the Highest Common Factor. Others describe the periodicity of cogging torque with Least Common Multiple between Q and 2p. The general idea is that a high number of periods, and so a small period, results in a smaller peak value.

To decrease the cogging torque a solution is that the number of slots should be almost equal to the number of poles [14]. In this way, the number of periods is increased and the amplitude of the cogging torque is minimized.
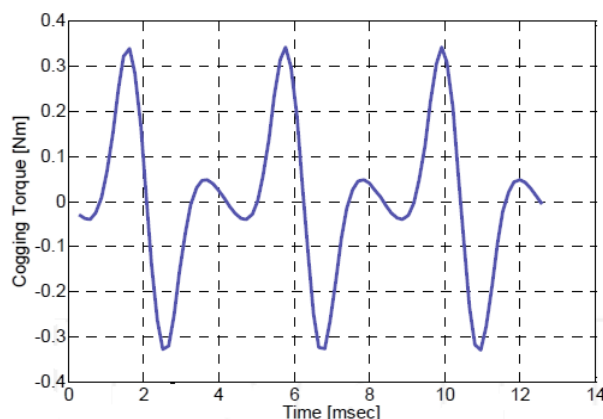
FIGURE 3.17: COGGING TORQUE WAVEFORM.

The two requirements about the number of slots are the opposite to each other. To obtain a EMF as sinusoidal as possible a high number of slots would be needed, while here it should be near a low number. The trade off is commonly solved with a fractional number of slots per pole per phase. The number of slots can be drastically reduced without affecting the distribution factor [14]. The choice permits to reduce the cogging torque without affecting the sinusoidal waveform of the EMF produced by the stator. Fractional slots per pole per phase are commonly produced with concentrated windings.

Moreover, another important factor that influences the evolution of the cogging torque is the length and the shape of the magnets. In fact, the optimization of the shape of the magnet and of the arc pole is effective [20] in order to improve the motor performance and decrease the rotor iron losses.

3.2.3 Control of PMSM machine

The adjustable speed drives are always under improvement from the control point of view. The diffusion of frequency converters and high computational capability of the digital signal processors arise the possibility of accurate control of synchronous and asynchronous motors. Thanks to the use of modulation as PWM the inverter can produce the frequency requested and therefore the speed of the motor can be regulated precisely and follow a reference profile. Concerning the synchronous machines, Fig. 3.18 shows the vector representation of the armature and excitation voltages and flux linkages:
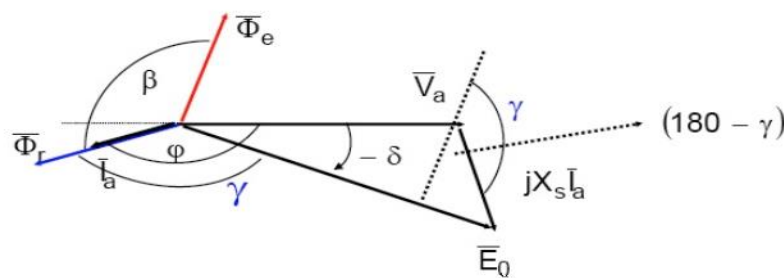
FIGURE 3.18: BLONDEL DIAGRAM FOR SYNCHRONOUS MACHINE.

From the principle of electrical machines is known that for isotropic synchronous machine:

$$T = -\frac{3p}{\omega_m} \left(\frac{V_a E_0}{X_s} \sin \delta \right)$$

(3.13)

With the simple trigonometric equivalence (3.14), it can be said also that:

$$V_a \sin(\delta) = X_s I_a \cos(180° - \gamma)$$
(3.14)

$$T = -\frac{3p}{\omega_m} E_0 I_a sin\beta = K \, \Phi_E I_a sin\beta$$
(3.15)

Where K is a constant value and Φ_E is the excitation flux of the magnet in [Wb].

To optimize the performance the angle β should be chosen and kept constant at 90°. As it can be seen in Fig. 3.19 this brings that the excitation and the armature field are perpendicular between each other as a DC machine. To obtain this condition permanently the Field Oriented Control was developed.
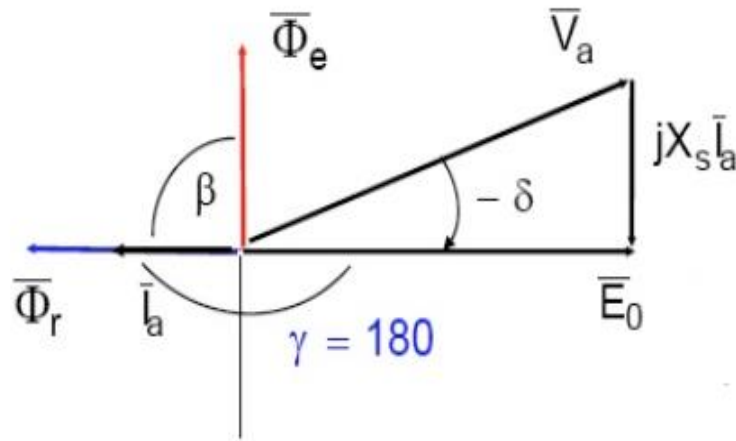
FIGURE 3.19: QUADRATURE OF ARMATURE AND EXCITATION FIELD.

Thanks to the transformation in an arbitrary "dq" reference frame it is possible to obtain the maximum Nm/A ratio from the machine. The degree of freedom of the control is the choice of the initial position and of the speed. The choice is unique for the synchronous machine (it is not for Induction machine) and it is called Rotor Oriented control. As shown in Fig. 3.20. the initial position of the d-axis is chosen on the axis of the excitation field. The q-axis leads of 90° electrical degrees. While the speed of the reference frame is the speed of the rotor and of the excitation field that are equal in synchronous machines.
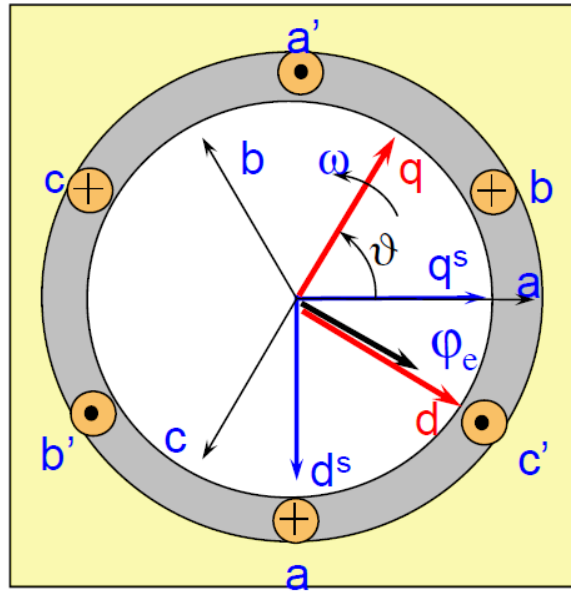
FIGURE 3.20: ROTOR ORIENTED CONTROL.

While in the three-phase system the waveform of the currents is sinusoidal in the reference frame chosen the two currents are constant as a DC.

The equation (3.2) and (3.3) are written in this reference frame. The model of the machine is adapted to decouple the effects of the current on the torque or on the excitation field. In fact, the current of the q-axis is proportional to the torque while the d axis has no effect on it. For this reason, the Maximum Torque per Ampere ratio is maximized keeping the d axis current to 0. However, when the base speed is reached the d-axis is used to decrease the back EMF. This allows the machine to work at higher speed even though the torque achievable is decreased. The great dynamic of the FOC is achieved thanks to the use of the control scheme in Fig. 3.21. In a closed loop control the use of Proportional Integral controller permits to force the machine to follow a specific reference.

The speed controller gives an output proportional to the q-axis current needed to extinguish the error between the speed reference and the measured or estimated one. That current produces a torque that will accelerate or decelerate the motor chasing the speed reference. To achieve them, the desired combination (Iq=Torque/Kt and Id=0) is the input of two current controllers. It is strictly important that the inner current loop is about 10 times faster than the outer loop for the rules of control theory.

Those two controllers produce the output that indicates the proper voltages for each axis in order to extinguish the error between the reference and the measured values.
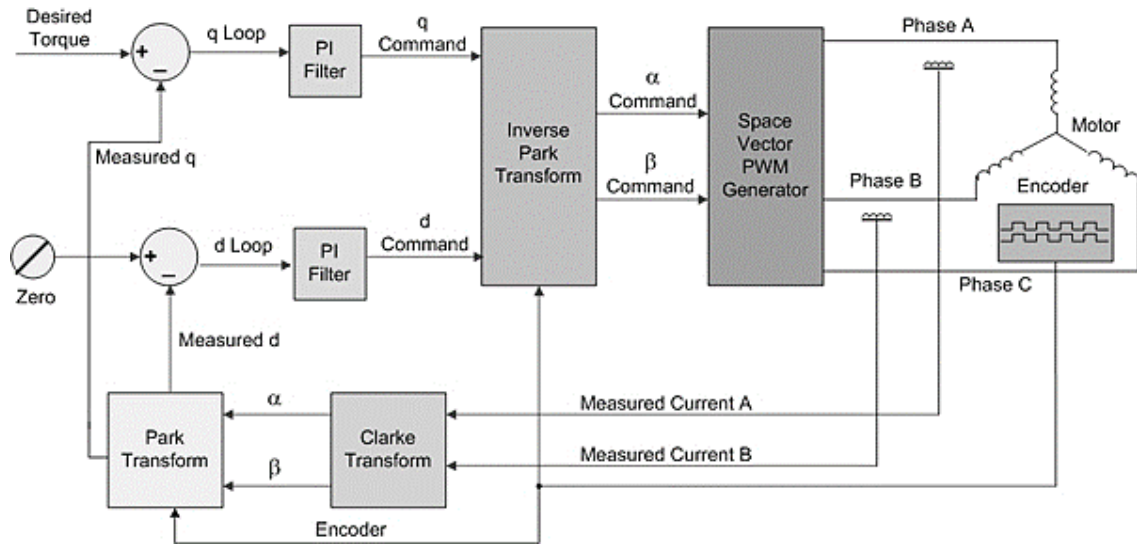
FIGURE 3.21: GENERAL CONTROL SCHEME OF FOC FOR PMSM MOTOR.

After the transformation, the input of SVPWM are the voltages in abc or αβ reference, the modulation provides the pattern of the gate driver to send to the inverter. This is generally the structure of the FOC control for PMSM motor. Its main advantages lie in the use of PI controller and its easy implementation in microprocessor. The tuning of the controller aims to achieve the higher dynamic without exceeding in the overshoot. The tuning is a crucial part of the control and for each application and load the optimal choice may be different.

An important update to the traditional FOC control is the Sensorless capability. In Fig. 3.21 the measurement of the speed is direct. This means that additional tools as resolver or encoder are needed. Resolver works through Hall effect sensors while the encoder is optical and it is more accurate and expensive. The angular position is derived from the integral of the speed once that an initial position is fixed. However, the possibility of avoiding the use of these devices is attractive. In fact, the absence of these tools reduces the length of the shaft, the price, the size, the number of connections and of components and eventually it improves the reliability of the entire system. To avoid the use of these devices the speed and therefore the position have to be estimated. The information about the angular position of the rotor is fundamental for the Park transformation and even minor errors may compromise the quality of the entire control.

The estimation thus must be precise and reliable at any operating condition. Many different strategies are developed [21], [22], [23]. The main concepts of most common methods are

mentioned hereby but the topic is too wide to be fully investigated in this chapter. Artificial intelligence methods are not discussed.

They can be divided mainly as in Fig. 3.22. The key is to derive information about the speed from voltages and currents because they are measured or known in any case. The most common method was the one exploiting the Back EMF. This system shows effective performance over a certain speed when the value measured is high and stable thanks to more kinetic energy. The inherent drawback of this strategies is that at low or zero speed the back EMF may be so small that the measurement is strongly affected by any inaccuracy as: error in the values of the parameter, noise and non-linearity of the power electronics due to the blanking time. More complex systems estimate the flux to obtain speed information and nowadays as Observer-based Estimators or Adaptive methods [22]. These systems analyse on line the performance of the motor predicting the changing of the parameters.

Stator resistance changes rapidly with the temperature therefore it should be measured or predicted. While the inductance brings even bigger challenge since it changes with temperature and with the condition of the magnetic circuit: when the iron is saturated in some points of the stator core the value of the inductance drastically decreases.
Many different possibilities are found and often the choice of the estimator depends on the application and it is a trade-off between the computational effort of the algorithm and the robustness against varying parameters or noise.

At low speed, as mentioned, any inaccuracy may yield a remarkable error in all the model based methods.
A very popular strategy nowadays that does not present any difficulties in low speed operation is the High Frequency injection [23]. This method injects High Frequency signal added to the voltage references that generates correspondent currents. These currents partially saturate the iron core and generate saliency in the rotor, this means that the inductance of d and q axis are different. Then a comparison between the measurement and the predicted behaviour of an isotropic model helps to track the position of the magnet pole.
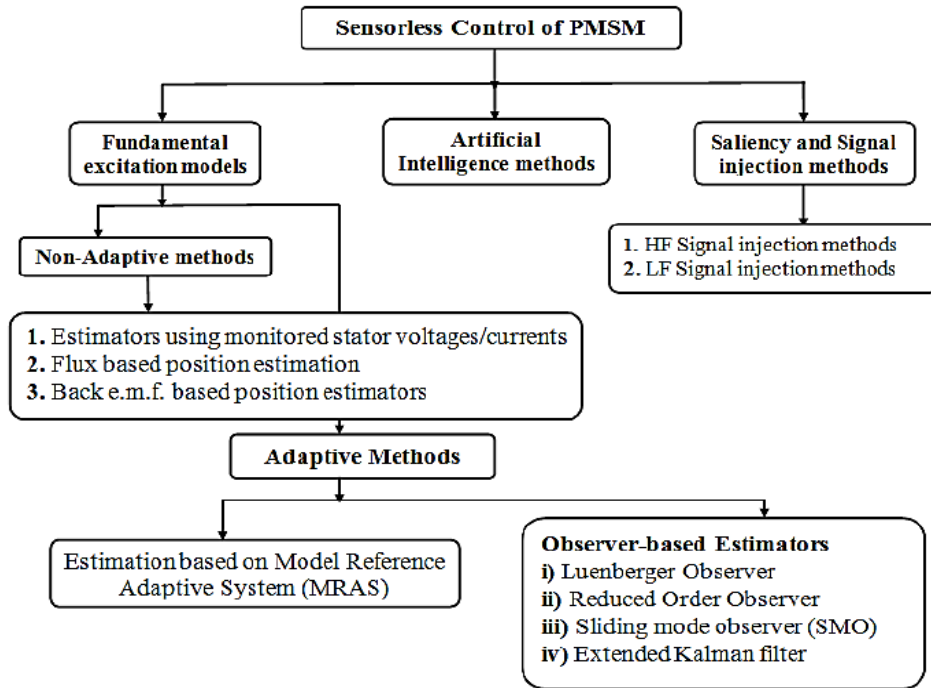
FIGURE 3.22: REVIEW OF SENSORLESS CONTROL FOR SPEED/POSITION ESTIMATION [21].

Reference Chapter 3:

[1] P. Sanjeev, "Analysis of Conduction and Switching losses in two level inverter for low power applications," *IEEE INDICON*, 2013.

[2] Innovative Power Devices for a Sustainable Future-SiC power modules (2015). Mitsubishi Electric.

[3] Kin L. (2016). POWER SiC 2016: "MATERIALS , DEVICES , MODULES" (June 2016). Yole Developpement

[4] Mecke, R.. "Multilevel NPC inverter for low-voltage applications" Power Electronics and Applications (EPE 2011), Proceedings of the 2011-14th European Conference on (2011).

[5] Alamri, B. Darwish, M. 2014 IEEE Precise Modelling of Switching and Conduction Losses in Cascaded H-Bridge Multilevel Inverters.

[6] Floten, S. Haug, T. (2010). Modulation Methods for Neutral-Point- Clamped Three-Level Inverter, Norwegian University of Science and Technology.

[7] Da Silva, E, Dos Santos, E. Jacobina, C. Pulsewidth Modulation Strategies, (June 2011), *IEEE Industrial Electronics* 37–45.

[8] Y. Wu, M. A. Shafi, A. M. Knight and R. A. McMahon, "Comparison of the Effects of Continuous and Discontinuous PWM Schemes on Power Losses of Voltage-Sourced Inverters for Induction Motor Drives," *IEEE Trans. Power Electron.*, vol. 26, no. 1, pp. 182–191, 2011.

[9] A. M. Trzynadlowski, S. Legowski, "Minimum-Loss Vector PWM Strategy for Three-phase Inverters," *IEEE Trans. Power Electron.*, vol. 9, no. 1, pp. 26–34, 1994.

[10] Kolar, J. W., Hans, & Zach, C. (n.d.). Influence of the modulation method on the conduction and switching losses of a pwm converter system. *IEEE Transactions on Industry Applications* (1999) Volume: 27, Issue: 6, Pages: 1063–1075

[11] Novotny, D.W. Lipo, T.A: "Dynamics of AC Drives" Department of Electrical Engineering University of Wisconsin.

[12] Zarri, L. Casadei, D (2014) Lectures of electrical drives for industry and wind application. University of Bologna.

[13] Abraham, D.S. (2015) The elements of Power: the Rare Metal Age.

[14] Serra, G. (2015) Lectures of "Design methodologies for electric machines" (metodologie di progettazione per le macchine elettriche) University of Bologna.

[15] Rossi, C. (2015) Lectures of "Electric traction systems" (sistemi per la propulsione elettrica) University of Bologna.

[16] J. A. Güemes, A. M. Iraolagoitia, M. P. Donsión, and J. I. Del Hoyo, "Analysis of Torque in Permanent Magnet Synchronous Motors with Fractional Slot Windings," *Int. Conf. Electr. Mach.*, pp. 3–6, 2008.

[17] N. Bianchi and S. Bolognani, "Design Techniques for Reducing the Cogging Torque in Surface-Mounted PM Motors," *IEEE Trans. Ind. Appl.*, vol. 38, no. 5, pp. 1259–1265, 2002.

[18] T. M. Jahns and W. L. Soong, "Pulsating Torque Minimization Techniques for Permanent Magnet AC Motor Drives-A Review," *IEEE Trans. Ind. Appl.*, vol. 43, no. 2, 1996.

[19] N. Bianchi, S. Bolognani, M. D. Pré, and G. Grezzani, "Design Considerations for Fractional-Slot Winding Configurations of Synchronous Machines," *IEEE Trans. Ind. Appl.*, vol. 42, no. 4, pp. 997–1006, 2006.

[20] F. Chai, P. Liang, Y. Pei, and S. Cheng, "Magnet Shape Optimization of Surface-Mounted Permanent-Magnet Motors to Reduce Harmonic Iron Losses," *IEEE Trans. Ind. Appl.*, vol. 52, no. 7, pp. 7–10, 2016.

[21] J. Agrawal, "Low Speed Sensorless Control of PMSM Drive Using High Frequency Signal Injection," *IEEE INDICON 2015*, pp. 4–9, 2015.

[22] N. Bianchi, S. Bolognani, J. Jang, and S. Sul, "Comparison of PM Motor Structures and Sensorless Control Techniques for Zero-Speed," *IEEE Trans. Power Electron.*, vol. 22, no. 6, pp. 2466–2475, 2007.

[23] O. Benjak and D. Gerling, "Review of position estimation methods for PMSM drives without a position sensor, part III: Methods based on saliency and signal injection," *Electr. Mach. Syst. (ICEMS), 2010 Int. Conf.*, 2010.

Chapter 4

EFFICIENCY MAPS for SERVO MOTORS

An effective method to describe completely the efficiency of a motor is an efficiency map. The value of the efficiency can be derived for each combination of torque and speed, therefore a more accurate analysis for the load cycle requested can be performed. This chapter deals with the strategies to obtain a reliable efficiency maps for PMSM motors. At the end of the chapter the efficiency map of a planetary gearbox is presented as well because it has been used in the following chapters.

The use of efficiency maps became popular to optimize the design of electrical motor for traction applications since the typical profile of torque and speed of a car is peculiar with many sudden accelerations. Furthermore, the efficiency is a key point in electric vehicles to exploit the energy of the battery in the best way. Different methods are found in the literature that discusses this topic [1], [2]. In a similar way, Servo Drives often exhibit varying working cycles that impose to the components sudden accelerations or braking. The speed requested and the load may vary continuously, thus the working points are not fixed and they might be very different from the nominal point.

Chapter 2 described the nature of the losses involved in the power transmission. These are generally very difficult to be calculated precisely because of the huge number of factors involved. Furthermore, it is known that the efficiency in the nominal working point is the highest one; the design process effectively, aims to optimize the performance and the heat dissipation in that condition. Any differences in the percentage of the load or in the speed of the motor decrease that value. Thus, an efficiency map should be able to give the value of the losses produced by the components with each combination of torque and speed. The losses can be calculated in a certain number of points and then using interpolation techniques, it can be extended to the entire torque speed diagram.

The accuracy of the map might depend both on the level of details of the calculation and on the number of points used for the interpolation.

The efficiency map for the electrical motor exploits the physical dependence of the losses on only one of the input. Iron and mechanical losses are linked only to the speed while joule losses are proportional to the square of the torque. A method to derive efficiency maps for PMSM motor for Servo drives is described. The map for gearbox is presented as well even

though it is not discussed in details. The maps presented are used in the following chapter in an experimental test in which the two components are flanged together.

4.1 Method to derive an efficiency map for Servo Drives

As mentioned before, the no salient pole electrical motors in servo drives are often controlled with the current of the d axis kept to zero. This kind of control coincides with the Maximum Torque Ampere ratio inside the torque constant operating region. The reason to choose this kind of control is firstly its simplicity. Moreover, since the field weakening region is not exploited completely in this kind of application for the need of constant torque operation, there is no need for a more complicated control. When high nominal speed are required, the windings can be adapted to decrease the back EMF constant. Without the field weakening control the calculation of the joule losses is very simplified because in all the situations the current can be directly derived from the torque. If the constant torque is valid for all the points of the operating region they can be calculated as:

$$P_{cu} = 3R_s(\Theta) \frac{T^2}{k_{TRms}^2} \tag{4.1}$$

The constant torque is referred to the ratio of torque and Rms of current needed to produce that torque. The resistance has to be corrected with the expected operating temperature and different considerations can be done to predict the steady state temperature of the windings according to the load cycle. For instance, assuming that with the nominal torque the windings experience an overtemperature of 105 °C (limit for insulation of class F).

The major idea is described in [3] and [4]. The most practical and effective way is to assume that different losses depend only either on torque or on speed. In this way, it is possible to extend the analysis to the whole operating region. This general method can be applied to different kinds of machines. In [4] it is explained in details the dependence of the losses either in the constant torque region that in the power constant region. The one of interest for Servo Drives is for PMSM motor in constant torque region and it is reported in Table 4.1. Iron losses are mainly eddy currents losses and so the main dependence is on the square of the speed as in (4.2). Magnet and rotor losses are neglected. Windage losses are instead considered later.

$$P_{loss}(T, \omega) = k_{20}T^2 + k_{02}\omega_m^2 \qquad (4.2)$$

	Surface PM							
	Constant Torque				Constant Power			
T^3								
T^2	cu-s		mgnt		cu-s		mgnt	
T								
1		fe	fe	wdge	cu/fe		mgnt	wdge
	1	ω	ω^2	ω^3	1	ω	ω^2	ω^3

Table 4.1: LOSSES DEPENDANCE ON TORQUE AND SPEED FOR PMSM MOTOR [4].

The quality of the procedure depends on the level of details of the initial information. For instance, if a very approximated model is sufficient the only information provided may be the efficiency in the nominal point. With the (4.1) Joule losses can be calculated quite precisely: thus, an idea can be to separate joule and iron (and other) losses, then find the coefficients that link the torque and the speed to the respective losses and use that coefficient in all the operating region. The information about the losses can be also derived from a working point at very low speed and high load where almost all the losses are Joule. This brings to know the maximum losses allowed, since the motors are designed to be able to dissipate a certain amount of losses that cannot be exceeded. As in Fig. 4.4 the losses are assumed to be the same in the points of the limit curve.

Moreover, the script must check the voltage limit to avoid calculating points that are out of the real operating region, therefore information about the flux is needed to derive the back-EMF voltage.

To enhance the accuracy, detailed information of the motor is requested. For instance, the iron should be divided in different areas since the flux density changes significantly between the yoke and teeth of the stator. Moreover, detailed information about the skew of the magnet should be considered as well as the peculiar characteristics of the iron and of the magnet used. All this information may be often difficult to be obtained by the customer.

Thanks to the help of the R&D department of Bonfiglioli Mechatronic Research the author received specific data of the company's product.

In this case a FEM analysis was conducted with the software FEMM. A 2D magneto static analysis is sufficient to achieve accurate results.

In particular, the routine uses 16 FEA simulations with selected couple of the current of d-axis and q-axis. High detailed description of the materials and of the geometry is implemented. Furthermore, a script in LUA derives for 16 points the information about: flux linkages, torque, maximum flux density in the yoke and in the teeth, currents and voltages.

These data are exploited by a Matlab code in order to generate the efficiency map.

Fig. 4.1 sums up the step of the algorithm.

The equations used in the algorithm are shown with the reference cited in the Fig.4.1. Firstly, for Iron losses calculation:

$$P_{Iron}(\omega) = \left(k_{ph} \frac{\omega}{2\pi 50} + k_{pe} \frac{\omega^2}{(2\pi 50)^2} \right) (B^2_{t\,yoke} W_{yoke} + B^2_{t\,teeth} W_{teeth}) \qquad (4.3)$$

Where the different values of the flux density are the maximum ones respectively in the yoke and in the teeth and W means the weight of the iron. The speed is meant in radiant per seconds. The coefficient K_{ph} is the specific loss for hysteresis losses while K_{pe} is for the eddy currents. Those coefficients are available from the data sheet of the electrical steel used.

The mechanical losses are instead derived from the (4.4)

$$P_{mech}(\omega) = k_3 n^3 + k_2 n^2 + k_1 n + k_0 \qquad (4.4)$$

Here the speed "n" is needed in round per minute. The coefficients are derived from experimental test previously conducted.
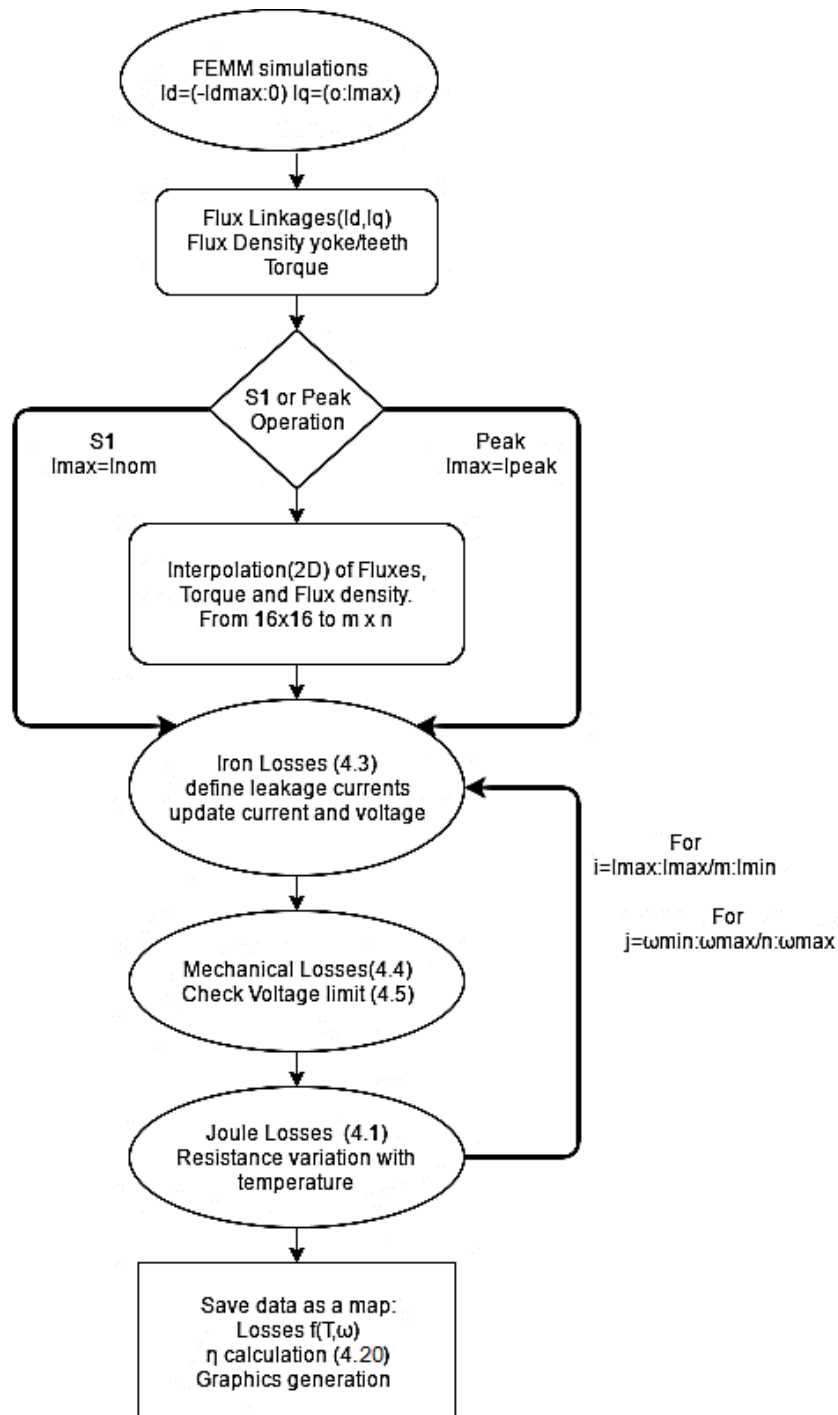
FIGURE 4.1: ALGORITHM USED FOR EFFICIENCY MAP GENERATION.

The voltage limit is derived from the back EMF generated on the stator windings. This depends on the speed and on the fluxes.

With the decomposition in d and q axis the voltage limit may be checked with the (4.5) while (4.7) – (4.18) are needed to derive the values used in (4.5) and (4.6).

$$|V_{pk}| > V_{nom} \qquad (4.5)$$

$$V_{pk} = \sqrt{V_d{}^2 + V_q{}^2} \qquad (4.6)$$

$$V_d = R_s I_{dtot} - \omega \Phi_{Ld} \qquad (4.7)$$
$$V_q = R_s I_{qtot} + \omega \Phi_{Lq} \qquad (4.8)$$
$$\Phi_{Ld} = L_s I_d + \Phi_{mag} \qquad (4.9)$$
$$\Phi_{Lq} = L_s I_q \qquad (4.10)$$

$$I_{dtot} = I_d + I_{fd} \qquad (4.11)$$
$$I_{qtot} = I_q + I_{fq} \qquad (4.12)$$

$$I_f = \frac{2}{3} \frac{P_{Iron}}{E_{pk}} \qquad (4.13)$$

$$I_{fd} = I_f \frac{E_d}{E_{pk}} \qquad (4.14)$$

$$I_{fq} = I_f \frac{E_q}{E_{pk}} \qquad (4.15)$$

$$E_{pk} = \sqrt{E_d{}^2 + E_q{}^2} \qquad (4.16)$$

$$E_d = -\omega \Phi_{Ld} \qquad (4.17)$$
$$E_q = \omega \Phi_{Lq} \qquad (4.18)$$

All the equations (4.5) -(4.18) are linked to each other and they are needed to check the voltage limit. (4.13) defines the equivalent leakage current of the iron losses that increases the peak current. The leakage current is associated with a shunt resistance in any kind of equivalent circuit of electrical machines and it represents the part of energy not transmitted to the rotor. I_f in Fig. 4.2 represents the leakage current that permits to include the Iron losses in the analysis. The value of the resistance can be calculated as in (4.19):
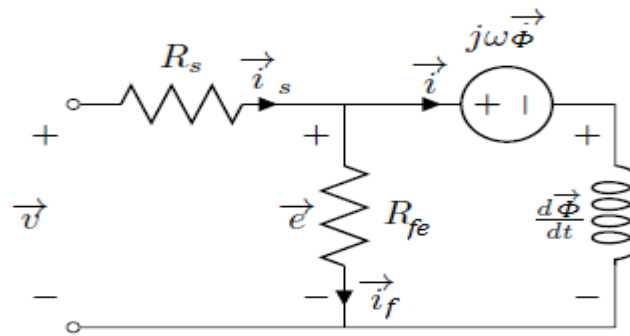

FIGURE 4.2: EQUIVALENT CIRCUIT WITH RESISTANCE FOR IRON LOSSES AND LEAKAGE CURRENT.

$$R_{fe} = 3 \frac{V_s^2}{P_{Iron}} \qquad \text{(4.19)}$$

Since the Joule losses are the main contribution to the total ones, the temperature plays a crucial role. The maximum overtemperature on the windings is considered to be 105°C. In the S1 operation it is calculated proportionally with the percentage of the load supposing that the overtemperature is the maximum one at the nominal load. For the peak or intermittent operation, instead it is assumed that the overtemperature is the maximum one in all the working points since the cycle may heat the motor up and it maintains a high temperature. Different load cycles change the evolution of the temperature since the thermal inertia of the motor is high and it takes time to change even with sudden changing in the operating condition. For this reason, if the evolution of the temperature can be measured, the information can be used to derive more precisely the joule losses occurred. Eventually the efficiency is derived with the (4.20)

$$\eta = \frac{P_{transmitted}}{P_{losses} + P_{transmitted}} \qquad \text{(4.20)}$$

Where the transmitted power is the mechanical power product of the torque and the speed in radians per second. Once the matrix is obtained to provide information of easy implementation the map is interpolated with a polynomial of 2nd or 3rd order. This permits to insert the equation even in software that can use only algebraic equations. Different types of interpolation should be considered and tested according to the number of points available.

4.2 Results for BMD 65

Firstly, the results are reported for the smallest size of the motor. As known the efficiency of electrical machines increases with the size therefore this small one should present the lowest values. Following the procedure explained in the chapter the code exploited the data achieved from the R&D division of the motor BMD65 that has a nominal torque of 1.7 Nm. The nominal speed of the motor of this map is 8000 rpm. Changing the nominal speed, both

the resistance and the current change therefore there are not big differences in the joule losses calculation.

The overall efficiency on the torque-speed diagram is depicted in Fig. 4.3. This case shows the map for continuous operation. Fig. 4.4 instead depicts the results of the total losses. The shape confirms the assumption described at the beginning. On the line of the limit of continuous operation the value of the losses is equal to the maximum one. That value can be easily derived considering a point at low speed and maximum torque since almost only Joule losses occur in that working point.
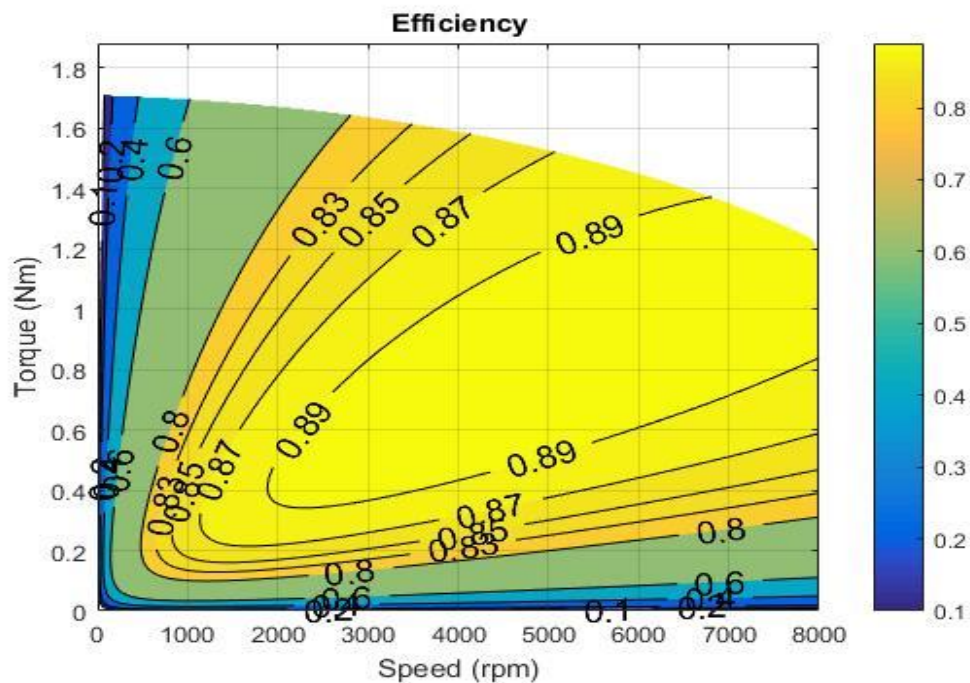
FIGURE 4.3: EFFICIENCY MAP FOR S1 FOR SMALL MOTOR: NOMINAL TORQUE 1.7 Nm.

Thanks to the division of the dependence of the type of losses the method is quite simplified. It is also possible to use the method for a wide range of different size of motor. In the following part the three-different kinds of losses are shown independently to highlight their dependence. Fig. 4.5 shows the Joule losses. It is noticed that the speed has no influence on it and they increase only with the torque. Fig. 4.6 and 4.7 show instead iron and mechanical losses. In those cases, it is the torque that has almost no influence in the calculation.
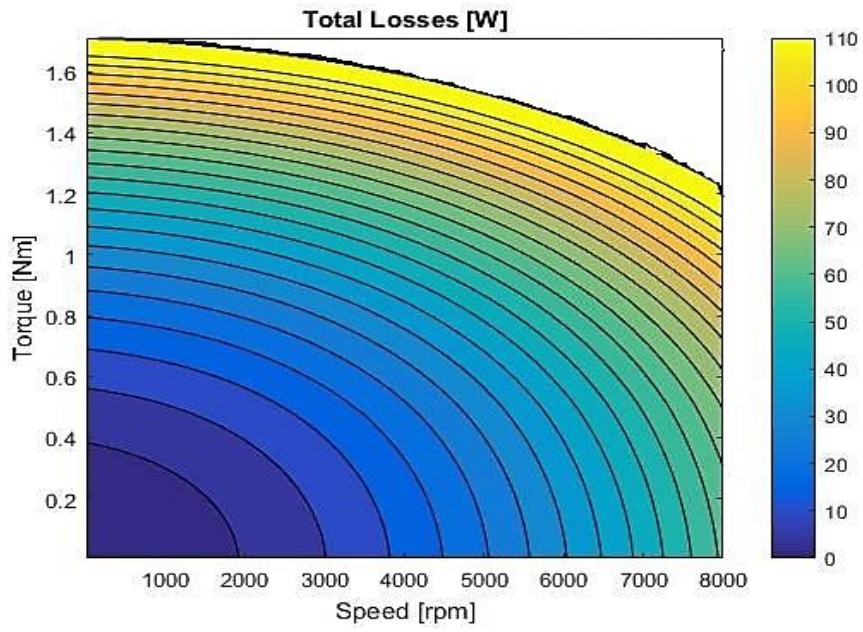
FIGURE 4.4: TOTAL LOSSES MAP ON TORQUE-SPEED DIAGRAM.
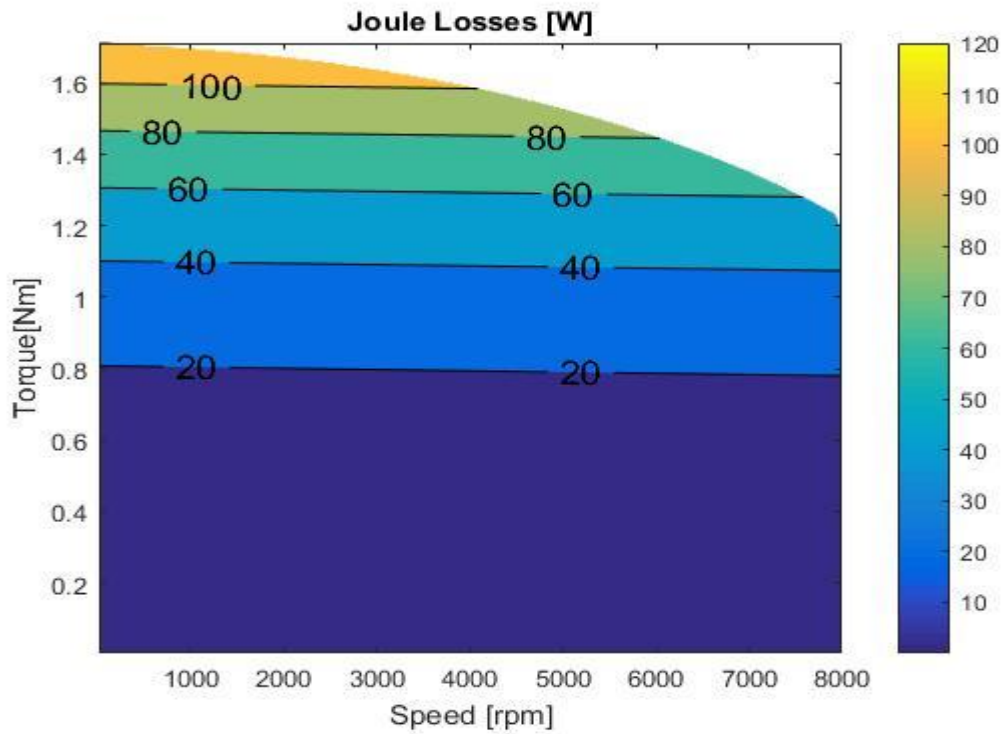
FIGURE 4.5: JOULE LOSSES MAP.
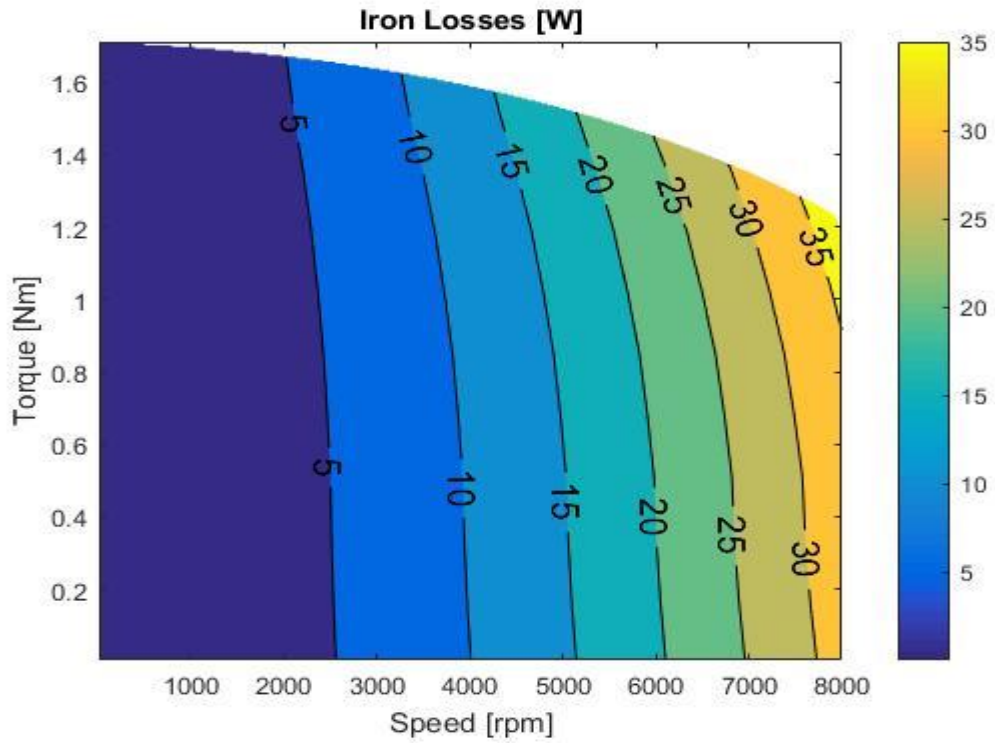
FIGURE 4.6: IRON LOSSES MAP.
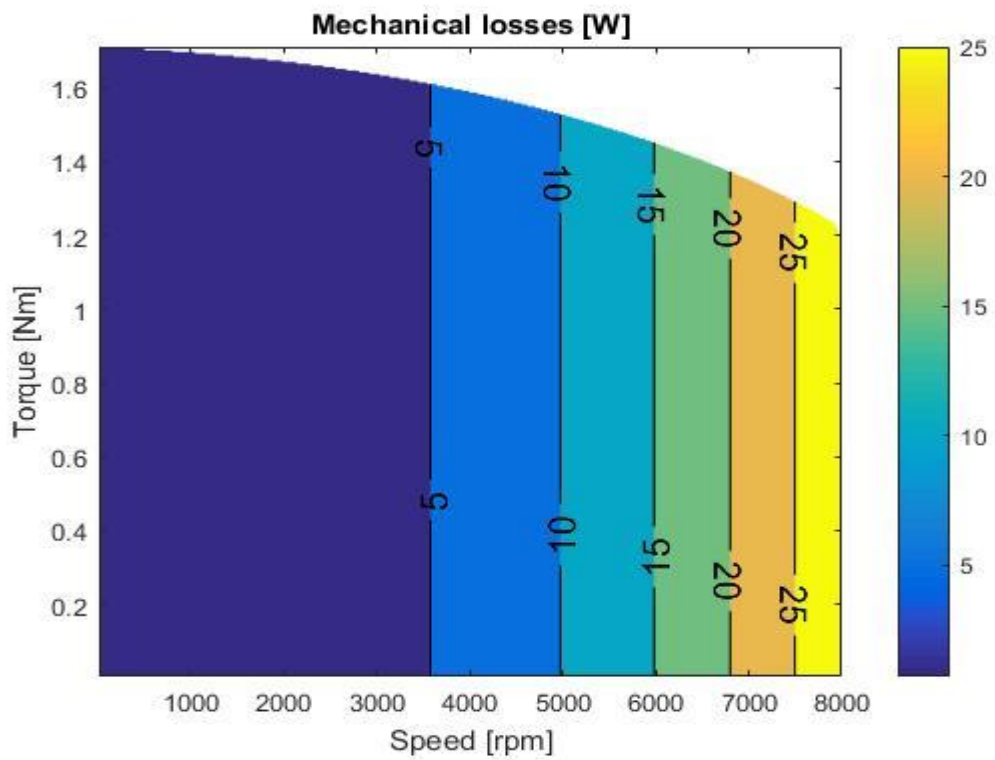
FIGURE 4.7: MECHANICAL LOSSES MAP.

In case of intermittent operation, it may be useful to be able to estimate the efficiency also in points out from the S1 operation. As seen in Fig. 4.1 the script for the peak operation uses the peak current value instead of the nominal one. The same procedure was applied to derive the values for the Peak operation but the temperature is considered the maximum one for all the working points.

Fig. 4.8 shows the efficiency map for intermittent or peak operation. The simulated motor has a nominal torque of 1.7 Nm and a peak torque of 4.5 Nm.
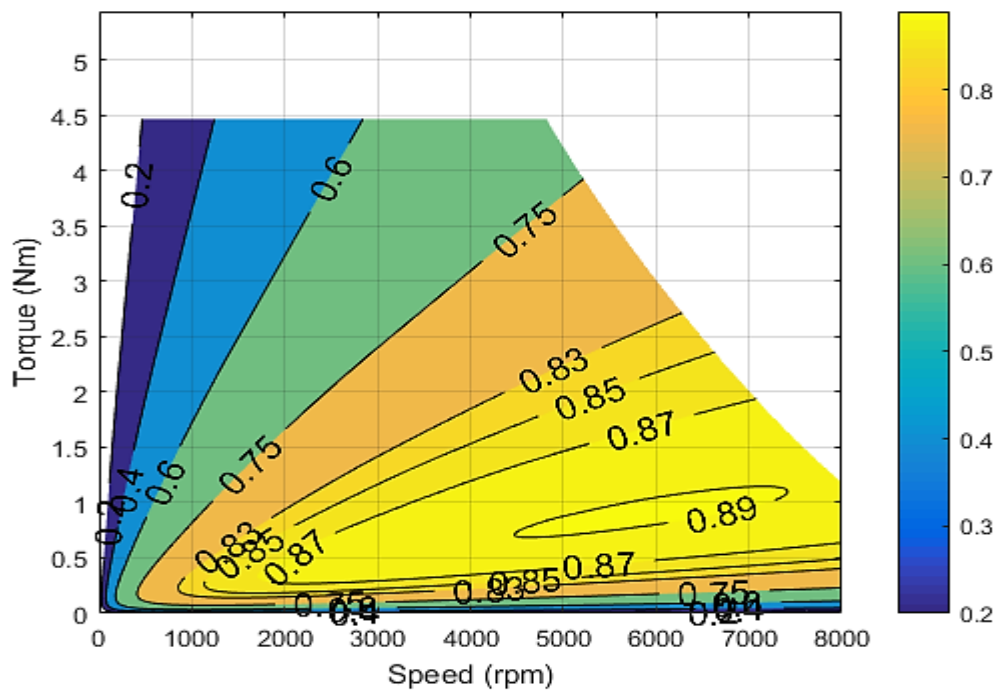
FIGURE 4.8: EFFICIENCY MAP FOR PEAK OPERATION OF BMD65.

4.3 Results useful for the experiment

Chapter 5 presents the results of an experiment in which these types of maps are tested therefore the map for the motor and the gearbox used are reported. Moreover, since the efficiency of electrical machines increases with the size it is useful to show another motor simulation. BMD 145 has a nominal torque of 16.8 Nm and 3000 rpm as nominal speed. The efficiency map for S1 operation is reported in Fig. 4.9.

The overall efficiency is higher than the one of the other motor presented since it is a bigger motor. It is worth to notice that it is necessary a specific analysis for each size of the motor. Assuming that different sizes have a similar efficiency may bring to error.

The method used is the same but it starts from different simulations since the stator and the magnet change with the size. Anyway, each specific loss shows the same evolution of the case presented in the previous paragraph.
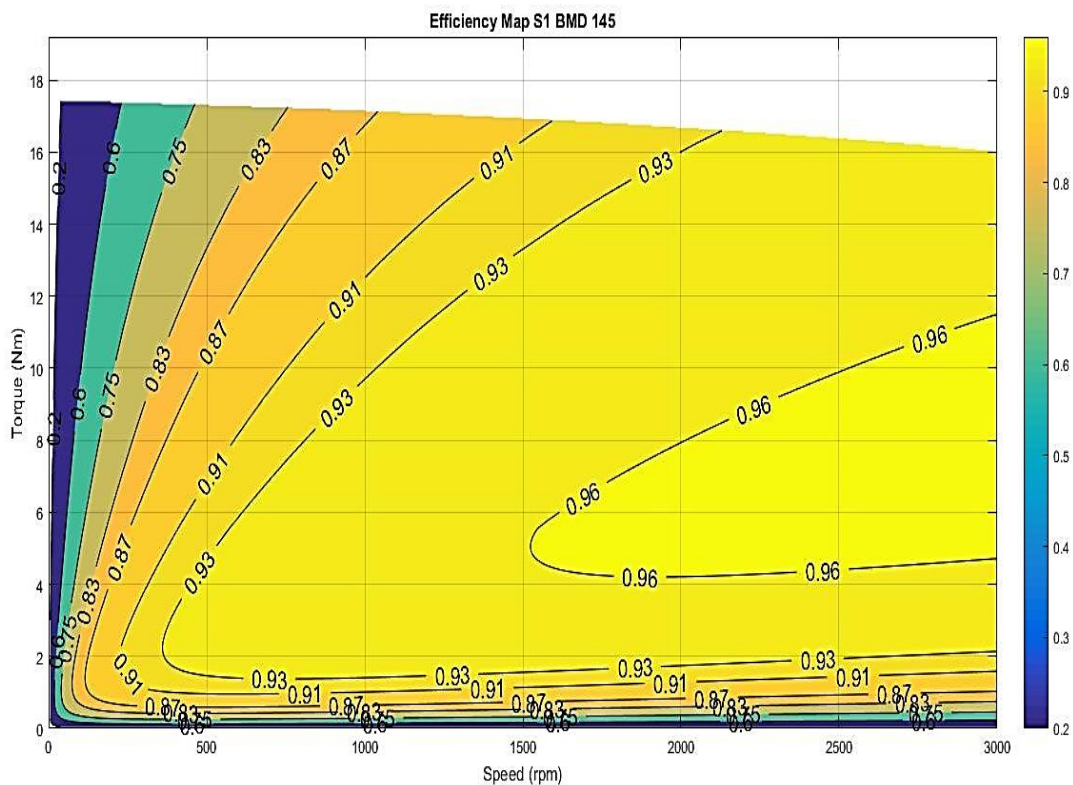
FIGURE 4.9: EFFICIENCY MAPS FOR BMD145 IN S1 OPERATION (3000rpm).

In the last part of the chapter the results used for the planetary gearbox are exposed. The procedure was not investigated in details. The losses described in Chapter 2 are derived for the specific geometry, dimensions and number of teeth involved for each gearbox. The main types of losses are reported in Fig. 4.10. In this case the map presented is for the TQ090 that has a gearbox ratio of 5. It has a nominal input torque of 36 Nm and a nominal input speed of 2500 rpm. The peak values are instead of 100Nm as input torque and 4500 rpm as input speed.

The procedure is validated in [5] for the same gearbox presented. The load dependent losses, the bearing losses and the seal losses can be derived through analytical expressions.

Main factors involved are the quality of the lubricant, its viscosity, the level of lubricant and the temperature.

Generally, a low level of oil increases friction losses but it decreases the load independent losses. Those latter are instead difficult to be calculated since CFD (Fluids dynamical) analysis are needed to derive velocity and pressure field. Moreover, the lubricant is moved, dragged and squeezed by the motion of the planet.

$$P_V = P_{VZ0} + P_{VZP} + P_{VL0} + P_{VLP} + P_{VD} + P_{VX}$$
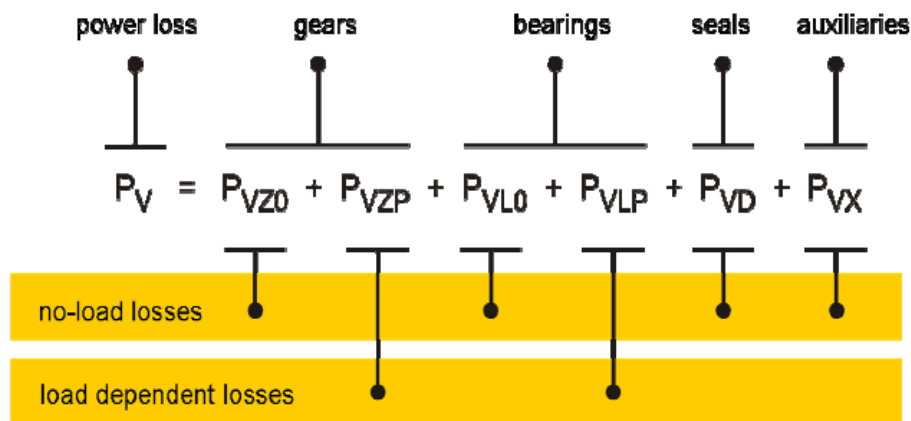
FIGURE 4.10: MAIN LOSSES FOR PLANETARY GEARBOX DIVIDED IN LOAD DEPENDENT AND INDEPENDENT.

The two phases fluid composed by air and lubricant may create foam and at high speed the temperature increases and the viscosity change therefore all the fluid dynamics event are completely different.

All the losses in fact strictly depend on the temperature but they contribute also to change it. An iterative procedure is done in [5], the amount of losses decreases with the increasing of the temperature while the heat exchange increases when the temperature grows. An equilibrium point is found and it represents the losses produced and the temperature that is created. This procedure is depicted in Fig. 4.11.

The x-axis of Fig. 4.11 represents the number of iterations.

Then the map presented in Fig. 4.12 shows the amount of losses while Fig. 4.13 the temperature derived for each working point.
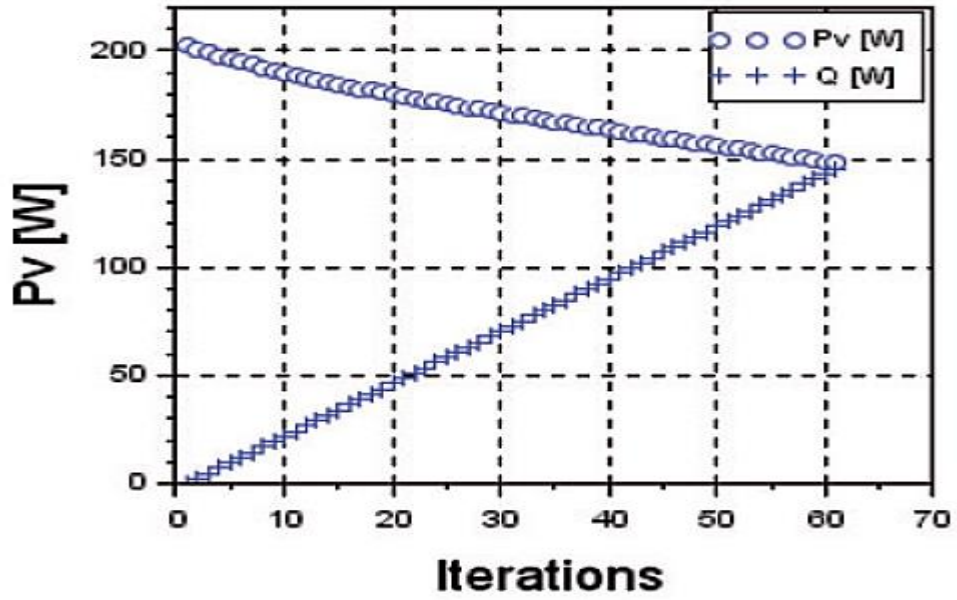
FIGURE 4.11: ITERATIVE PROCEDURE TO FIND TEMPERATURE FOR THE LOSSES CALCULATION OF GEARBOXES [5].
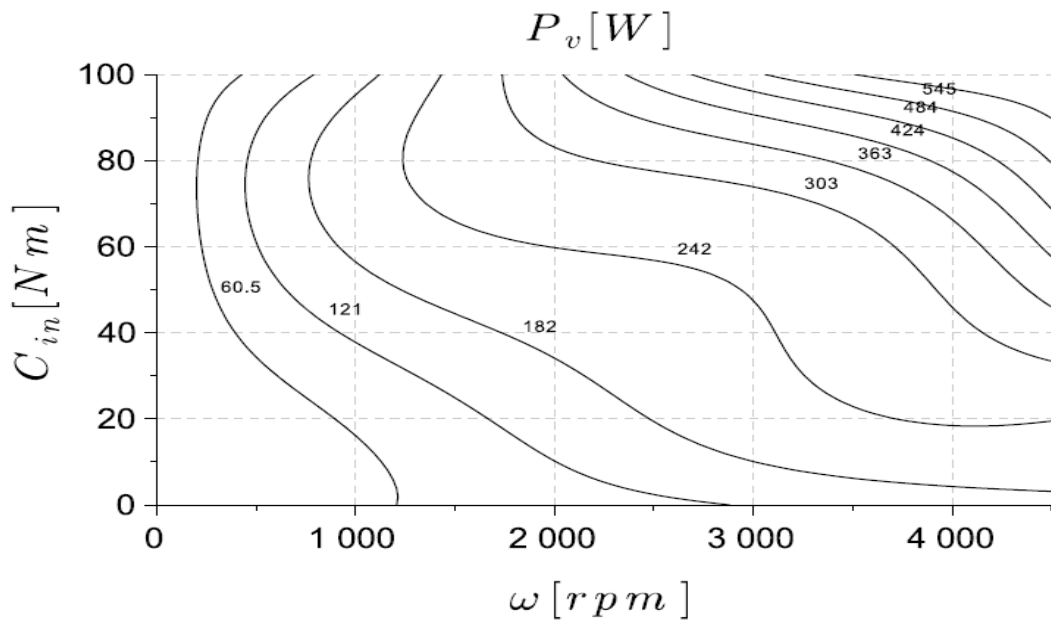
FIGURE 4.12: LOSSES MAP FOR GEARBOX TQ090 i5.
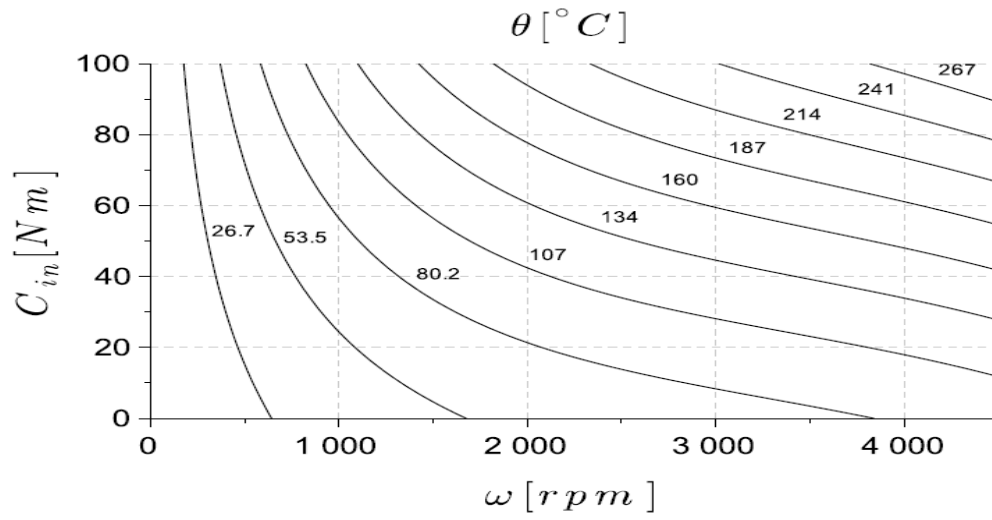
FIGURE 4.13: TEMPERATURE MAP FOR TQ090 i5.

References Chapter 4

[1] L. Song, "Efficiency Map Calculation for Surface-mounted Permanent-magnet In-wheel Motor Based on Design Parameters and Control Strategy," *ITEC Asia-Pacific*, no. 2, pp. 1–6, 2014.

[2] Q. Li, T. Fan, X. Wen, X. Tai, Y. Li, and G. Zhang, "Modeling of the efficiency MAP of surface permanent magnet machine for electrical vehicles," *2013 Int. Conf. Electr. Mach. Syst. ICEMS 2013*, pp. 1222–1225, 2013.

[3] V. Ruuskanen, P. Immonen, J. Nerg, and J. Pyrhönen, "Determining electrical efficiency of permanent magnet synchronous machines with different control methods," *Electr. Eng.*, vol. 94, no. 2, pp. 97–106, 2012.

[4] A. Mahmoudi, W., G. Pellegrino, "Efficiency Maps of Electrical Machines," 2016 XXII International Conference on Electrical Machines (ICEM) (2016) Volume: 1, Publisher: IEEE, Pages: 1043-1049.

[5] F. Concli, "Thermal and efficiency characterization of a low-backlash planetary gearbox: An integrated numerical-analytical prediction model and its experimental validation," *Institution of Mechanical Engineering*, 2015.

Chapter 5

EXPERIMENTAL VALIDATION

To validate the efficiency maps developed for the electrical motors and the gearboxes an experimental verification was conducted. This chapter presents the results of the measurement of the total efficiency of the combination motor plus gearbox. The two components are flanged together like in the real operating condition and thus the heat exchange is different from the one considered for the maps. The chapter includes a description of the setup and of the method used that follows the principle of IEC 60034-1. The efficiency measurement is done with the direct method. Moreover, an analysis of the inverter efficiency is presented.

The experiment was set up thanks to the Research & Development division of Bonfiglioli Mechatronic Research in Rovereto (TN).

The main purpose of the experiment was to highlight and quantify the difference in the efficiency prediction between the theoretical analysis and the real operating condition. The efficiency maps of the motor and of the gearbox were already validated in a test with the component alone. In that case both the motor and the gearbox are flanged with a metallic plate that optimizes the thermal exchange. Since the real operating condition imposes that the motor is flanged with the gearbox as in Fig. 5.1 the efficiency is expected to decrease because the quality of the heat exchange of the motor gets worse. Effectively, the frame of the gearbox may have approximately the same temperature of the frame of the motor, therefore the two surfaces are almost in thermal equilibrium. The measurement of test should be performed ensuring a steady state thermal behaviour at a constant temperature. The operating points were chosen in a peculiar order to reach the maximum. The first three points heat the motor up till the maximum temperature. The others are therefore evaluated in the worst case. The total number of operating points measured is 8 and this permits to analyse the torque speed chart.

Furthermore, measurements on the inverter efficiency are conducted as well and the dependence on the speed of the motor and on the torque, is highlighted.
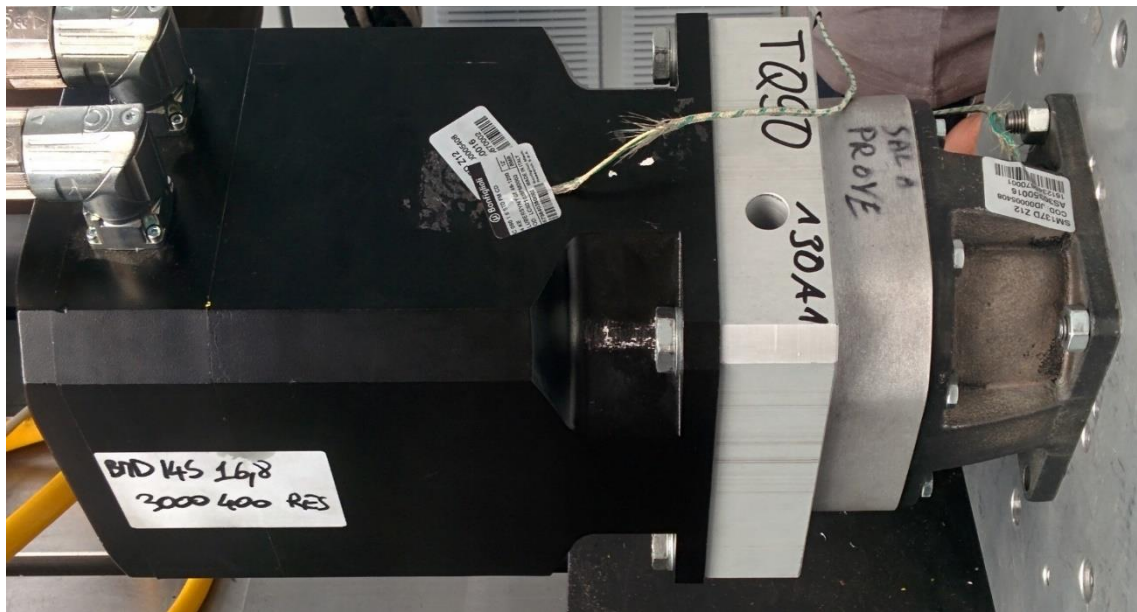
FIGURE 5.1: EXPERIMENTAL SETUP. COMBINATION OF BMD 145+TQ 90.

This information may confirm the expected high value of inverter efficiency and its slight dependence on the speed of the motor.

Fig. 5.2 shows a scheme of the setup of the experiment. It is a regenerative measurement because the second motor works as generator and gives energy back to the bus DC. The energy consumption from the grid is equal to the total losses. There are 3 different points in which the measurement of the power takes place:

- power DC before the inverter: through DC voltage measurement and a current transducer
- active Power AC after the inverter: through current sensors and a power analyser
- mechanical Power after the gearbox: through a torque meter and encoder.

The inverters themselves have their own measurement tools but generally they exhibit an uncertainty of 1% while with the current transducers used the uncertainty is about 100 times smaller (0.01%).
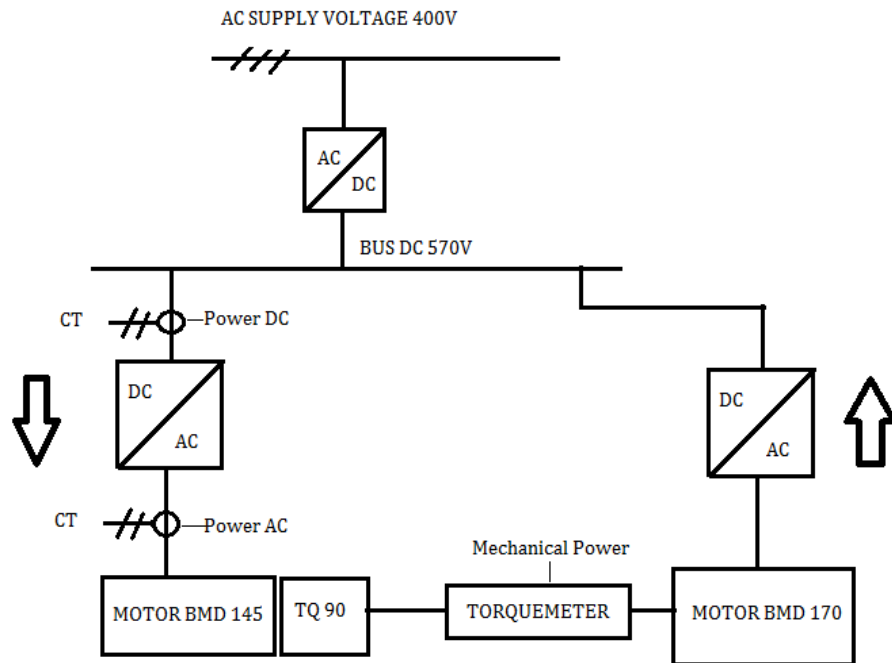
FIGURE 5.2: SCHEME OF THE MEASUREMENT SET UP.

5.1 Detailed description of the components used

Firstly, the components used in the experiment are hereby presented with their datasheet provided by the company.

The inverter is a servo inverter and one of the control implemented is the Field oriented control that was used during the test. Fig. 5.3 shows the datasheet of the ACU 401-19 chosen for this test. The inverter that feeds the generator motor is instead ACU 401-21.

The electrical motor is a permanent magnet surface mounted with fractional slot number and concentrated windings and Fig. 5.4 shows the commercial data sheet provided by the company. The motor in the experiment was a BMD 145 with 8 poles, 16.8 Nm as nominal torque, 3000 rpm as nominal speed and 400 V as supply voltage. While the motor used as generator is BMD 170 and it has a nominal torque of 36 Nm.

ACU401 - Technical data (from 4.0 to 15 kW)

ACU401-			18	19	21	22	23	25
			Size 2 (F, A)		Size 3 (- or F, A)		Size 4 (-, A)	
Output, motor side								
Rated motor current output	I_n	A	9.0	14.0	18.0	22.0	25.0	32.0
Rated motor voltage output	U_n	V	3 x (from 0 to mains voltage)					
Overload current	I_{pk}	A	13.5	21.0	26.3	30.3	37.5	44.5
Recommended rated motor power	P_n	kW	4.0	5.5	7.5	9.2	11.0	15.0
Switching frequency	f_c	kHz	From 2 to 16					
Rated motor frequency	f_n	Hz	From 0 to 1000					
Input, mains side								
Rated mains voltage	U	V	320 ... 528					
Rated mains frequency	f	Hz	45 ... 66					
Rated current 3 ph/PE	I	A	7.8	14.2	15.8	20.0	26.0	28.2
Mains fuses 3 ph/PE	I	A	10.0	16.0	25.0		35.0	

FIGURE 5.3: DATA SHEET OF THE INVERTER USED. ACU 401-19.

BMD 145 • 16.8 Nm - 400V

Parameter	Symbol	Unit	Speed [min⁻¹]				
			1600	3000	4500	5500	6000
Standstill torque (dT=105K)	M_0	[Nm]	16.8				
Motor rated frequency	f_n	[Hz]	107	200	300	367	400
Motor rated voltage	V_n	[V_{AC}]	314	308	314	319	305
Rated Torque (dT=105K)	M_n	[Nm]	16.5	16	14	13	12.5
Current at rated speed	I_n	[A]	6.8	12.5	16.4	17.5	19
Standstill current	I_0	[A]	6.9	13.0	19.0	22.8	26
Max Torque	M_{max}	[Nm]	46	46	46	46	46
Max Current	I_{max}	[A]	26.7	50	73	88	100
Back EMF constant	K_e	[V/1000min⁻¹]	156	83	57	47	42
Torque constant	K_T	[Nm/A]	2.42	1.29	0.88	0.74	0.65
Rated Power	P_n	[kW]	2.76	5.0	6.6	7.5	7.9
Stator phase-phase Resistance (at 20°C)	R_{PP}	[Ω]	2.53	0.72	0.34	0.24	0.18
Stator phase-phase Inductance	L_{PP}	[mH]	40.4	11.5	5.4	3.8	2.9
Rotor inertia	J_m	[kgm² x 10⁻⁴]	12.8				
Electric time constant (at 20°C)	τ_{el}	[ms]	16				
Thermal time constant	τ_{therm}	[min]	36				
Motor mass without brake	m_M	[kg]	15.2				
Motor mass with brake	m_{MB}	[kg]	17.8				

FIGURE 5.4:DATA SHEET OF PMSM MOTOR USED in THE EXPERIMENT: BMD 145/ 16.8 Nm/3000rpm /400V.

Fig. 5.5 shows instead the operational limits in the Torque-speed diagram of the same motor. The curve for 3000 rpm should be considered.

81
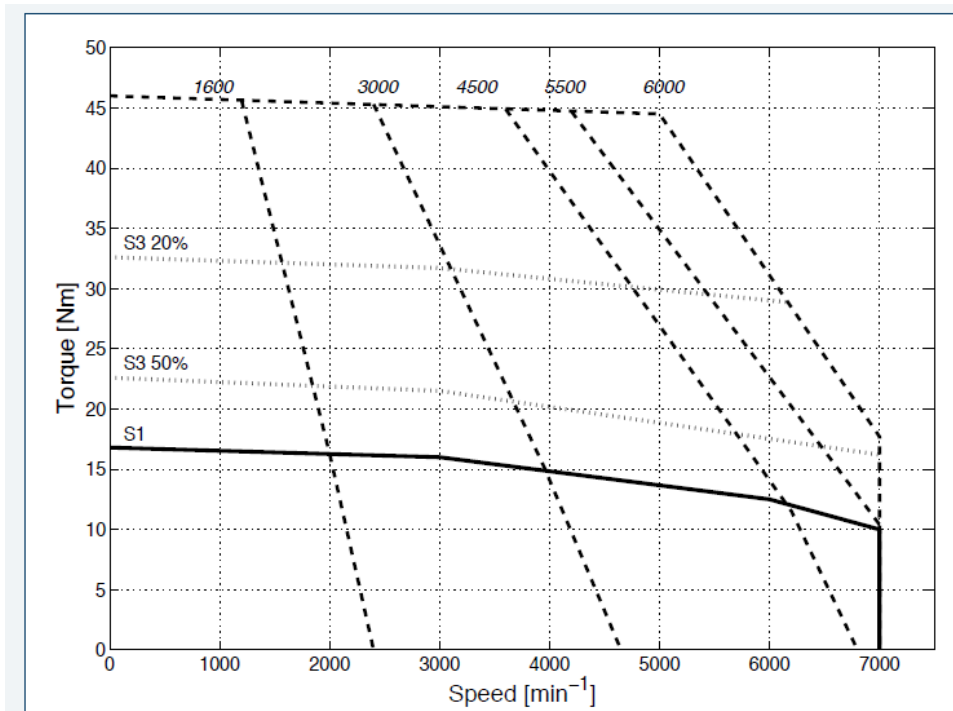
FIGURE 5.5: OPERATIONAL LIMITS FOR THE SERIES OF THE MOTOR SELECTED.

Furthermore, the gearbox flanged with the motor is presented like the previous components in its commercial data sheet provided by the company in Fig. 5.6. The gearbox used was a planetary gearbox with low backlash and high torsional stiffness. It has a gear ratio of 5, nominal input torque of 36 Nm.

		M_{n2}	M_{a2}	M_{p2}	n_1	$n_{1\,max}$	φ_S	φ_R	C_t	SB $R_{2\,max}$	SB $A_{2\,max}$	HB $R_{2\,max}$	HB $A_{2\,max}$	η	J_G [kgcm²]			
i		[Nm]	[Nm]	[Nm]	[min⁻¹]	[min⁻¹]	[arcmin]	≤	$\left[\frac{Nm}{arcmin}\right]$	[N]	[N]	[N]	[N]	%	11	14 - 19	24	28	32-38
TQ 090 1_3		130	200	400	2500	4500	3'	2'	28	4800	4300	6600	5900	97	–	2.18	2.30	2.69	4.48
TQ 090 1_4		200	300	500	2500	4500	3'	2'	28	4800	4300	6600	5900	97	–	1.63	1.75	2.14	3.93
TQ 090 1_5		180	280	500	2500	4500	3'	2'	28	4800	4300	6600	5900	97	–	1.39	1.52	1.90	3.70
TQ 090 1_7		160	250	500	3000	4500	3'	2'	28	4800	4300	6600	5900	97	–	1.19	1.32	1.70	3.50
TQ 090 1_10		110	170	350	3000	4500	3'	2'	28	4800	4300	6600	5900	97	–	1.08	1.21	1.59	3.39

FIGURE 5.6: DATA SHEET OF THE GEARBOX TQ 90 i5.

The measurement set up is depicted in the picture Fig. 5.7.

82

FIGURE 5.7: SET UP of the EXPERIMENT. MOTOR+GEARBOX UNDER TEST, TORQUEMETER AND GENERATOR MOTOR.

The data collected and measured are the following ones:

- DC voltage after rectifier (about 570 V)
- DC Current
- AC Current after the inverter
- Temperature of the case of the motor through thermocouple K
- Temperature of the case of the gearbox through thermocouple K
- Torque and speed after the gearbox

The electrical and mechanical measurements are input of a power analyser that collect, order and manipulate the data achieved. The data are saved online and fitted in an Excel file to be easily read and used. The main worry is to ensure that the motor and the windings have a steady state temperature. In this case the evolution of the temperature is monitored thanks to the thermocouple. When the variation of this latter is less than 5 degrees in an hour the motor is considered to be in thermal equilibrium and the measurement can start. The IEC 60034-1 suggests 2 degrees but since the evolution of the temperature follow a logarithmic law the difference is small. Moreover, to check moreover the maximum overtemperature of the winding IEC 60034-1 gives many recommendations to achieve an

accurate measurement of the resistance. Since the measurement occurs after shutting the motor off the temperature rapidly decreases and the value of the resistance should be extrapolated. This might bring to significant error in the estimation of the temperature even with a slight error in the resistance value. This measurement takes place to ensure that the insulation does not exceed its operational temperature defined by the insulation class: in this case class F defines a maximum temperature of 155°C. For the same reason mentioned in the beginning of the chapter this measurement is relevant for the test because the motor is tested in a different operating condition that is a worse case than the one usually checked with the motor alone. Thus, a derating factor might be necessary for the continuous operation.

The measurement tools are hereby presented in details:

- Current Transducer: LEM IT 60-S
- Power Analyser: Yokogawa WT 3000
- Torque meter: KTR Dataflex 16/50
- Thermocouple K type
- Thermocouple Transducer: LKM 232

The accuracy of the tools is quite high while as explained previously the accuracy of the efficiency prediction is unavoidably quite poor. Therefore, the analysis of the uncertainty propagation due to the use of several measurement tools, is not performed. The uncertainty would affect the efficiency values in a not significant way.

In this kind of setup mechanical oscillations may arise and compromise the accuracy of the measurement.

The two motors should be controlled in a way that avoids any kind of instability. One possible solution is to implement a speed control for the one that works as motor and a torque control for the other one that works as generator. Any kind of load profile might be simulated changing the torque produced by the generator.

Different possibilities were investigated in the past by the R&D department but for this case the choice described seemed the most reasonable.

5.2 Results

The working cycle chosen for the experiment is presented in Table 5.1. The maximum torque usable was the size of the torque meter that was 50 Nm. The choice of a gearbox ratio of 5 means that the input torque of the gearbox cannot exceed 10 Nm. The first three points are maintained for a long time in order to heat the motor up. The temperature is continuously monitored with the thermocouple and when the variation in an hour is less than 5 degrees the thermal exchange is considered as steady state. Therefore, the first point is calculated with a temperature of the frame of the motor of 80°C. The second with 100°C and in the third the motor is heated up to the maximum temperature of 125°C on the frame of the motor. The other 5 points between 120°C and 115°C are measured after the motor has reached a steady state temperature. The evolution of the temperature is depicted in Fig. 5.8.

	Motor Input Torque	Input Speed	Frame Motor Temp
1	9 Nm	1500 rpm	80 °C
2	5 Nm	3000 rpm	100°C
3	9 Nm	3000 rpm	125°C
4	9 Nm	2250 rpm	120°C
5	5 Nm	2250 rpm	118°C
6	5 Nm	1500 rpm	116°C
7	9 Nm	750 rpm	115°C
8	5 Nm	750 rpm	113°C

Table 5.1: working points of the experiment.

Figures 5.9, 5.10 and 5.11 show the working points of the cycle in the torque speed diagram and power speed diagram. Those graphs help visualizing and understanding how much of the available performance of the component is exploited.
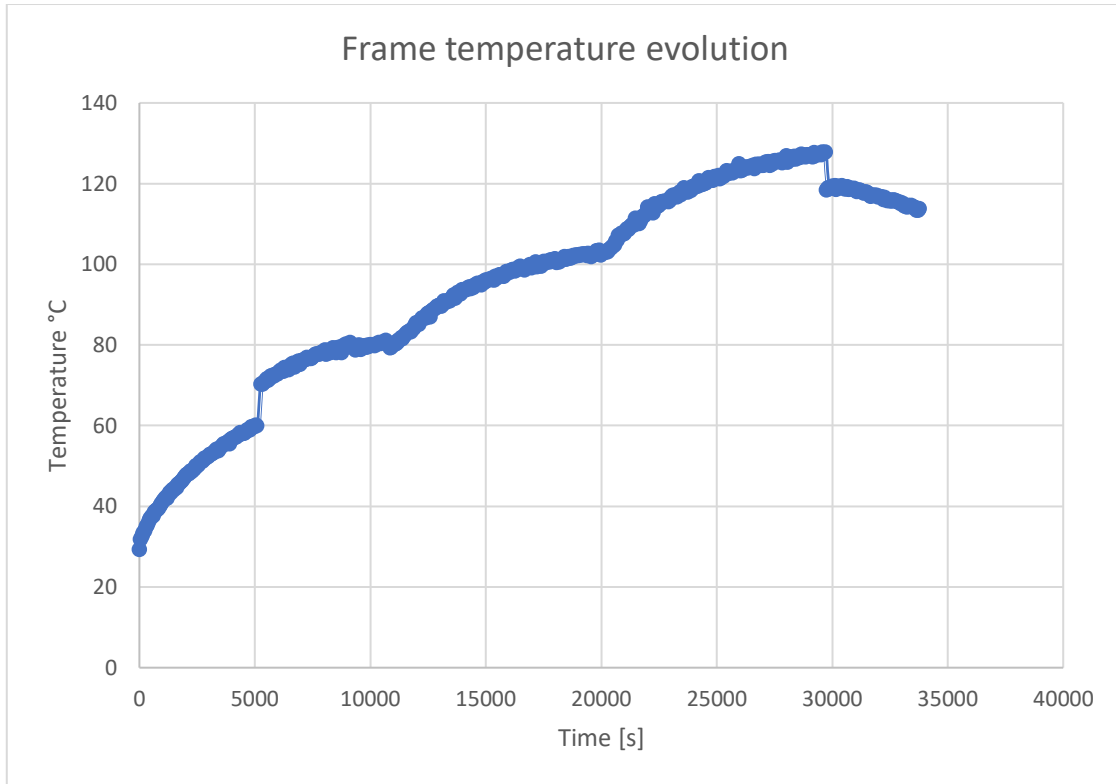
FIGURE 5.8: EVOLUTION OF THE TEMPERATURE ON THE FRAME OF THE MOTOR.
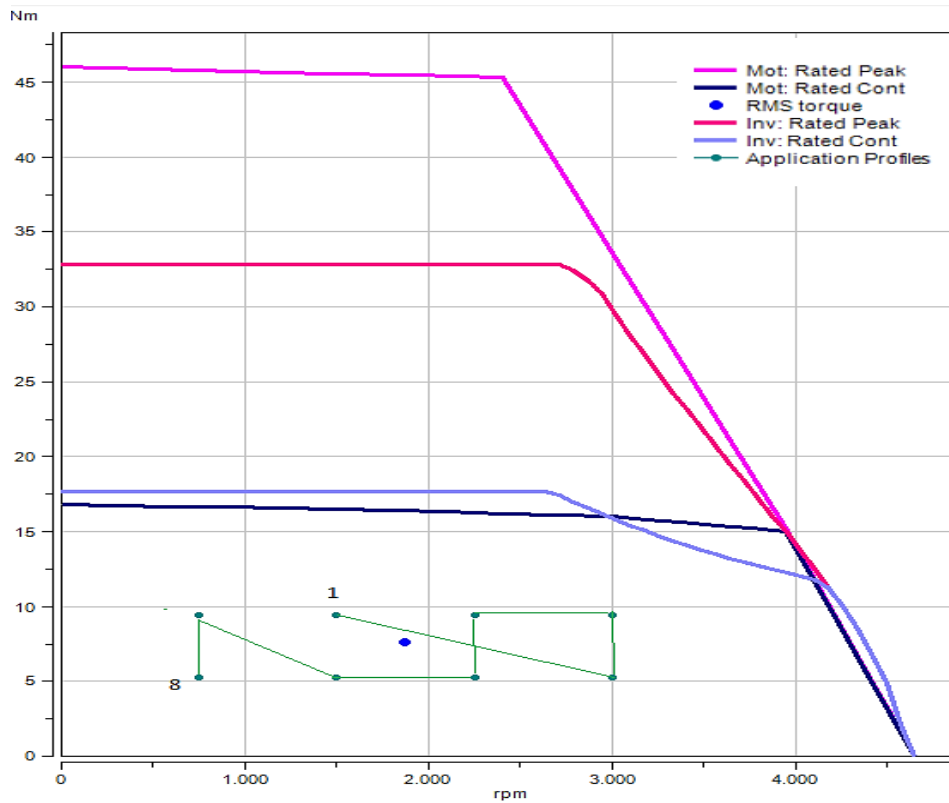
FIGURE 5.9: WORKING POINTS ON THE TORQUE SPEED DIAGRAM FOR MOTOR AND INVERTER WITH OPERATIONAL LIMITS.
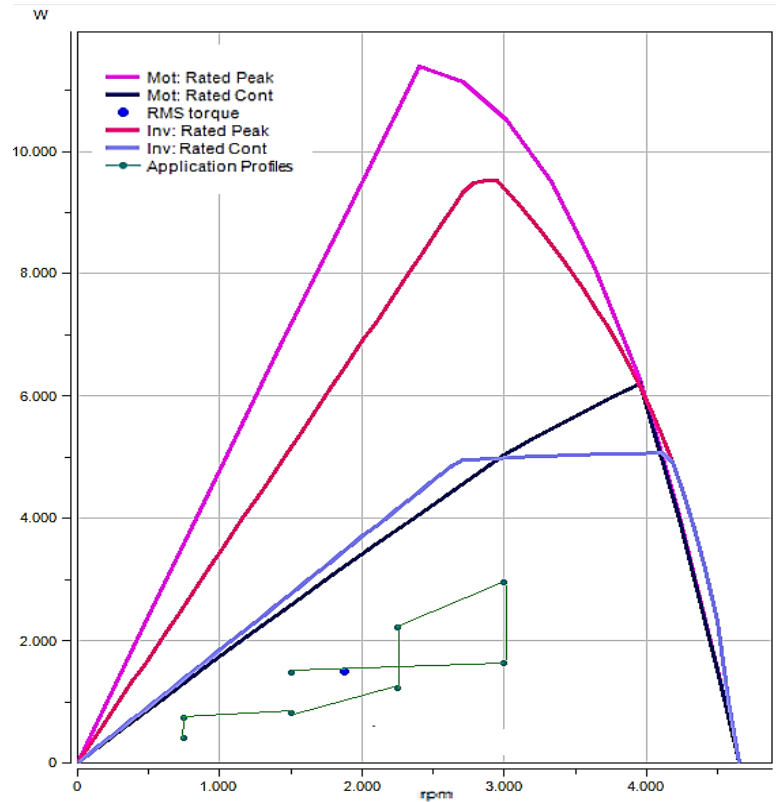
FIGURE 5.10: WORKING POINTS ON THE POWER SPEED DIAGRAM OF THE MOTOR AND INVERTER.
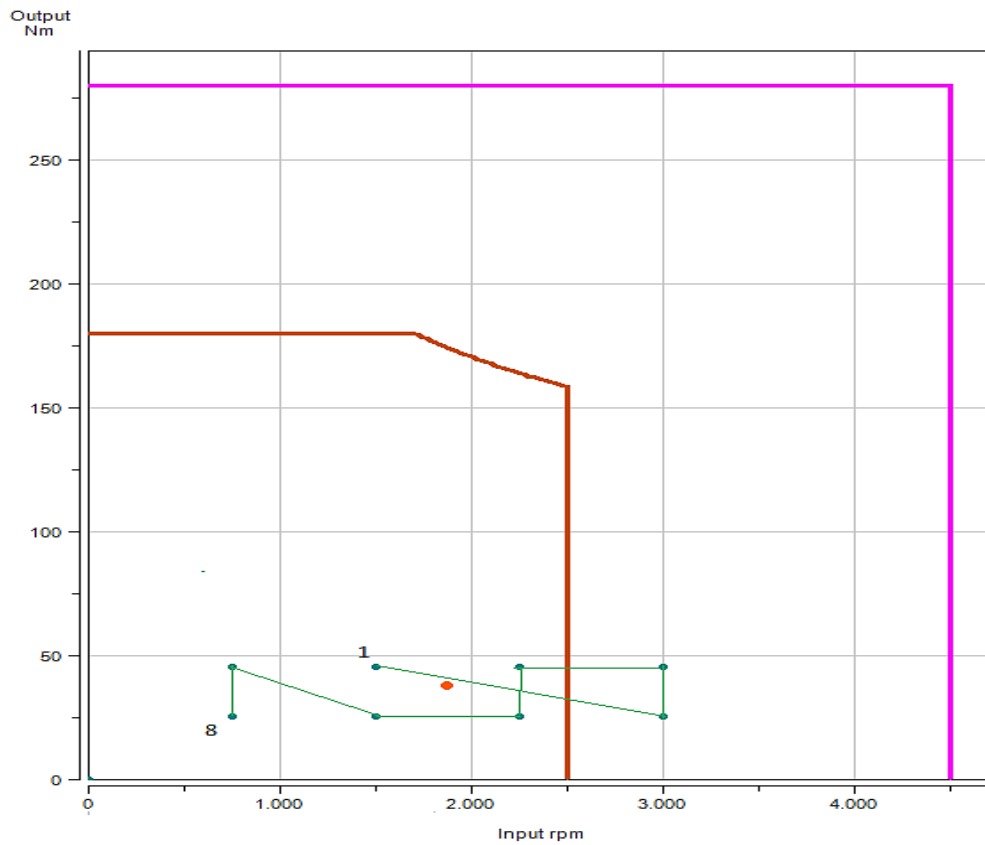
FIGURE 5.11: WORKING POINTS ON THE TORQUE SPEED DIAGRAM OF THE GEARBOX WITH OPERATIONAL LIMITS.

5.2.1 Resistance Measurement

The measurement of the resistance is reported for the point in which the frame motor is the highest one. This kind of measurement is useful to evaluate the maximum temperature of the windings. Since they are not accessible, the motor is stopped and unplugged and the measurement takes place with an ohmmeter. As the IEC 60034-1 suggests the value of the resistance should be extrapolated from the data achieved because the time needed to disconnect the motor and connect the ohmmeter is relevant. In fact, even minor change in the value of the resistance affects significantly the temperature derived from the calculation. The temperature of the windings is derived with the (5.1).

$$\Theta_x = \frac{R_x\,(234.5 + \Theta_{cool})}{R_{cool}} - 234.5 - \Theta_{amb} \qquad (5.1)$$

The case of the third point is presented. This one in fact heats the motor till the maximum temperature among the one used in the experiment and therefore the temperature of the windings is verified for the worst case. These are the results of the ohmmeter in Fig. 5.12.
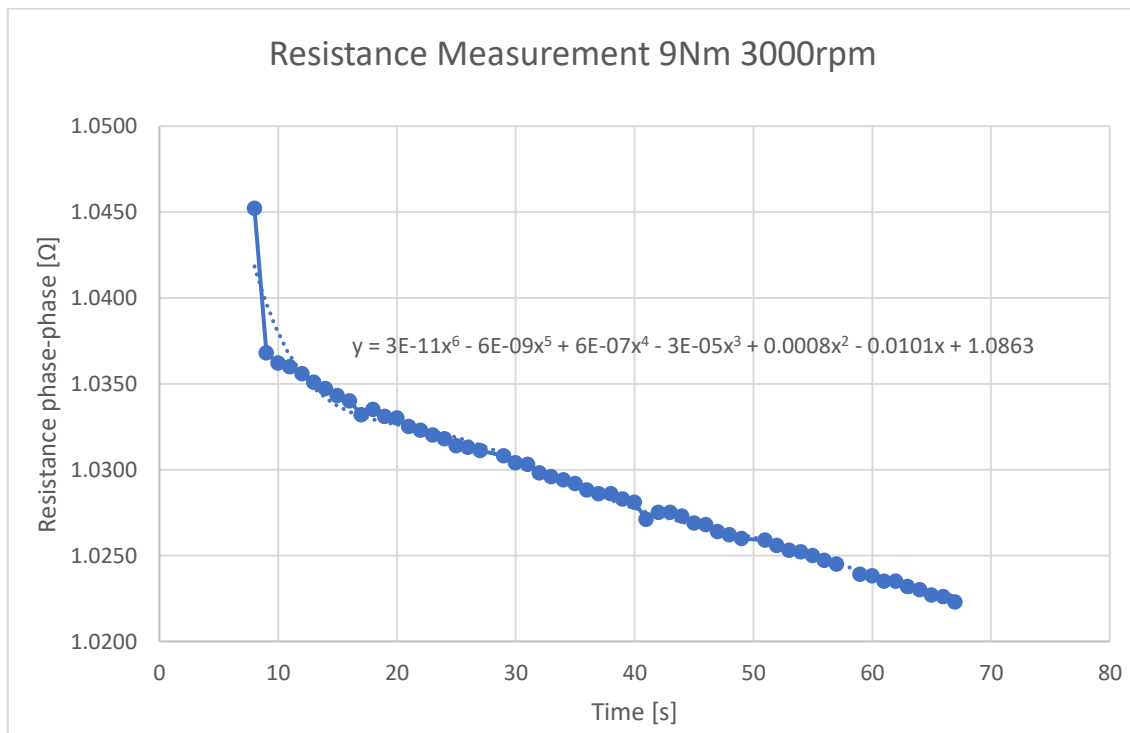
FIGURE 5.12: RESISTANCE EXTRAPOLATION.

The data are interpolated with a polynomial and the value considered for the resistance is the value extrapolated for the time equal to zero.

In (5.1) the resistance of the data sheet, that is measured at 20°C, can be used or to enhance furthermore the accuracy the resistance should be measured while the motor is still cool before starting the experiment. The ambient room temperature while the measurement occurred was 32°C. The maximum temperature of the windings is 149.7°C with an overtemperature of 117.7°C. The value of the overtemperature exceeds the 105°C for insulator of class F. The fact occurs since a derating factor must be applied when the motor is flanged with a gearbox. The R&D division commonly tests for half of the nominal load (8Nm) while the case presented has a bigger load (9Nm). Results are depicted in Table 5.2.

|	Rpp [Ω]	Ambient Temp [°C]
Resistance Cool	0.72	20
Resistance Max Temp	1.0863	32
	Temp [°C]	
Overtemperature	117.7	
Windings Max Temp	149.7	

Table 5.2: Resistance measurement and overtemperature calculation.

5.2.2 Efficiency calculation comparison

With the information of the resistance then the joule losses can be derived and separated from the total ones.

The main purpose of the experiment was to investigate the error of the efficiency map presented in Chapter 4. Hereby the results of the experiment and of the map are compared. The losses are calculated as the difference between the power measured after the inverter and the mechanical power measured with the torque meter.

The error in the prediction is significant and it increases at high speed. This seems reasonable since the gearbox heats up more at high speed and therefore the differences between the condition of the heat exchange in which the maps are derived and the one considered for the experiment are even more different.

Table 5.3 shows in details the prediction with the efficiency map for each working point and the efficiency values. Table 5.4. includes the total efficiency results from the experiment and from the method with the maps.

	Motor and gearbox losses with efficiency maps	Motor and gearbox losses from experiment	Error in the prediction
9Nm-1500rpm	205 W	222 W	-17 W
5Nm-3000rpm	238 W	327 W	-89 W
9Nm-3000rpm	307 W	386 W	-79 W
9Nm-2250rpm	258 W	319 W	-61 W
5Nm-2250rpm	192 W	232 W	-40 W
5Nm-1500rpm	142 W	146 W	-4 W
9Nm- 750rpm	149 W	153 W	-4 W
5Nm- 750rpm	89 W	81 W	+8W

Table 5.3: Losses calculation comparison.

	Motor		Gearbox		Total with maps	Experiment
1	89 W	94%	116 W	92%	87%	86%
2	65 W	96%	173W	90%	86%	83%
3	122 W	96%	185 W	94%	90%	88%
4	104 W	95%	154 W	93%	89%	86%
5	48 W	96%	144 W	89%	86%	83%
6	34 W	96%	108 W	88%	85%	84%
7	77 W	90%	72 W	90%	83%	82%
8	23 W	94%	66 W	85%	81%	83%

Table 5.4: Efficiency comparison.

The efficiency is overestimated in the high-speed region while it seems more reliable in the low speed one. A derating factor might be introduced to consider this deterioration after other experiments are conducted.

With the precise information about the resistance Joule losses can be calculated with high accuracy with (5.2).

The Table 5.5. shows the separation between the losses of the motor in joule and others.

$$P_{cu} = \frac{3R_{pp}}{2}(\theta)\frac{T^2}{k_{Trms}^2} \tag{5.2}$$

The torque constant should be the ratio between the torque and the Rms of current needed. The approximation of the method with the map is significantly. In the map for the S1

continuous operation the temperature is scaled with the level of the load so the joule losses for 9 Nm or 5 Nm are calculated with a lower temperature than in the experiment. This error may be corrected deriving the values of the other losses and inserting then the real joule losses.

	Resistance p-p	Joule Losses real	Joule Losses with map	Other Losses (Iron+ mechanical) with map	Real joule losses+ others with map
1	0.897 Ω	66 W	56 W	33 W	99 W
2	0.9542 Ω	22 W	17 W	48 W	70 W
3	1.086 Ω	79 W	56 W	66 W	145 W
4	1.072 Ω	78 W	56 W	48 W	126 W
5	1.066 Ω	25 W	17 W	31 W	56 W
6	1.06 Ω	24 W	17 W	17 W	41 W
7	1.055 Ω	77 W	56 W	21 W	98 W
8	1.05 Ω	24 W	17 W	6 W	30 W

Table 5.5: Motor losses separation.

The Joule losses are underestimated in the method (for continuous operation) whenever the temperature is near the maximum one since the temperature was scaled with the percentage of the nominal load applied. In this case, instead, the temperature after point 3 is the maximum one and it slightly decreases from 125 °C to 113 °C. Part of the error seen in Table 5.3. can be removed introducing the error derived from the calculation of the Joule losses. It is worthy to notice that the evolution of the temperature strictly depends on the working cycle and on the environmental condition. It is not possible to predict its evolution for a wide range of cases but it seems reasonable to adapt the situation to the method used for the map calculation.

Table 5.6. shows the comparison of the results between the experiment and the maps prediction after the correction of the error in the Joule losses.

Efficiency motor +gearbox with maps after correction	Experiment	Losses motor and gearbox with efficiency maps	Losses motor and gearbox from experiment
87%	86%	215 W	222 W
86%	83%	243 W	327 W
89%	88%	330 W	386 W
88%	86%	280 W	319 W
85%	83%	200 W	232 W
84%	84%	149 W	146 W
80%	82%	170 W	153 W
81%	83%	96 W	81 W

Table 5.6: comparison after correction of the Joule losses.

The error in the prediction of efficiency with the maps is more significant at high speed because the gearbox produces more losses and the heat exchange is slower. Besides this inherent error, the results achieved with the maps are reasonable and they can be considered as valid values with an accuracy of ± 3 % in the overall efficiency value.

5.2.3 Inverter Efficiency

Eventually the results of the inverter efficiency are reported. The converters are known to be very efficient and it is common to consider value over 95%. The only direct influence considered is the switching frequency since it is a choice of the customer and it depends on the application. Higher switching frequency decreases the efficiency. Hereby the results highlight a strong dependence of the inverter efficiency on the speed of the motor and on the torque too. Deriving an efficiency map for the inverter was considered less important because of the very high values of it but, after these results instead, it seems necessary as for the other components. At low speed the inverter efficiency decreases significantly. If the motor is forced to work at low speed the overall efficiency is even poorer than the one described because of the converter. It is worth to notice, moreover, that the inverter has to transmit the power needed by the mechanism and the losses dissipated on the other components. A lower value of efficiency means thus higher amount of losses because the power is higher in comparison to the motor and the gearbox. Tables 5.7 and 5.8 report the results of the measurement of the inverter losses. Eventually, Fig. 5.13 shows the evolution of the efficiency with different speed and two level of torque.

Inverter Losses				
	750 rpm	1500rpm	2250rpm	3000 rpm
9 Nm	147 W	150 W	165 W	171 W
5 Nm	111 W	121 W	135 W	158 W

Table 5.7: Inverter Losses.

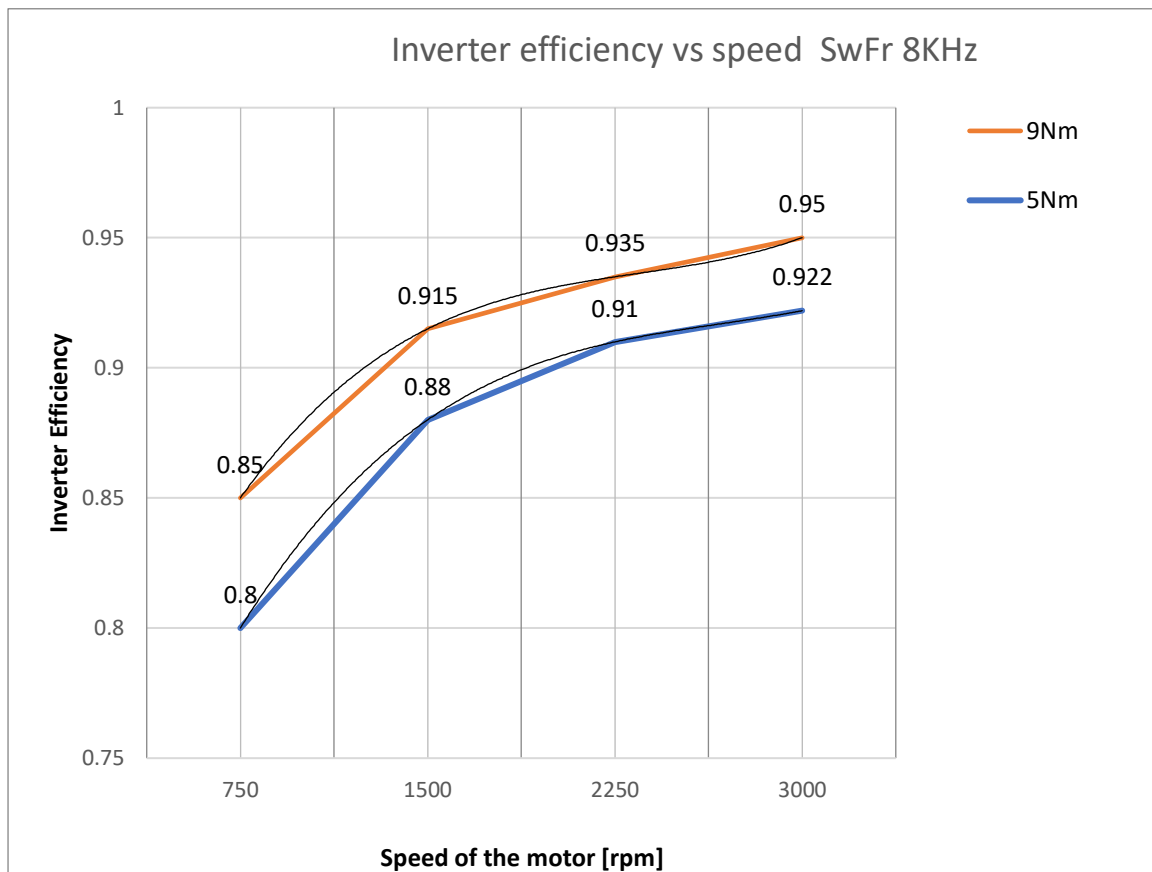| Inverter efficiency				
	750 rpm	1500rpm	2250 rpm	3000 rpm
9 Nm	85%	91.5%	93.5%	95%
5 Nm	80%	88%	91%	92%

Table 5.8: Inverter Efficiency.

FIGURE 5.13: EFFICIENCY OF THE INVERTER FOR DIFFERENT LOAD.

Chapter 6

SIZING PROCEDURE INCLUDING ACCURATE EFFICIENCY EVALUATION

Chapter 4 presented a way to increase the accuracy of efficiency evaluation without an excessive computational effort. The efficiency maps are tested and the results are reported in Chapter 5. This last chapter has the purpose to use the experimental and theoretical analysis to optimize the sizing procedure. When sizing a Servo-axis different project scenarios can be proposed to fulfil mechanical robustness and thermal criteria but usually the selection is not considering efficiency and TCO analysis. The criteria hereby considered aim to minimize the energy consumption and with the improved evaluation of the efficiency they may provide a more reliable prediction.

Increasing the efficiency of the single components is sometimes useless without checking the entire Servo chain. Firstly, the product of the efficiencies depends mostly on the worst one. In industrial applications for instance, when a worm gear is present (η=50-70%) even a revamping of an induction motor with a more efficient brushless motor may be less effective since the benefit is partly wasted. In the Servo control applications, instead, where planetary gearboxes are chosen all the three components exhibit a nominal efficiency over 85% therefore they all matter equally. The inverter shows the highest one and for this reason it is not characterized by an efficiency map like the others even though the results of the experiment suggest a deeper investigation. Slightly change can be considered introducing an option that decreases it with higher switching frequency chosen for the application.

The demanding improvement is to estimate the efficiency through all the work cycle and in the entire torque speed diagram. Due to the complexity of the losses prediction, as mentioned in chapter 1, dynamically simulating many different configurations of products from the efficiency point of view need many resources. What happens even in major mechatronic companies is a sizing procedure made to ensure the mechanical robustness and thermal loadability of the solution with an affordable initial cost on the components. This approach, although, has to be improved with the point of view of proposing the lowest Total Cost of Ownership in the next 5 or 10 years. In order to check the TCO the analysis about the efficiency plays the main role. It is worth to mention that considerations about

the reliability of the products to predict and to minimize unavailability and maintenance cost may be always more considered. In this chapter a common procedure for the sizing is presented and the increased accuracy of the efficiency evaluation is integrated in the method.

6.1 Servo Drives selection criteria

The mechatronic system is composed by [1]:

- mechanical components such as driving elements and gearboxes
- electromechanical components such as motor, brake and angle sensors
- the inverter as central electronic component
- software in the inverter for control and communication system

For each of these components several different types and options may be found in order to meet the requirements of the load. A solution should be found according to these principles:

- torque requirement and overload capacity: as fast as possible or as necessary
- position accuracy and repeatability: as precise as necessary
- economic criteria: as affordable as possible

The dynamic and static performance of the load has to be fulfilled ensuring an extended lifetime of all the components. The mechanical and electrical operation limits are therefore underlined. Firstly, overload can cause a mechanical damage to the gearbox. Secondly the continuous operating limits are defined by the overheating of the motor and of the gearboxes. Finally, the inverter defines the maximum speed limits through the maximum output voltage and the maximum torque through the maximum ampere. Higher temperature decreases the reliability of the insulators, capacitor, bearings and seals.

The crucial objectives can be summed up in 4 points:

- performance demanded: torque, speed and acceleration ramps required
- mechanical strength
- thermal design within the limits of the components
- economic aspects to optimize costs throughout the life cycle

Inside the economic design the total cost of ownership should be also taken into account as explained in the chapter 1.

The load profile is fulfilled combining a high acceleration capability with a gearbox able to adapt the slow motion of the load to the quite high-speed operating region of the motor. The use of gearbox is fundamental since the electrical motors can easily rotate at high speed and the use of gearbox may reduce remarkably the size and the price of the motor. The proper ratio minimizes the size of the motor (or the torque) reducing its cost. The gearbox ratio is the major degree of choice of the selection and it is defined as:

$$i = \frac{n_{motor}}{n_{load}} \tag{6.1}$$

The basic principle is to adapt the operating limits of motor to the load requirements through a proper ratio of the gearbox. Commonly, this choice is done in order to run the motor at its nominal speed and to reduce as much as possible the torque size of the motor. In fact, different maximum speeds change only the number and the section of the conductors in the stator, while increasing the torque means generally an increase in the radius therefore in the size and significantly in the cost too. From this approximated reasoning a reasonable estimated ratio can be found, subsequently an algorithm is developed to find the proper size of the gearbox [2].

Another crucial side of the choice of the ratio is the effect on the inertia mismatch that is defined as:

$$r = \frac{J_{load}}{J_{motor} i^2} \tag{6.2}$$

The ratio describes how relatively big is the inertia of the load "seen" by the motor through the gearbox. The presence of the gearbox decreases the inertia of load more than proportionally. A high value of the coefficient of (6.2) means that a remarkable part of the available torque is needed to accelerate. The Fig. 6.1 shows the problem of the coupling between two different inertial loads and the factors involved. The motor has the only rotor that exhibits low inertia for the need of high acceleration capability. To maximize the dynamic between motor and gearbox the value of the gear ratio may be optimized [3], for a pure inertial load, as:

$$i = \frac{\sqrt{J_{load}}}{\sqrt{J_{motor}}}$$

This means that if the inertia of the load and of the motor are the same the gearbox would not be needed. The optimized value would bring to an inertia mismatch (defined in (6.2)) equals to 1. The inertia of the motor can be much lower than the load (up to thousand times) if the proper gearbox is interconnected. A common rule of thumb in companies is to keep the inertia mismatch between 5 and 10. While under 5 there is mainly a matter of economical convenience, not exceed a value of 10 has a deeper and fundamental reason that may compromise the stability of the system.

The Fig. 6.1 shows the factors involved in the quality of the mechanical transmission. $B_{M/ML/L}$ are the viscous damping of the coupling between the motor and the ground, motor and load, load and the ground respectively. K_S is the coupling elasticity.
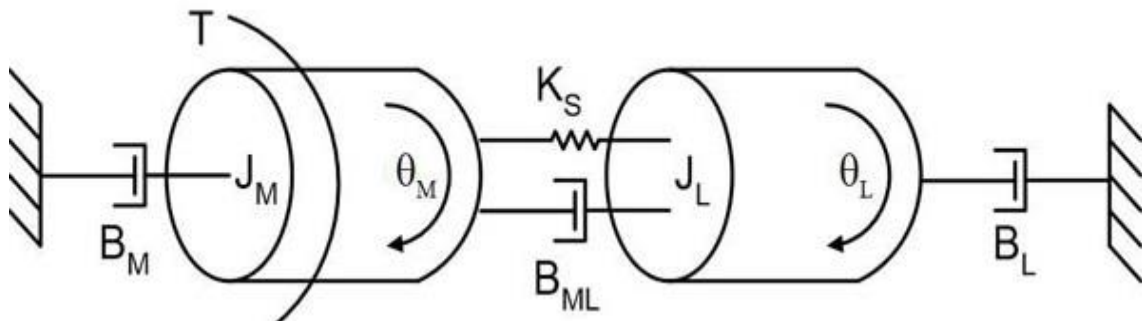
FIGURE 6.1: FACTORS THAT INFLUENCE THE MECHANICAL RESONANT FREQUENCY.

The inertia of the gearbox is neglected in this part of the analysis because it is very small for planetary gearbox [4]. In the following the limit value less than 10 for inertia mismatch is justified.

Firstly, a higher value would decrease the acceleration capability since the load would be much bigger than the rotor. But more important, the inertia mismatch defines the resonant frequency of the mechanical system. One of the main worries in the sizing procedure for Servo drives is the Servo stiffness. This quality means that a static and dynamical torsional stiffness is ensured in the system. The inertia mismatch, moreover, is involved in the quality of the mechanical transmission. Since every system shows compliance and elasticity (though neglectable in some cases) there is a mechanical resonant frequency in which the

system would lose the stability. This frequency decreases with the increasing of the compliance and of the inertia mismatch. When the resonant frequency is low there is a concrete risk that the bandwidth of the speed controller may be similar and it may bring to instability.

Since the controllers are tuned to ensure the stability with the possible fastest time response, the bandwidth of the speed controller is desirably quite high (order of hundreds of Hertz). If the inertia of the load changes a new tuning is necessary to ensure the proper answer of the system.

Because of the discretization of the control, the motor receives torque command not continuously. The interval of time is so fast that the inertia filters the oscillations. If the Servo stiffness has low quality due to compliance or high inertia mismatch firstly the system may not satisfy the requirements of the motion profile but it may also risk entering in an unstable behaviour [5].

From the control theory, the transfer function of the system gets far more complicated when an elastic coupling is introduced in the modelling while without it the inertia acts as a low pass filter as in (6.5). Moreover, it is evident that the ratio between load and motor inertia plays the crucial role. Systems that may exhibit remarkable compliance and elasticity are the ones in which a belt or a pulley is present for instance. To derive the transfer function of the mechanical system the equation at the shaft is reported in (6.4):

$$T_m - b\omega_m - T_L = (J_m + J_L)\frac{d\omega}{dt} \tag{6.4}$$

J_m and J_L are the inertia of the motor and of the load. b is a coefficient for the friction. After introducing the load torque as a disturbance, in the Laplace domain the function transfer can be written as:

$$\omega_m(s) = \frac{1}{(J_m + J_L)s + b}T_m(s) \tag{6.5}$$

If an elastic coupling is present, the (6.4) should be modified as:

$$T_m - b\omega_m - K_s(\theta_m - \theta_L) - T_L = (J_m + J_L)\frac{d\omega}{dt} \tag{6.6}$$

Where θ_m and θ_L are the angular position of the motor and of the load respectively. K_s is instead a constant for the elastic coupling. Since the position is equal to the integral of the speed (6.6) can be brought in the Laplace domain but a very complicated system describes now the dynamic of the system and it does not act as a low pass filter anymore. All in all the Servo stiffness may be affected by compliance in the system and by a high ratio of the inertia mismatch because the mechanical resonant frequency might decrease until the value of the bandwidth of the speed controller.

The inertia mismatch must be, therefore, checked with attention for any different loads and configurations of the mechanical parts to avoid the risk of instability. The ratio of the gearbox must be chosen considering its effect on this aspect. However, the value of the inertia mismatch can be changed also in other ways since an external mass can be added to the shaft to increase the inertia of the motor, often called flywheel. This last solution permits to avoid that the choice of the ratio only depends on the choice of the inertia mismatch.

Once that the quality of the servo stiffness is ensured the selection can consider a wider approach and different criteria to satisfy the customer.

The selection criteria considered more often in industry are [2]:

- minimization of motor torque
- minimization of weight and size
- minimization of Peak Power or peak current
- energy consumption

6.2 Calculation of the required performance

Fig. 6.2 shows which parameters are needed in the calculation. Each load requests a specific profile and exhibits singular weight and size. T_L, the load torque, includes the inertial and resistant torque of the load. Application engineer, during Servo sizing, proposes a specific combination of the products that satisfies the performance needed by the specific load.
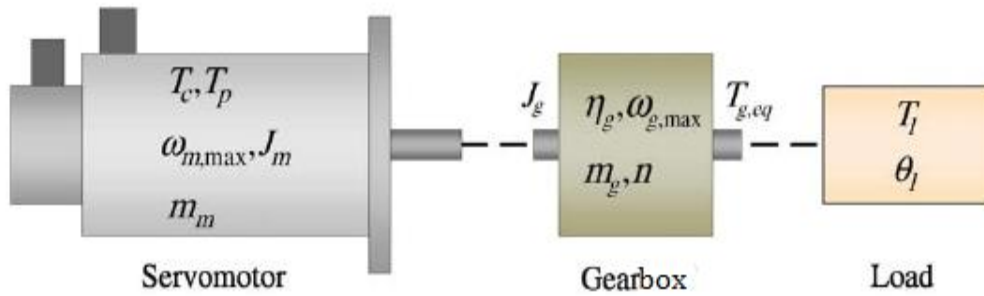
FIGURE 6.2: NEEDED PARAMETER FOR THE SIZING PROCEDURE.

To properly select the size of the component the operational limits of the latter are considered. For the type of the electrical motors considered (PMSM motor) the limits are cited in table 6.1. These limits are applicable for all permanent magnet motors but for brushed motors, where the peak torque limit is defined to avoid a faster decreasing of the life of the brushes.

	Reason
Continuous torque	Overheating of winding insulator
Peak torque	Demagnetization
Mechanical speed	Mechanical limit/voltage supply

Table 6.1: operational limits of electrical motors.

The peak motor speed can be sometimes adapted through the design of the windings and so if this possibility is available the only limit is the mechanical constraint.
The torque imposed to the motor is equal to:

$$T_m(t) = (J_m + J_g)\ddot{\theta}_m + \frac{T_L(t)}{i\,\eta_g} \tag{6.7}$$

Since the operational limit is for continuous operation the equivalent torque of a cycle of work is calculated as the RMS value. This choice derives from the equivalent thermal energy produced by the motor. Assuming that the main contribution is given by the joule losses the energy produced is proportional to the square of the torque (and of the current) and the equivalent torque for a load cycle can be calculated as:

$$||T_m(t)||_{Rms} = \sqrt{\frac{1}{\tau}\int_0^\tau ((J_m + J_g)\ddot{\theta}_m + \frac{T_L(t)}{i\,\eta_g})^2 dt} \qquad (6.8)$$

Instead, to verify the maximum peak torque, applied even for a small interval of time, the value that must be considered is the highest experienced in the entire cycle.

$$||T_m(t)||_{peak} = \max |((J_m + J_g)\ddot{\theta}_m + \frac{T_L(t)}{i\,\eta_g})| \qquad (6.9)$$

The torque of the motor depends therefore on the load, on the acceleration needed, on the inertia of the motor and on the inertia and the efficiency of the speed reducer.

For the gearbox, the phenomena behind the operational limit are more complex than for the motor. As mentioned in the Chapter 2 the prediction of the temperature of the oil or of the gears is really demanding. Moreover, the environmental condition and the type of working operation timing may affect the maximum performance. Therefore, because of the complexity behind the limiting factors, there is not a universal procedure as for the motors. In some gear catalogues a root mean cube is suggested to calculate the equivalent continuous torque as in (6.10). The pedix 2 indicates the output shaft, thus T_2 is the torque at the output of the gearbox and n_2 the speed of the slow shaft at the output of the gearbox.

$$T_{2RMC} = \sqrt[3]{\frac{(|T_{2\,(1)}^3||n_{2\,(1)}|t_1 + |T_{2\,(2)}^3||n_{2\,(2)}|t_2 + \dots + |T_{2\,(n)}^3||n_{2\,(n)}|t_n)}{n_{2\,(1)}t_1 + n_{2\,(2)}t_2 + \dots + n_{2\,(n)}t_n}} \qquad (6.10)$$

And an equivalent speed for the cycle as:

$$n_{2EQU} = \frac{|n_{2\,(1)}|t_1 + |n_{2\,(2)}|t_2 + \dots + |n_{2\,(n)}|t_n}{\Sigma t_i} \qquad (6.11)$$

The majority of real-world gear applications need an infinite life dimensioning ($>2\times10^6$ load cycles). For this reason, the recommendation of nearly all gear standards (ISO, DIN, AGMA) is to base the gearbox torque ratings on endurance limits and minimum bearing

life. The Fig. 6.3 shows instead the selection method for the gearboxes reported in the catalogue of Bonfiglioli.
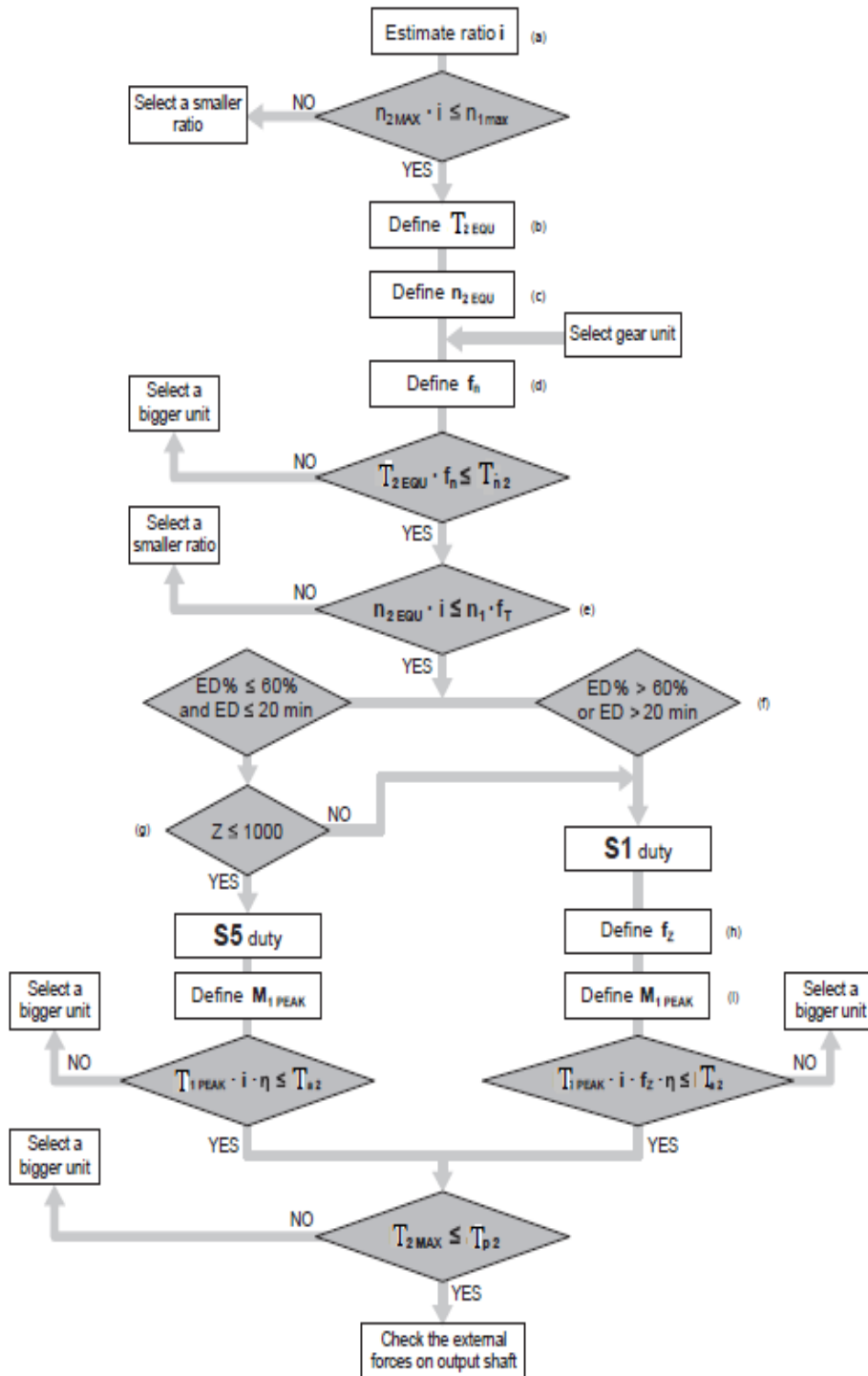

FIGURE 6.3: GEARBOX SELECTION METHOD [6].

The method used in a company should be able to cover a wide range of industrial application. Moreover, it has to ensure a reliable selection and to satisfy the lifetime requested for the specific application.

As it can be seen in Fig. 6.3 there are some derating factors that consider stress factor as high speed, high number of cycles and environmental condition.

f_n is a speed factor that imposes a derating in high speed conditions. f_t is a temperature adjusting factor and f_z is a cycles factor and it may decrease the maximum performance if the number of cycles designed for the application is particularly high.

Besides the equivalent torque there are several other factors involved in the selection of the proper size of the gearbox as environmental condition and limiting factors for high speed or continuous operating cycle. This selection method shows that for the selection of the gearbox many factors are involved and therefore many different possibilities would be possible. The one in Fig.6.3 exploits years of experience of the company and it may be more reliable than any other theoretical approach. About the gearbox, the manufacture's information should be considered in the calculation.

Last important parameter for the sizing procedure is the peak power requested to the drive system. Because of the small thermal inertia of the devices the converter should not be overloaded. The overload capacity of the converter is generally smaller than the PMSM motor since the electronic devices don't have much thermal inertia. The peak power thus, has to be precisely considered and not exceeded during all the operation cycle of the drive. The total power used by the motor is the sum of the one transmitted to the load and the one dissipated in heat during the performance.

$$P_m = P_{mech} + P_{loss} \tag{6.12}$$

In [2] the losses are approximated with the only joule losses that are the most important and they can be easily calculated.

The improvement inserted in the selection is to use the value of the losses derived from the efficiency maps for the specific load cycle. This information is more accurate because the total losses include iron and mechanical losses and depend on the speed besides the torque. Thus, the peak power that the drive must satisfy is:

$$P_{peak} = \max(P_{mech} + P_{loss}) \tag{6.13}$$

For the efficiency evaluation, what matters more is the total energy consumption. This can be derived as in (6.14) where P_{in} is the power flowing through the inverter:

$$W_{in} = \int_0^t P_{in} dt \tag{6.14}$$

Where

$$if\ P_m > 0 \rightarrow\ P_{in} = P_{in}$$
$$if\ P_m < 0 \rightarrow P_{in} = 0$$

The energy consumption strictly depends on the duration of the cycle and on the number of cycles per day. Only for continuous application (S1 cycle) the value becomes significant because the power involved in this application may be small.

As mentioned in Chapter 1 regenerative applications are not examined since they are still not so common in Servo drives due to the limited power involved. If a regenerative system would be present when the power is negative it is sent back to the grid or the other axis. Without it when the motor is braking and the power is negative, all the energy is dissipated in heat resistors.

6.3 Integration of Efficiency Maps in the selection

The components feasible for the application can be found following the principle presented. The following step is to select the most convenient combination of inverter, motor and gearbox to fulfil the requirements of the loads. The factors involved in the selection may be very different as mentioned in this chapter. Some applications may present specific requirements (as high inertia mismatch, compactness demanded, high radial forces on the bearings . . .) and it is worth to underline that each application may need a specific analysis. Nevertheless, there are specific softwares to help Customer Application engineers in the optimization but generally they still do not focus on efficiency with accuracy and a comparison between the software and the proposed method is presented.

The improvement proposed in this paragraph is to insert the more accurate calculation of the losses in the process of selection and in the energy consumption prediction. For an easy implementation, the efficiency maps described in Chapter 4 are approximated by a polynomial function of torque and speed. The torque and the speed experienced by the load should be discretized in a reasonable amount of points that describes the entire cycle. Then, couple of values of torque and speed are the input of the polynomial equation and the total losses for each working point are derived.

To better understand the comparison, a characterization of the assumption of the professional software is also needed.

In the software settings, the motor has an efficiency that reaches the nominal value and decreases at low speed as in Fig. 6.4.
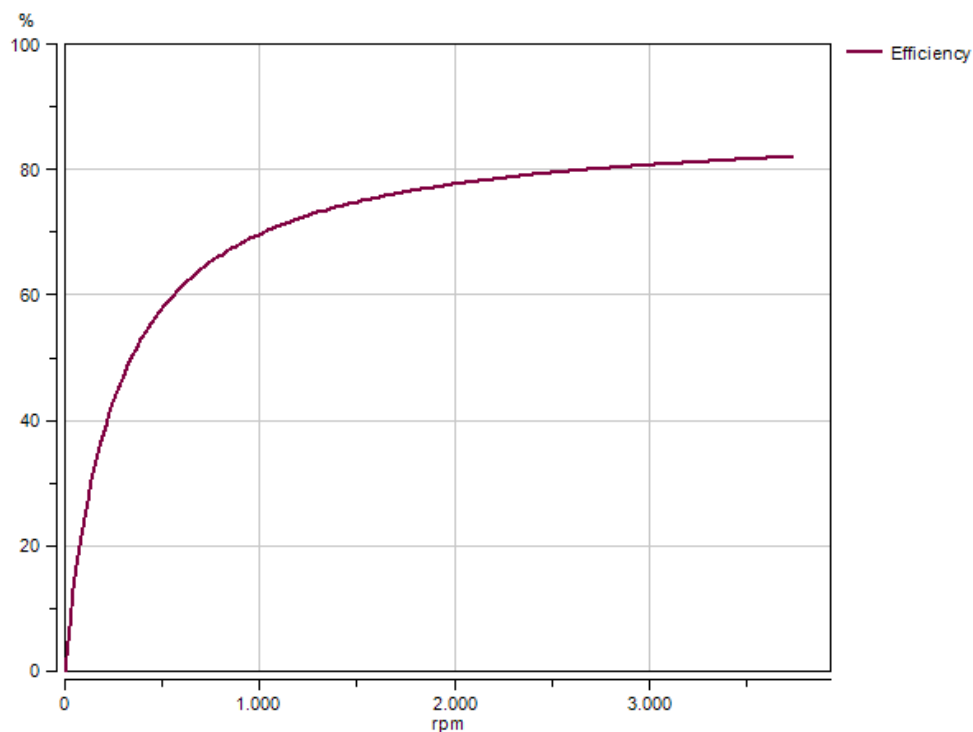

FIGURE 6.4: EFFICIENCY CHARCTERIZATION FOR MEDIUM SIZE MOTOR (AROUND 10Nm) IN THE PROFESSIONAL SOFTWARE.

The nominal value is about 80 % for small sizes and it increases until 90 % for bigger ones. Then the constant torque is considered slightly smaller at higher speed. This analysis includes only Joule losses of the motor and it is not possible to change the resistance

following the operating temperature of the windings. The inverter has a fixed nominal efficiency about 97 %.

Finally, the efficiency of the gearbox, without considering how many stages it has, is considered at 97 % and slightly decreases at low speed as in Fig. 6.5.
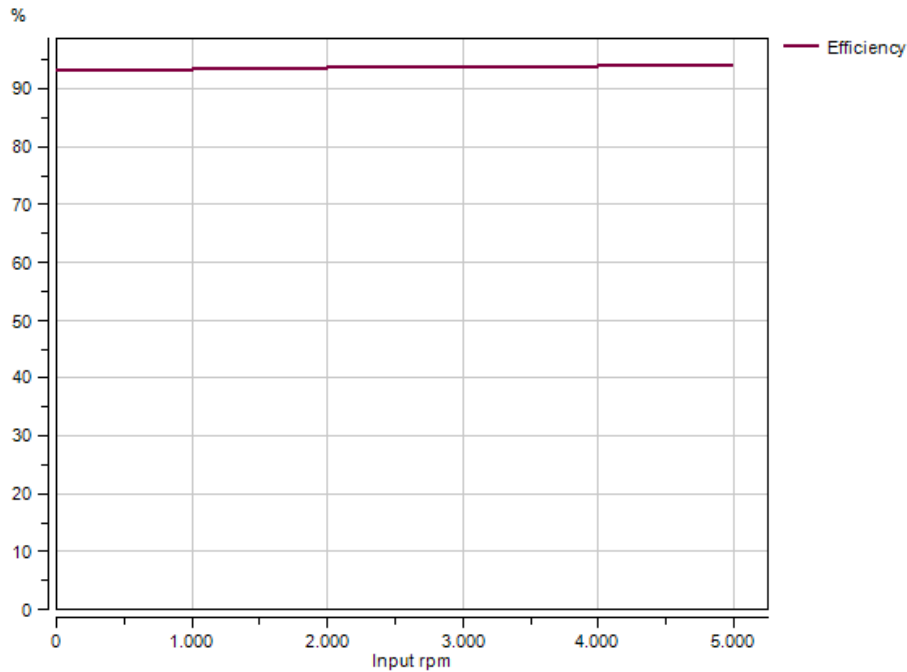

FIGURE 6.5: GEARBOX EFFICIENCY CHARACTERIZATION IN THE PROFESSIONAL SOFTWARE.

Firstly, the comparison between the results of the calculation with the proposed method and the ones obtained with the professional software for sizing procedure are presented. Table 6.2 shows the working cycle used and the losses predicted for the gearbox and for the motor with the proposed method. The cycle is the same used in the experiment of Chapter 5. This allows a comparison of the two methods with the results of a real application.

The torque of the motor is derived considering the efficiency of the gearbox that increases the torque asked by the motor. The temperature of the windings is measured and the resistance is corrected. The energy consumption can be calculated following (6.14).

Torque	Speed	Time	Gearbox Losses	Motor Losses	Total Eff
9 Nm	1500 rpm	0 s	116 W	111 W	86%
5 Nm	3000 rpm	60 s	173 W	73 W	86%
9 Nm	3000 rpm	120 s	185 W	145 W	89%
9 Nm	2250 rpm	180 s	154 W	126 W	88%
5 Nm	2250 rpm	240 s	144 W	56 W	85%
5 Nm	1500 rpm	300 s	108 W	41 W	84%
9 Nm	750 rpm	360 s	72 W	98 W	80%
5 Nm	750 rpm	420 s	66 W	30 W	81%

Table 6.2: Results with the method proposed.

To simplify the approach, losses and power equivalent for the cycle can be found as in (6.15) and (6.16).

$$Losses_{EQ} = \frac{\sum Losses_i t_i}{\Sigma t_i} \tag{6.15}$$

$$Power_{EQ} = \frac{\sum Power_i t_i}{\Sigma t_i} \tag{6.16}$$

Hereby the comparison between the energy consumption calculated with this method and with the values obtained by the professional software is presented. The price of KWh for industries is considered 0.15 €/KWh. The cycle is considered to last continuously 24 h per day per 365 days a year. Therefore, there are 180 cycles a day that last 480 s each. This justifies the correction of the resistance with the maximum temperature since it is a continuous and varying cycle, as confirmed in the experiment. Table 6.3 shows the comparison with the results obtained by the professional software.

Energy cost per year	Method with efficiency map	Professional software
Cost of the mechanism per year	1818 €	1818 €
Cost of losses of the motor per year	109 €	175.8 €
Cost of losses of the gearbox per year	167 €	64.8 €
Total Losses per year (from the experiment: 306.5 €)	276 €	240.6 €
Total cost of energy per year	2094 €	2058 €

Table 6.3: comparison between the proposed method and a professional software.

The slight difference in the total cost is the result of a balance between significant differences in the calculation of the single components. The software seems to underestimate motor efficiency, in particular for medium and big sizes, while it overestimates for all the gearboxes, in particular if more stages are used.

Moreover, with the results for the efficiency of the inverter a comparison between the prediction of energy consumption with the experiment and with the software is also presented to underline the difference in the results. Table 6.4 reports the comparison between the professional software and the results from the real measurements.

	Experiment	Professional software
Inverter Losses	190.5 €	63.7 €
Motor + Gearbox Losses	306.5 €	240.6 €
Total Cost per year with inverter	2315 €	2121.7 €

Table 6.4: comparison between the professional software and the results from experiment.

The inverter is considered almost ideal in the software. The results of the experiment instead highlight the significance of the inverter losses and therefore the prediction of the software seems very different from the real consumption.

6.4 Application case: scenarios comparison for hoist

Moreover, a case of a real application is presented. The method developed is used to predict the energy consumption.

The purpose of the method aims to help the Application engineers to make the most convenient choice for the customers. Different scenarios are always possible and it is sometimes difficult to choose a specific combination of products instead of another one. In this example that deals with a hoisting application, two different gearbox ratios are chosen. The first example has a ratio of 5 while the second of 16. This changes the size of the motor and the average speed in which the motor will work.

The size of the motor may be very important, if a compact solution is needed for instance, but the method focuses only on the efficiency evaluation assuming that no specific needs are demanded for the application. The bigger motor will show higher nominal efficiency

but it is more expensive and it may work at very low speed since the ratio of the gearbox is smaller. The smaller motor instead, even though it has a lower nominal efficiency, it may work at higher speed and it may show less losses. Furthermore, the gearbox with one stage has a better nominal efficiency than the one with two stages, but it is also longer in dimensions and more expensive.

Without an accurate analysis, it is impossible to have a reliable prediction of which one of the two cases is the most efficient.

A hoist application may include lifting and lowering. A very common structure is similar to the one depicted in Fig. 6.6 with a ball screw coupled with the output shaft of the gearbox. The figure is only an example and the software inserts an inclination of 90° degrees to consider a lifting application. The load cycle only includes the lifting because the lowering part involves many considerations about the regenerative braking that are not studied in this work. For this kind of application, the customers would receive many benefits from a regenerative setup or even only with increasing of the capacitance to increase the energy stored in the bus DC. Nevertheless, for the small power involved in Servo application it is still not so common that the customers decide to invest to install this improvement.

A professional software derives the load and the speed profile from the type of mechanism and the weight and the inertia involved. The requirements of the load at the output shaft of the gearbox are depicted in Fig. 6.7. Moreover, the torque speed diagram for different choices of the gearbox ratio are shown in Fig. 6.8 and 6.9.
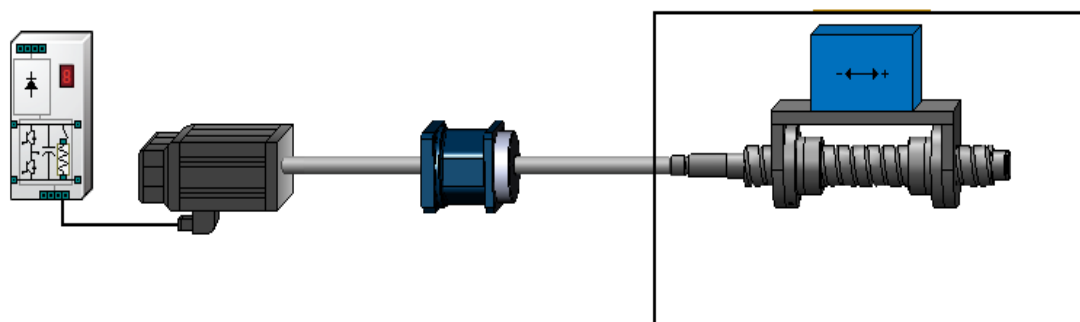

FIGURE 6.6: SCHEME OF THE COMPONENT FOR HOIST APPLICATION. (INCLINATION=90°).

The two scenarios are presented in Table 6.5.

	GEARBOX RATIO	MOTOR NOMINAL TORQUE	MOTOR NOMINAL SPEED	INVERTER NOMINAL CURRENT
SCENARIO 1	5	16.8 Nm	3000 rpm	7.8 A
SCENARIO 2	16	3.2 Nm	4500 rpm	3.8 A

Table 6.5: Main parameters for the two different Scenarios.

Two different scenarios are compared. They both fulfil the requirements of the load but they use a different gearbox ratio. Scenario 1 uses a lower ratio and so a bigger motor: it shows a higher nominal efficiency but it may work in low efficient points and at low speed (as in Fig. 6.8).
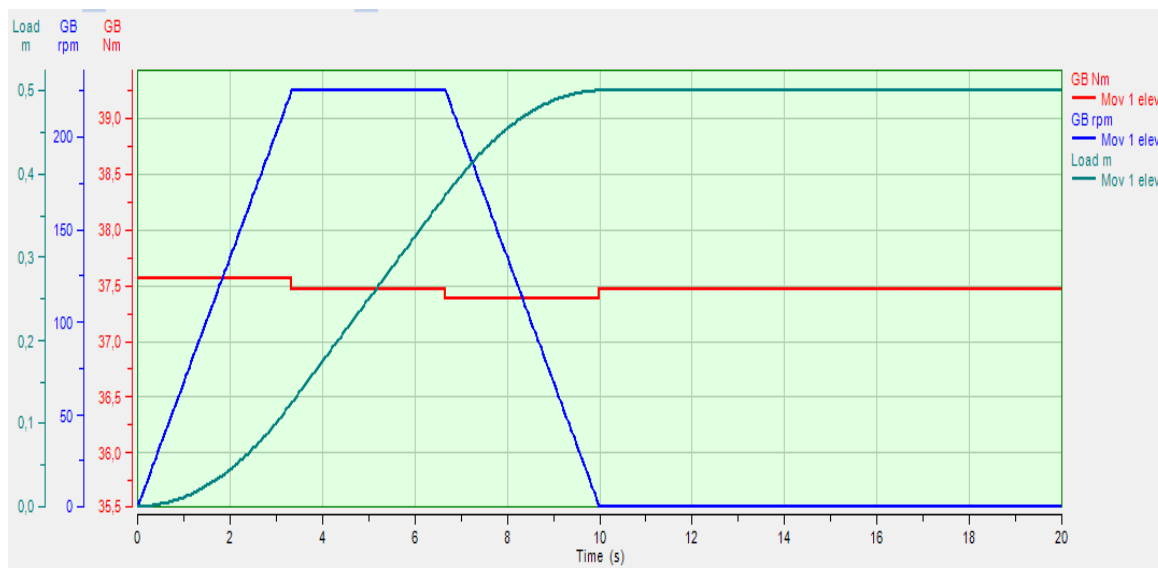

FIGURE 6.7: LOAD AND SPEED PROFILE REQUIRED AT THE OUTPUT SHAFT OF THE GEARBOX.

Scenario 2 uses a two stages gearbox that may increase the losses, but it allows it to use a smaller motor and a smaller drive and they are expected to work near the nominal point (as in Fig. 6.9).
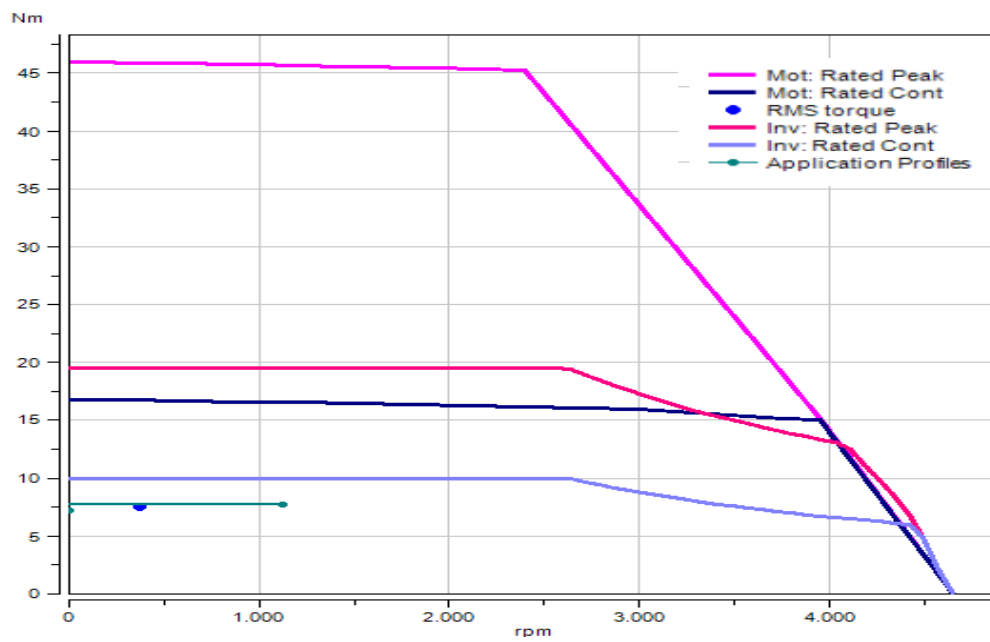
110

FIGURE 6.8: MOTOR AND DRIVE WORKING POINTS FOR A GEARBOX RATIO OF i=5. SCENARIO 1.
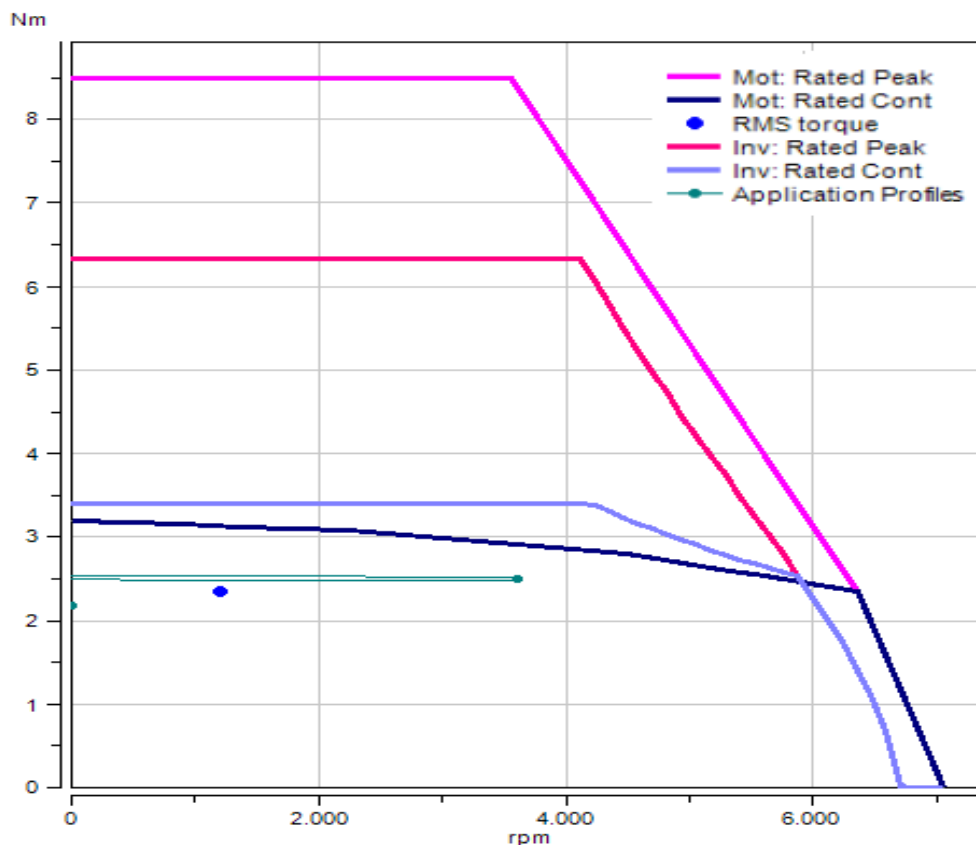

FIGURE 6.9: MOTOR AND DRIVE WORKING POINTS WITH A GEARBOX RATIO OF i=16. SCENARIO 2.

The torque and speed profiles are the input of polynomial equations that describe the losses produced by each component. The results of the calculation of the losses are reported in Table 6.6 and 6.7.

Torque 1 [Nm]	Speed 1 [rpm]	Losses TQ70i5 [W]	Losses BMD 145 [W]	Inverter Power [W]	Inverter Losses [W]
7.512	562.50	72.26	56.92	571.7	24.27
7.494	1125.00	74.75	56.13	1013.7	33.99
7.476	562.50	71.97	56.32	568.7	24.20
7.494	0.00	0.00	0.00	0.0	11.69
7.494	0.00	0.00	0.00	0.0	11.69
7.494	0.00	0.00	0.00	0.0	11.69
Average Losses [W]		36.50	28.23		19.59

Table 6.6: Results for Scenario 1.

Torque 1 [Nm]	Speed 1 [rpm]	Losses TQ70i16 [W]	Losses BMD 82 [W]	Inverter Power [W]	Inverter Losses [W]
2.347	1800.00	195.80	157.47	795.77	31.58
2.341	3600.00	317.22	156.52	1356.61	45.61
2.336	1800.00	195.01	156.04	791.42	31.48
2.341	0.00	0.00	0.00	0.00	11.69
2.341	0.00	0.00	0.00	0.00	11.69
2.341	0.00	0.00	0.00	0.00	11.69
Average Losses [W]		118.01	78.34		23.96

Table 6.7: Results for Scenario 2.

The inverter is characterized by the nominal efficiency provided by the manufactures and considering the stand by losses that occurs continuously even when the motor is still.

The total cost of the energy needed by the mechanism is the same for both the scenarios. Once the total cost of the losses per year is achieved an economic comparison can be done. Scenario 1 has a higher initial price since the drive and the motor are bigger and they are the most influent part in the bill of material. Even though the gearbox with two stages costs almost the double of the single stage the Bill of Material is higher of 210 € for the Scenario 1. Fig. 6.10 shows the economical comparison of the two scenarios.

Even though the initial price is higher, the first Scenario appears as the most convenient. The losses are significantly smaller and in less than 2 years the difference in the initial price would be completely paid back.

The assumption is that the cycle is repeated continuously for the entire year without stopping; the price of energy is considered 0.15 €/KWh.

The cost of the mechanism per year is the same for both scenarios and it is of 386 €/year. Total cost of energy per year is therefore: 497 €/year for scenario 1 and 676 €/year for scenario 2.
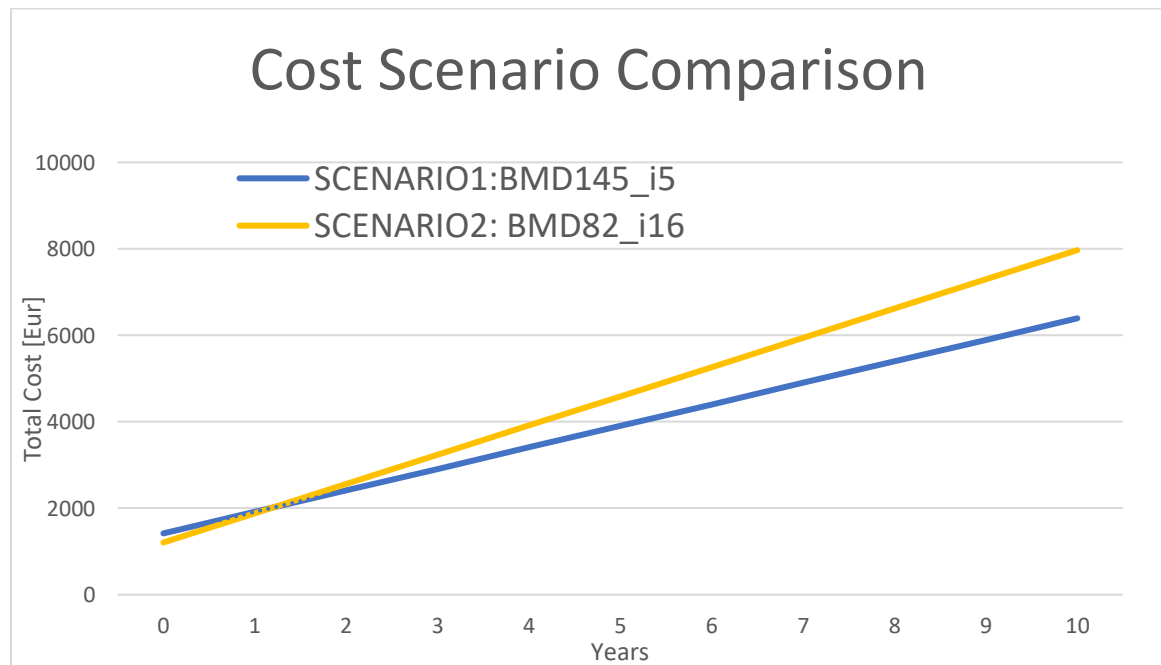

FIGURE 6.10: ECONOMICAL COMPARISON OF THE TWO SCENARIOS FOR HOIST.

The meaning of the results can be deducted from Fig. 6.11 in which the working points are shown on the efficiency map. Even though the choice of a small gearbox ratio forces the motor to work at low speed, since the motor is quite big it has good efficiency values also at low speed.
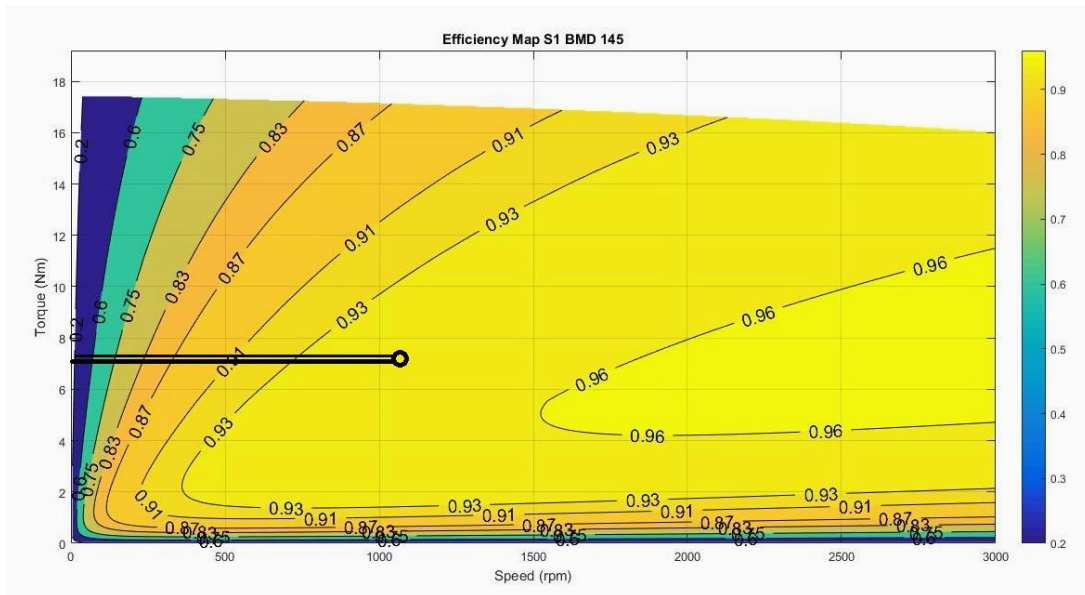

FIGURE 6.11: WORKING POINTS ON THE EFFICIENCY MAP FOR SCENARIO 1: MOTOR BMD 145.

Comparing with Fig. 6.12 it can be noticed that the higher gearbox ratio determines working points very near to the nominal efficiency. But the values are in any case smaller than for scenario 1.
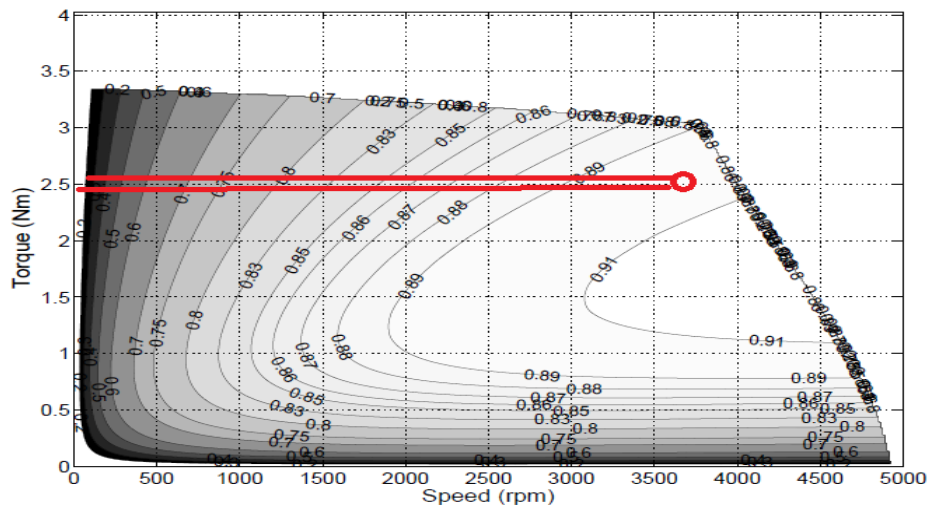

:

FIGURE 6.12*: WORKING POINTS ON THE EFFICIENCY MAP FOR SCENARIO 2: MOTOR BMD 82.

Reference Chapter 6

[1] Kiel, E. "Drive solutions: mechatronics for production and logistics", Springer (2007).

[2] Roos. F, Johansson. H, and Wikander. J, "Optimal selection of motor and gearhead in mechatronic applications," *Mechatronics*, vol. 16, no. 1, pp. 63–72, 2006.

[3] Pasch KA, Seering WP, "On the drive system for high performance machines" *ASME J Mech Transmiss Automat Des* 1984 vol.106, no. 1, 102-8.

[4] Ross. F, Spiegelberg. C, "Relations between size and gear ratio in spur and planetary gear trains". Technical Report, TRITA-MMK 2005:01, ISSN 1400-1179, November 2004

[5] Armstrong. RA, "Load to motor inertia mismatch: Unveiling the truth" Drives and Control Conference 1998, Telford, England. Kollmorgen Motion Technologies.

[6] Precision Planetary Gearboxes Catalogue (2015) Bonfiglioli Tecnoingranaggi.

Conclusions

The thesis aimed at an improvement in the prediction of the energy consumption of a mechatronic chain in order to provide a more reliable information to the customers in the TCO analysis. Since the losses produced are strictly linked with the environmental and operating condition the accuracy of the calculation has an inherent error and assumptions are necessarily needed.

The main losses which occur in a mechatronic chain are analysed. Switching and conduction losses are considered for the inverter; joule, iron and mechanical losses are studied for the electrical motor; and lubricant, meshing, bearing and seals losses are reported for the gearbox.

Servo control applications need usually high dynamics, high power density and high precision in the positioning. Therefore, the most common strategies in industries to achieve the best performance and to reduce the main losses are investigated.

Since the calculation of the losses is necessarily approximated, the accuracy of the results might be poor. For this reason, the approach chosen was to develop a simplified mathematical model able to calculate the most relevant type of losses.

The efficiency maps for the electrical motor (as PMSM) was studied and a code was developed. The code needs input data derived from FEM simulations and it exploits them to generate a map in which the losses are reported for each combination of torque and speed.

Moreover, the Joule losses can be derived more precisely if measurement of the resistance and of the frame temperature takes place. Without any information, different assumptions are done to predict the operating temperature according to the type of working operation.

An experiment was conducted to ensure the validity of the approach. In fact, while the maps consider the component alone, in the real operation the motor and the gearbox are flanged together. This situation change the quality of the heat exchange assumed in the map and therefore the losses produced.

The experiment shows that the efficiency maps overestimate the efficiency of the couple motor + gearbox in particular at high speed when the temperature of the gearbox frame

increases. Eventually, the map of motors and the map of gearboxes seems to be accurate below ±3%.

The experiment highlights also the need for further investigation on the inverter. The amount of losses measured on this component was relevant, comparable with the ones produced by the PMSM motor or the planetary gearbox. Specially at low speed and low torque applied the efficiency drops.

The improved efficiency calculation was integrated in the sizing procedure. The results were compared with the ones achieved with a professional software that the company uses to help the selection. The theoretical and experimental analysis might provide a more reliable prediction of the energy consumption of the Servo chain. This value should be considered when a comparison between different scenarios is conducted.

An example including a hoist application is presented in which different gearbox ratios were feasible. It might happen that a higher initial cost of the components ensures a lower TCO in 5 or 10 years. Any specific case should be analysed individually because changing the size or the ratio both change the efficiency map and the working points of the components.